

**North Field, Qatar:
A Study of Condensate Blockage and Petroleum
Streams Management**

M.Sc. Thesis

**BY
ARIF KUNTADI**

SUPERVISOR: PROF. CURTIS H. WHITSON

Trondheim, June 2004



**DEPARTMENT OF PETROLEUM
ENGINEERING AND APPLIED GEOPHYSICS**

**NORWEGIAN UNIVERSITY OF
SCIENCE AND TECHNOLOGY**

NTNU**Norges teknisk-naturvitenskapelige universitet****Fakultet for ingeniørvitenskap og teknologi***Faculty of Engineering and Technology***Studieprogram i Geofag og petroleumsteknologi***Study Programme in Earth Sciences and Petroleum Engineering***Institutt for petroleumsteknologi og anvendt geofysikk***Department of Petroleum Engineering and Applied Geophysics***HOVEDOPPGAVEN/DIPLOMA THESIS/MASTER OF SCIENCE THESIS****Kandidatens navn/ The candidate's name: ARIF KUNTADI****Oppgavens tittel, engelsk/Title of Thesis, English:****North Field, Qatar: A Study of Condensate Blockage and Petroleum Streams Management****Utfyllende tekst/Extended text:**

This thesis aims to study the behaviour North Field gas condensate reservoir mainly in term of condensate blockage phenomenon near the wellbore which gives very significant well deliverability loss. Radial and Full Field reservoir model are simulated and some observations at the region near the wellbore have been done. Petroleum streams management has been developed for North Field to generate a complete compositional streams database.

Studieretning/Area of specialization: Reservoir Engineering**Fagområde/Combination of subjects: PVT, Reservoir Simulation and Petroleum Streams Engineering****Tidsrom/Time interval: January –June 2004**

.....
Faglærer/Teacher

Original: Student

Kopi: Fakultet

Kopi: Institutt

Acknowledgments

I wish to express my sincerest gratitude to my supervisor Professor Curtis H. Whitson for his invaluable personal and academic guidance throughout the whole work of this thesis and also for his fresh ideas and insights when discussing every topic in this thesis.

I especially thank to Dr. Mohammad Faiz ul Hoda and Dr. Knut Uleberg who helped me to develop petroleum streams management of North Field and with whom I had interesting discussions for improving the quality of this thesis.

I also thank to QUOTA Programme for giving me financial support in two years studying at the Department of Petroleum Engineering and Applied Geophysics of the Norwegian University of Science and Technology.

I would like to give my thanks to the office staffs at IPT, NTNU, and also all my friends for their cares and “smart” discussions in this latest two years.

Finally, I would like to dedicate this thesis to my parents who always give me constant encouragement. I am indebted to my wife, Astri, who always be patient to stand by me and encourage me to finish my study and thesis. Last but not least, I am also indebted to my son, Akhtar, a “little star” who has been my new spirit to finish this thesis.

Trondheim, June 2004

Arif Kuntadi

Table of Contents

ACKNOWLEDGMENTS.....	3
TABLE OF CONTENTS.....	4
ABSTRACT	6
1. INTRODUCTION	7
2. EQUATION OF STATE (EOS) AND RESERVOIR MODEL	8
2.1. EOS MODEL.....	8
2.2. RESERVOIR MODEL	8
3. CONDENSATE BLOCKAGE PHENOMENON.....	10
3.1. INTRODUCTION	10
3.2. GAS CONDENSATE RATE EQUATION	10
3.2.1. <i>Flow Regions</i>	11
3.2.2. <i>Calculating Pseudopressure</i>	11
3.3. RELATIVE PERMEABILITY NEAR WELLBORE.....	13
3.4. RELATIVE PERMEABILITY IN KHUFF FORMATION.....	14
4. RADIAL MODEL SIMULATION.....	17
4.1. RESERVOIR MODEL DESCRIPTION.....	17
4.1.1. <i>Gridding and Layering</i>	17
4.1.2. <i>Permeability distribution</i>	17
4.2. RADIAL MODEL SIMULATION AND RESULTS	18
4.3. OBSERVATION AT AREA NEAR WELL BORE.....	18
4.3.1. <i>Gas Rate distribution</i>	18
4.3.2. <i>Capillary number profile</i>	19
4.3.3. <i>Oil Gas Ratio (OGR) profile</i>	19
4.3.4. <i>Oil Saturation profile</i>	19
4.3.5. <i>Correlations</i>	19
4.3.6. <i>Permeability Effect</i>	20
5. SKIN FACTOR PREDICTION.....	23
5.1. CONDENSATE SKIN FACTOR PREDICTION	23
5.2. EFFECTIVE SKIN FACTOR PREDICTION	25
6. SENSITIVITY ANALYSIS	27
6.1. COREY-LIKE EQUATION EXPONENT AND PRODUCTION TUBING SIZE.....	27
6.2. PRESSURE CONSTRAINTS AND TUBING SIZE	27
6.3. PERMEABILITY DISTRIBUTION.....	28
6.3.1. <i>Radial Model Simulation</i>	28
6.3.2. <i>Full Field Model Simulation</i>	28
7. PETROLEUM STREAM MANAGEMENT	30
7.1. PETROLEUM STREAMS MANAGEMENT IN NORTH FIELD.....	30
7.2. GENERATING STREAMS DATABASE OF NORTH FIELD.....	32

7.3. SOME APPLICATIONS IN STREAMS DATABASE	33
8. CONCLUSIONS.....	35
NOMENCLATURE	36
REFERENCES	39
TABLES	40
FIGURES	47
APPENDIX A.....	106
1. FULL FIELD RESERVOIR MODEL DATASET	106
2. RADIAL RESERVOIR MODEL DATASET	112
APPENDIX B.....	119
1. EXTRACT OF MAIN STREAM FILE WHICH IS CONVERTED FROM THE SIMULATION RESULT STREAMS.....	119
2. EXTRACT OF WELL STREAM FILES WHICH IS THE RESULT OF FILTERING OPERATION OF MAIN STREAM FILE.....	120
3. EXTRACT OF AVERAGE WELL STREAM FILES WHICH IS THE RESULT OF AGGREGATION AND AVERAGING OPERATIONS OF WELL STREAM FILE.	121
4. EXTRACT OF AVERAGE WELL LAYER STREAM FILES WHICH IS THE RESULT OF AGGREGATION AND AVERAGING OPERATIONS OF WELL LAYER STREAM FILE.	122
APPENDIX C.....	123
1. SPREADSHEET CALCULATION EXAMPLE FOR PREDICTING THE GAS RATE WITH EXCLUDING AND INCLUDING THE CAPILLARY NUMBER EFFECT	123
2. SPREADSHEET CALCULATION EXAMPLE FOR PREDICTING THE DRY GAS RATE	123

Abstract

North Field is a giant gas condensate reservoir in Qatar which has estimated gas reserves more than 900 Tcf. This field is a part of Khuff formation and has four main productive layers: K1, K2, K3 and K4. The main objectives of this thesis are to study the condensate blockage phenomenon in this reservoir and to develop petroleum streams management procedures for given production line structure. This thesis uses an Equation of State (EOS) model and reservoir model which have been developed previously³. The developed EOS model was a Soave-Redlich-Kwong (SRK) EOS with 24 components. The developed reservoir model was a full field Cartesian model, no communication layering system between geological layers, uniform porosity and permeability in each geological layer and produced by 20 wells.

A radial well model is developed as a representation of one production well in the full field reservoir model. This model then is run for different permeability distributions to study the effect of condensate blockage. Near well region observations have been made specifically for gas rate, oil saturation, producing OGR and capillary number profiles. Observation in the log normal permeability distribution model simulation shows that there are some correlations between capillary number, oil saturation and producing OGR at the near-well region. The very low permeability model gives higher producing OGR and oil saturation compared than the moderate low model (the original model). In both permeability models the capillary number is proportional to the production gas rate.

Another observation result from the radial model simulation shows that most well deliverability loss happens in the region near the wellbore where both gas and condensate are flowing. The k_{rg} dramatically drops in this region due to condensate banking. The ratio $k_{rg}/k_{ro}(P)$ and $k_{rg}(k_{rg}/k_{ro})$ are the most important parameter to describe the phenomena in this region. The $k_{rg}/k_{ro}(P)$ can be predicted by PVT simulation of the developed EOS model. Both PVT simulation and reservoir simulation give the same range of this parameter from 1 – 100.

This thesis demonstrates how to use the spreadsheet calculation to accurately reproduce the gas production rate of the radial simulation model when the produced GOR is given. The condensate blockage skin factor is also able to be predicted by this hand-calculation. The effective skin factor which represents the condensate blockage effect in the full field model simulation is predicted by matching the full field simulation to the radial model simulation. This matching gives effective skin factor ranges from 3 (for high capillary number) to 15 (not including capillary number effect). This range is independent of the permeability distribution.

Some sensitivity analyses have been done to see the effect of permeability distribution, capillary number and tubing size in the simulation of North Field. The capillary number gives significant improvement of the gas production plateau period when simulated in the very low permeability model but it doesn't for moderate low permeability model. Log normal and uniform permeability model give almost identical simulation result.

Petroleum streams management has been developed by performing some sequences to generate the streams database from the simulation output file for one block concession of North Field. The streams database gives a complete description of the streams in all production nodes of the model and could be used to perform a reservoir production optimization. Some plots are generated to show the usefulness of the developed streams database.

All data used in this thesis was based directly or founded on information in the public domain. Complete references are given at the end of this thesis.

1. Introduction

North Field, firstly discovered in 1971, is situated just offshore to the North East of the peninsular landmass of Qatar as shown in **Fig. 1** and, geologically, in communication with Iran's South Pars. North Field has gas reserves estimated more than 900 Tcf and considered as the world's second largest holder of gas reserves after Russia or the largest single gas field in the world. This field covers an area of more than 6000 square kilometers which is nearly half the size of Qatar land. North Field reservoir which is a part of Permian Khuff formation mainly consists of mixture of dolomite and limestone and has 4 geological layers (starting from the top): K1, K2, K3 and K4⁸.

Previous work³ developed an Equation of State (EOS) model and reservoir model for North Field. In the following chapter there will be a brief description about the developed EOS model and full field reservoir model.

Condensate blockage phenomenon in the near-wellbore can be important issue in the deliverability of a gas condensate reservoir. This phenomenon significantly reduces the well deliverability and for a given pressure constraint (e.g. bottom hole flowing pressure) it gives reductions in the recovery both of gas and condensate accordingly. The radial model with single production well and fine grid is run to capture the effect of condensate banking in the near-wellbore during the field production life. The log normal distribution model of permeability is introduced to study the effect on gas rate, capillary number, oil gas ratio (OGR) and oil saturation at the first radial block. The very low and uniform permeability model is also run and then compared to the log normal model.

Fevang and Whitson¹ described how significant the ratio k_{rg}/k_{ro} in the region near the wellbore is. They mentioned that by being given an accurate OGR it is possible to reproduce the gas rate almost exact as the gas rate which was produced from the radial and fine grid model simulation. This thesis work will demonstrate how the spreadsheet calculation is able to reproduce the simulation gas rate for a given OGR and predict the condensate blockage skin factor. The full field model (FFM) which has been developed in the previous work has a coarse grid model that can not capture the condensate banking near the wellbore. To include this near well phenomenon it needs to put some skin factor in the FFM which then makes the FFM simulation behaves like the radial model simulation. The procedures to match FFM wells to a fine gridded radial model will also be discussed in this thesis.

In the sensitivity analysis there will be discussions about some parameters which are considered important factors to understand the behavior of a gas condensate reservoir. Corey-like exponents, production tubing size, pressure constraints and permeability distribution have been examined.

Petroleum streams management is basically not only important to study in gas condensate reservoir, but in gas condensate reservoir the compositional streams are more valuable than in oil reservoir because the compositional streams determine how much the part of the produced reservoir fluids will be as natural gas or Liquefied Natural Gas (LNG), Liquefied Petroleum Gas (LPG) and as condensate. This thesis work has developed an early step of a complicated petroleum stream management of North Field, Qatar. A further study is still needed to be done to develop a comprehensive petroleum streams management in such huge gas condensate reservoir.

2. Equation of State (EOS) and Reservoir Model

Cubic equations of state (EOS's) are simple equations relating pressure, volume, and temperature (PVT). They accurately describe the volumetric and phase behavior of pure compounds and mixtures, requiring only critical properties and acentric factor of each component. The same equation is used to calculate the properties of all phases, thereby ensuring consistency in reservoir processes that approach critical conditions (e.g., miscible-gas injection and depletion of volatile-oil/gas-condensate reservoirs). Problems involving multiphase behavior, such as low-temperature CO₂ flooding, can be treated with an EOS, and even water-/hydrocarbon-phase behavior can be predicted accurately with a cubic EOS¹³.

Due to its huge gas reserves so an appropriate development of North Field is needed to be done carefully in order the gas reserves which have been discovered in this field could be recovered optimally. One of the tools usually used in petroleum engineering to give comprehensive evaluation of the potentiality of the reservoir is reservoir simulation. Simulation will give accurate result if uses an accurate description of the reservoir fluid phase behavior and the appropriate reservoir model. This chapter gives the description about the EOS model and the full field reservoir model which have been developed in Ref. 3.

2.1. EOS Model

Almarry and Al-Saadoon⁶ developed an EOS model for North Field fluids, particularly for K4 formation fluids. They used the Peng Robinson (PR) EOS model but unfortunately they did not provide the detail component properties of their model. The new EOS model was developed with SRK EOS as described in Ref. 3. SPE 13715 only provided the composition of original reservoir fluids which dealing with single carbon number up to C₆ and one heaviest fraction of C₇₊. This heaviest fraction was characterized by Gamma distribution model to get 13 new components with the heaviest components C₃₀₊. The developed SRK EOS model had 24 components which then it was named SRK EOS24.

Ref. 3 discussed the procedure to characterize the C₇₊ fraction using *PhazeComp* and it also explained the way to match this SRK EOS24 model to some experiment data which were obtained from SPE 13175. **Fig. 2 - Fig. 3** show the agreements between the CVD experiments data and what the SRK EOS24 model predicted. The final SRK EOS24 model parameters resulted from C₇₊ fraction characterization and EOS model matching are presented in **Table 1** and its complete BIPs are presented in **Table 2**.

The SRK EOS24 model was developed from the reservoir fluid properties of K4 formation but then it was also used to model the reservoir fluid of the other three formations: K1, K2 and K3. Some papers^{8,9} mentioned that K2 and K3 have H₂S contents slightly higher than K4 so the difference then only at initial composition of K2/K3 and K4, still can use the same EOS model. The reservoir fluid of K1 is basically similar to K4. The calculated initial gas compositions of North Field's fluids are presented in **Table 3**.

2.2. Reservoir Model

The full field reservoir model (FFM) which was developed in Ref. 3 only modeled one block concession of North Field since it is really needed numerous grid blocks to model the whole area which covers more than 6000 sq km. The FFM covers the area of 100 sq km or equivalent to 10 km x 10 km. Both the previous work and this thesis work use the free version of *Sensor* simulator which has maximum active grid blocks of 6000.

The North Field FFM was a grid coarse Cartesian model with DX = DY = 500 m. The geological layers K1, K2 and K3 were divided into 3 numerical layers each and then K4 was

divided into 4 numerical layers. So finally the reservoir model had dimension of 20 x 20 x 17 including the 3 seal layers between each geological layer and one bottom seal layer. The final layering model of North Field (Khuff formation) is presented in **Fig. 4**.

Al-Shiddiqi and Dawe⁸ explained that this formation has porosity ranging from 4–20%, and average permeability of 30 md. They also described that the permeability of K2/K3 ranging from 3 – 1800 md and K1/K4 have somewhat lower permeability. The FFM used permeability of 45 md for K2/K3 and 15 md for K1/K4. It used uniform porosity for each geological layer which were 10% for K1/K4 and 15% for K2/K3. The vertical permeability used was 10% of the horizontal permeability. The analytical relative permeability correlation used was a Corey-like equation. Detail formation properties and relative permeability correlation parameters are presented in **Table 4**.

As previously discussed, the PVT properties used in the FFM were the SRK EOS24 model with two different initial gas compositions of K1/K4 and K2/K3. Since the FFM had 2 different initial gas composition then it was initialized by two different initialization regions, one was for K1/K4 and the other was for K2/K3. The gas plateau rate was set at 2000 MMSCF/D with 20 production wells which means each well producing 100 MMSCF/D. The wells positions are shown at **Fig. 5** and all wells were perforated in all numerical layers. Detail description of the North Field FFM is presented at **Table 4**.

3. Condensate Blockage Phenomenon

3.1. Introduction

The typical chemical composition of a gas-condensate mixture is dominated by volatile components such as methane, and a rather ‘small’ amount of heavy hydrocarbon components (<15 mol-%), though these heavier components make up a considerably larger percentage of the liquid phase (‘retrograde condensate’) formed during pressure decrease below an upper dew point. For practically any retrograde condensate reservoir, the condensate saturation is, throughout most of the reservoir, so low that its mobility is much less than gas mobility and for practical purposes can be considered immobile. Nevertheless, this gas-dominated flow behavior is not correct in the near-well vicinity where condensate saturations often reach high values (>50%), and oil permeability may exceed gas permeability ($k_{rg}/k_{ro} < 1$)².

Condensate blockage near the wellbore may reduce gas well deliverability appreciably, though the severity depends on a number of reservoir and well parameters. Condensate blockage is important if the pressure drop from the reservoir to the wellbore is a significant percentage of the total pressure drop from reservoir to delivery point (e.g. a surface separator) *at the time (and after) a well goes on decline*. Reservoirs with low-to-moderate permeability (<10–50 md) are often ‘problem’ wells where condensate blockage must be handled properly. Wells with high *kh* products (>5–10,000 md-ft) are typically not affected by reservoir pressure drop because the well’s deliverability is constrained almost entirely by the tubing. In this case, condensate blockage is a *non-issue*².

3.2. Gas condensate rate equation

The general volumetric rate equation for a gas condensate well of any geometry (e.g. radial, vertically fractured, or horizontal) is, for a compositional formulation,

$$q_g = C \left(\frac{RT_{SC}}{P_{SC}} \right) \beta_S \int_{P_{wf}}^{PR} \left(\frac{\rho_o k_{ro}}{M_o \mu_o} \right) + \left(\frac{\rho_g k_{rg}}{M_g \mu_g} \right) dp \dots\dots\dots (1)$$

or in terms of black-oil PVT,

$$q_g = C \int_{P_{wf}}^{PR} \left(\frac{k_{ro}}{B_o \mu_o} R_s \right) + \left(\frac{k_{rg}}{B_{gd} \mu_g} \right) dp \dots\dots\dots (2)$$

where

$$C = \frac{2\pi a_1 kh}{\ln(r_e/r_w) - 0.75 + s} \dots\dots\dots (3)$$

$a_1=1/(2\pi \cdot 141.2)$ for field units, and $a_1=1$ for pure SI units. The constant C includes basic reservoir properties such as permeability *k*, thickness *h*, drainage radius r_e , wellbore radius r_w , and other constants. Skin *s* is a composite factor that includes non-ideal flow effects such as damage, stimulation, drainage geometry, and partial penetration. Fevang and Whitson¹ mentioned that relative permeabilities k_{rg} and k_{ro} are defined relative to absolute permeability, and not relative to permeability at irreducible water saturation.

3.2.1. Flow Regions

Fevang and Whitson¹ introduced a model of a gas condensate well undergoing depletion which consists of 3 regions:

Region 1: An inner near-wellbore region where both gas and oil flow simultaneously (at different velocities).

Region 2: A region of condensate buildup where only gas is flowing.

Region 3: A region containing single phase (original) reservoir gas.

These three regions define pseudosteady-state flow conditions, meaning that they represent steady-state conditions at a given time but that the steady-state conditions change gradually during depletion. **Fig. 6** shows these three regions with the pressure profile for a given time in North Field undergoing depletion while **Fig. 7** depicts the regions with the oil saturation profile.

Region 1. This region contributes the most deliverability loss in gas condensate well as shown in **Fig. 6** where the pressure drop mainly occurs in this region. The gas mobility dramatically drops in Region 1 due to condensate banking, and as shown in **Fig. 7** the oil saturation (S_o) in this region is higher than critical oil saturation which means that in this region both phases, oil and gas, are flowing together to the wellbore. Fevang and Whitson¹ describe that the flowing compositions (GOR) in this region is constant throughout, equal to the gas entering Region 1 and the same composition as the produced wellstream. Knowing the wellstream composition defines the composition of the gas entering Region 1 and we can predict the pressure at the boundary of Region 1 and Region 2 which is the dew point of the wellstream mixture. The size of Region 1 increases with time. For steady state condition, the oil saturation is determined along this region (as a function of distance) *specifically* to ensure that all liquid that condenses from the single-phase gas entering Region 1 has sufficient mobility to flow through and out of Region 1 without any net accumulation. Region 1 always exists when the flowing bottom hole pressure (BHP) is lower than the original dew point pressure and vice versa.

Region 2. This region has a net accumulation of condensate since only the gas flows in this region and the condensate is immobile or, if no, only has very small mobility. Basically the phenomenon of the gas in this region is similar to the behavior of gas in CVD experiment which then implies to the oil saturation distribution in this region with correction in water saturation. The size of Region 2 is largest just after the reservoir pressure drops below the dew point. It decreases in size with time because Region 1 is expanding.

Region 3. This region only exists when the reservoir pressure is higher than the initial dew point pressure of the reservoir gas. The composition of gas is constant throughout and equal to the original gas composition. The contribution of this region in well deliverability is quantified by the treatment of single phase gas flow.

3.2.2. Calculating Pseudopressure

Fevang and Whitson¹ proposed a model to calculate the pseudopressure integral as described in Eqs. (1) and (2) by using the extension of pseudopressure method of Evinger and Muskat which was originally proposed for solution gas drive oil wells. The First step is breaking the pseudopressure intergral into 3 parts corresponding to the regions developed in gas condensate well:

$$\text{Total } \Delta p_p = \int_{P_{wf}}^{PR} \left(\frac{k_{ro}}{B_o \mu_o} R_s \right) + \left(\frac{k_{rg}}{B_{gd} \mu_g} \right) dp =$$

$$\begin{aligned}
 \text{Region 1} \quad & \int_{p_{wf}}^{p^*} \left(\frac{k_{ro}}{B_o \mu_o} R_s \right) + \left(\frac{k_{rg}}{B_{gd} \mu_g} \right) dp \quad + \\
 \text{Region 2} \quad & \int_{p^*}^{p_d} \frac{k_{rg}}{B_{gd} \mu_g} dp \quad + \\
 \text{Region 3} \quad & k_{rg}(S_{wi}) \int_{p_d}^{p_R} \frac{1}{B_{gd} \mu_g} dp \quad \dots\dots\dots(4)
 \end{aligned}$$

From the producing GOR, R_p , we know the dew point of the producing wellstream mixture. Using black-oil PVT, with r_s defined as the solution oil-gas ratio, we locate the pressure in the PVT table where $r_s=1/R_p$ and define this pressure as p^* . In a compositional treatment the dew point of the producing wellstream composition is defined as p^* . If $p^* > p_R$, then integration of the Region 1 integral should only be from p_{wf} to p_R ; in this case, Regions 2 and 3 don't exist.

Region 1. The Region 1 pseudopressure integral is solved using the modified Evinger-Muskat approach. At pressures $p < p^*$ the PVT properties R_s , B_o , r_s , B_{gd} , μ_o , and μ_g are found directly. Next, the equation defining producing GOR

$$R_p = R_s + \left(\frac{k_{rg}}{k_{ro}} \right) \left(\frac{\mu_o B_o}{\mu_g B_{gd}} \right) (1 - r_s R_p) \quad \dots\dots\dots(5)$$

is used to calculate k_{rg}/k_{ro} as a function of pressure,

$$\left(\frac{k_{rg}}{k_{ro}} \right) (p) = \left(\frac{R_p - R_s}{1 - r_s R_p} \right) \left(\frac{\mu_g B_{gd}}{\mu_o B_o} \right) \quad \dots\dots\dots(6)$$

where PVT properties are known as a function of pressure. It is also shown that Eq. (6) can be expressed in terms of the oil relative volume of the flowing gas during a constant composition expansion, $V_{roCCE} = V_o / (V_g + V_o)$

$$\left(\frac{k_{rg}}{k_{ro}} \right) (p) = \left(\frac{1}{V_{roCCE}} - 1 \right) \left(\frac{\mu_g}{\mu_o} \right) \quad \dots\dots\dots(7)$$

From Eqs. (6) and (7), V_{roCCE} can be expressed in terms of black-oil PVT properties, for any producing GOR R_p ,

$$V_{roCCE} (p) = \left[1 + \left(\frac{R_p - R_s}{1 - r_s R_p} \right) \left(\frac{B_{gd}}{B_o} \right) \right]^{-1} \quad \dots\dots\dots(8)$$

As shown by Evinger and Muskat, relative permeabilities k_{rg} and k_{ro} can be expressed directly as a function of the ratio k_{rg}/k_{ro} (when both phases are mobile). This means that we can evaluate k_{rg} and k_{ro} directly as a function of pressure in the Region 1 pseudopressure integral, $k_{rg}(p) = f[k_{rg}/k_{ro}(p)]$ and $k_{ro}(p) = f[k_{rg}/k_{ro}(p)]$, using Eq. (6).

Region 2. When Region 2 exists ($p^* < p_R$), the Region 2 integral is evaluated using $k_{rg}(S_o)$, where S_o is estimated as a function of pressure from CVD relative oil volumes $V_{roCVD}(p) = V_o(p) / V_d$, yielding $S_o(p) = [V_{roCVD}(p)](1 - S_w)$. If V_{roCVD} values are not known for the black-oil PVT data set, they can be calculated using the following equations:

$$(V_{roCVD})_k = \frac{N_{k-1} - G_{k-1}(r_s)_k (B_o)_k}{1 - (r_s R_s)_k} \dots\dots\dots(9)$$

with $N_{k-1} = \left(\frac{V_{roCVD}}{B_o} + \frac{1 - V_{roCVD}}{B_{gd}} r_s \right)_{k-1}$

and $G_{k-1} = \left(\frac{V_{roCVD}}{B_o} R_s + \frac{1 - V_{roCVD}}{B_{gd}} \right)_{k-1}$

where k represents the current pressure, k-1 represents the previous pressure, and $(V_{roCVD})_0 = 0$.

Region 3. Only PVT properties are found in the Region 3 integral, where the traditional single-phase gas pseudopressure function can be used.

3.3. Relative permeability near wellbore

Region 1 is the most important region to observe when examining the condensate blockage in a gas condensate well. The biggest pressure drop occurs in this region and also the gas mobility or k_{rg} decreases significantly due to the condensate banking. As described earlier the *key correlation* to calculate the pseudopressure integral in this region is *the relationship between the k_{rg} and the ratio k_{rg}/k_{ro}* . The ratio k_{rg}/k_{ro} which is pressure dependent basically can be calculated from the PVT experiment or PVT simulation and by solving Eq. (7). The relevant range of k_{rg}/k_{ro} depends upon the pressure range of Region 1 which is from the dew point pressure of the wellstream mixture to BHP. Whitson et al² mentioned that the relevant range of k_{rg}/k_{ro} in Region 1 is from 0.1 to 100. The correlation $k_{rg} = f(k_{rg}/k_{ro})$ then can replace the correlation $k_{rg}(S)$ and $k_{ro}(S)$ which means that the measurement of fluids saturation is not required anymore.

Gas condensate well productivity would be predicted properly when high velocity phenomena such as non-Darcy flow and high capillary number effect are taken into account in the calculation/simulation. In most gas condensate wells the net effect of these two phenomena is to improve productivity, reducing the impairment due to condensate blockage⁵. This thesis work is trying to see the effect of capillary number in terms of relative permeability changes.

When the capillary forces are very high the relative permeability is absolutely function of rock relative permeability correlation or the mixture behaves as immiscible. On the other side if the capillary forces are very low then the mixture will behave as miscible and the curve of relative permeability becomes ‘straight line’. Finally for the system which has capillary force in between those extreme cases will have relative permeability situated between the ‘immiscible’ or ‘rock’ curves and the ‘miscible’ or ‘straight line’ curves. To link these two curves Fevang and Whitson¹ proposed a term called immiscibility factor, f_i , which is function of capillary number (N_c). For low capillary numbers, the immiscible curves apply and $f_i = 1$. For sufficiently high capillary numbers the miscible curves apply and $f_i = 0$. A constant k_{rg}/k_{ro} value (used instead of saturation) defines the immiscible and miscible relative permeability values used in the generalized correlation.

Capillary number is defined as the ratio of viscous forces to capillary retaining forces

$$N_c = \frac{\Delta P_v}{P_c} \dots\dots\dots(10)$$

or, which is the same:

$$N_c = N_{cg} \equiv \frac{v_{pg} \mu_g}{\sigma_{go}}, \quad v_{pg} = \frac{v_g}{\phi(1 - S_{wi})} \dots\dots\dots(11)$$

where v_{pg} is a ‘pore’ gas velocity and v_g is Darcy’s gas velocity. Relative permeability of gas including capillary number dependence is given by Whitson and Fevang⁴

$$k_{rg} = f_I k_{rgI} + (1 - f_I) k_{rgM} \dots\dots\dots(12)$$

where k_{rgI} is the immiscible ($N_c = 0, f_I = 1$) gas relative permeability, and k_{rgM} is the miscible ($N_c = \infty, f_I = 0$) straight line gas relative permeability, calculated as

$$k_{rgM} = k_{rg}^o \frac{1}{1 + (k_{rg} / k_{ro})^{-1}} \dots\dots\dots(13)$$

Then the immiscibility factor, f_I , can be defined as

$$f_I = \frac{1}{(\alpha N_c)^n + 1} \dots\dots\dots(14)$$

where α is a constant dependent only on rock properties, and a good estimation for α can be written as

$$\alpha = \frac{2 \cdot 10^4}{\sqrt{k \phi}}, \quad n = 0.7 \dots\dots\dots(15)$$

where k is absolute permeability and ϕ is porosity.

3.4. Relative permeability in Khuff formation

The ratio k_{rg}/k_{ro} of Region 1 is readily calculated from PVT. The range of k_{rg}/k_{ro} during the production life is determined. In the early period of production, North Field has three regions due to the initial undersaturated reservoir pressure, note: p_R initial = 5300 psig and p_d initial = 5120 psig (5135 psia). Once the reservoir pressure has reached the initial p_d then only two regions are developed in North Field, and the fact that initial p_R is only slightly higher than initial p_d leads this reservoir will only have 2 regions (1 and 2) almost during its production life when the depletion mechanism is applied.

CVD experiment is conducted from the p_d initial to any lower pressure to observe the behavior in Region 2 and then CCE experiments are performed for equilibrium gases produced from each pressure nodes of CVD experiment. The CVD experiment represents the mechanism in Region 2 where the equilibrium gas of each pressure step is basically the same as the gas leaving Region 2 or the gas entering Region 1. The CCE experiment represents the mechanism in Region 1 so when the equilibrium gas of any pressure step of CVD is fed for CCE experiment then basically we simulate the behavior of Region 1 for given p^* . Hence, the pressure steps of the CVD experiment are the representation of p^* of the reservoir during its production life.

Fig. 8 shows the relative liquid volume of CVD and CCE experiments which are performed for North Field SRK EOS24 model. The retrograde condensation of this EOS model gives a maximum liquid relative volume of 2.3% at 1750 psig. The red line shows the

behavior in Region 1 when p_R is equal to p_d initial or the first time in the production history when only 2 regions are developed in this reservoir. This plot gives us the maximum liquid relative volume of 1.5% at 2750 psig. The relevant range of fluids behavior in Region 1 depends upon how high the pressure constraint we put as the BHP is. The behavior of flowing reservoir fluids in Region 1 for p^* lower than p_d initial are represented by the others CCE relative liquid volume plots.

Eq. (7) is used to calculate the relative permeability ratio k_{rg}/k_{ro} , **Fig. 9** shows the range of k_{rg}/k_{ro} for the whole production life of Khuff formation. It is seen that the relevant range of k_{rg}/k_{ro} is from 2 – 100. There are some k_{rg}/k_{ro} higher than 100 but these occur for very low p^* s. The p^* of 1750 psig or lower practically only happens in the late of reservoir production history or under depletion production scenario it is the period when the reservoir could not produce the plateau production rate any longer (note: in the original scenario of this thesis the plateau rate is set at 100 MMSCF/D/well).

The developed reservoir model of North Field applied analytical permeability correlation. The Corey-like correlation which is used in *Sensor* simulator is described below

$$k_{rog} = k_{rocw}^o \left(\frac{1 - S_{org} - S_{wi} - S_g}{1 - S_{org} - S_{wi}} \right)^{nog} \dots\dots\dots(16)$$

$$k_{rg} = k_{rgro}^o \left(\frac{S_g - S_{gc}}{1 - S_{org} - S_{gc} - S_{wi}} \right)^{ng} \dots\dots\dots(17)$$

$$k_{row} = k_{rocw}^o \left(\frac{1 - S_{orw} - S_w}{1 - S_{orw} - S_{wi}} \right)^{now} \dots\dots\dots(18)$$

$$k_{rw} = k_{rwo}^o \left(\frac{S_w - S_{wi}}{1 - S_{orw} - S_{wi}} \right)^{nw} \dots\dots\dots(19)$$

The correlation parameters used are presented in **Table 4**. This model uses exponent $nog=no=3$; the exponent parameter (n) basically affects the curvature of the plot of saturation vs. relative permeability; $n=1$ gives a ‘straight line’ correlation and the higher exponent (e.g. 3 or 4) have significant curvature. Exponent equal to 1.5 could be considered as the representation of relative permeability model for a system which has high capillary number and the infinity capillary number is represented by exponent 1. **Fig. 10** shows the relative permeability vs. gas saturation of the developed model ($n=3$) and the representation of high capillary number model ($n=1.5$), while **Fig. 11** depicts the relationship between k_{rg} vs. k_{rg}/k_{ro} for both models.

Simple 1D radial model simulation with a single well has been done for Layer K4 to see the condensate blockage effect in Khuff formation in general. The results of the simulation are shown in **Fig. 12 - Fig. 15**. Again, it is clearly seen in **Fig. 12** that the most pressure drop occurs in the region near the wellbore (Region 1) and three regions exist in early production period (40 days) where $p_R > 5135$ psia (p_d initial) and afterward only two regions (1 and 2) exist in the reservoir. The exact boundary of Region 1 and Region 2 is predicted by calculating the dew point of producing wellstream (p^*) at a given time, but one quick way to locate this position is by pointing out where the oil start flowing or when S_o is already higher than S_{oc} ($S_{oc}=20\%$). **Fig. 13** shows that these boundaries are located at around 10 ft from the wellbore

after 40 days simulation and around 50 ft after 500 days. It means that Region 1 is expanding by time and Region 2 is reducing accordingly. **Fig. 15** also gives indication that the position where condensate begins being mobile is getting farther from the wellbore.

Fig. 14 tells us how big the k_{rg} drops when gas flows near the wellbore, this is the key reason explaining why Region 1 contributes the most productivity loss in gas condensate well production history. This figure also shows that in Region 1 the relevant range of k_{rg} is 0.05 - 0.2 and then if we confirm this k_{rg} range to **Fig. 11** we will get the ratio k_{rg}/k_{r0} situated from 1 - 100. This range of k_{rg}/k_{r0} , which is calculated from radial simulation, is very close to the range predicted from PVT simulation. This agreement becomes the evidence that the most relevant range of k_{rg}/k_{r0} in practical is from 1 - 100.

4. Radial Model Simulation

The fine grid model is required to study condensate blockage phenomenon in gas condensate reservoir. Radial reservoir model with one production well in the center is the suitable reservoir model when fine grid is needed. Basically full field model is still able to use to capture the condensate blockage effect but it needs to have local grid refinement in the area near the production wells. This thesis work has developed a radial model for North Field and then simulated this model to observe some phenomena near wellbore such as oil saturation, capillary number, oil gas ratio, and production gas rate.

4.1. Reservoir model description

The main purpose of developing the radial model in this thesis work is to study gas condensate reservoir behavior in appropriate way which then its result could be taken into account in the FFM. The developed radial model is a representation of one production well in the FFM where the volumetric drainage used in radial model is equal to 1/20 of the FFM volumetric drainage. All the parameters used in the radial model are the same as the FFM except the gridding, layering and permeability distribution. Detail description of North Field radial model is presented in **Table 5**.

4.1.1. Gridding and Layering

To capture the phenomena near wellbore this radial model uses fine grid at the region near well and getting larger for the area far away from the wellbore. Logarithmic propagation is used to generate 25 radial blocks. This model has well radius, r_w , equal to 0.583 ft (7") and outer boundary radius, r_e , equal to 4140 ft. Radial coordinate of this model is presented in **Table 5**.

This radial model still uses the same reservoir thickness as used in the FFM but the numerical layers in this model has 10 ft thickness where K1, K2, K3 and K4 are divided into 20, 32, 25 and 64 numerical layers respectively. Totally this model has 145 numerical layers with 141 active layers and 4 sealing layers. This model only has one block in the θ direction. Finally the developed radial model has grid model as 25x1x145.

4.1.2. Permeability distribution

The FFM has the uniform permeability distribution in each geological layer where K1/K4 have permeability 15 md and K2/K3 have 45 md. The log normal permeability distribution is introduced in the radial model for each geological layer. Al-Shiddiqi and Dawe⁸ explained that the permeability in Khuff formation has extreme vertical variation, for example they mentioned that in interval of 1 meter the permeability can change from 3 to 1800 md. To include this extreme variation phenomenon, during generating the permeability distribution for each geological layer we set at least one layer has very high permeability and one other layer has very low permeability, in addition we tried to keep the average permeability as used in FFM.

Fig. 16 shows the permeability distribution in K1 which has average permeability of 16.7 md, minimum permeability 0.1 md and maximum permeability 299 md. **Fig. 17 - Fig. 19** show the permeability distribution of K2, K3 and K4 respectively. The summary of the permeability distribution of Khuff formation radial model is presented in **Table 6**.

4.2. Radial Model Simulation and Results

The developed radial model was simulated for 50 years with plateau rate of 100 MMSCF/D, the same scenario as used in FFM simulation. This radial simulation has pressure constraint of minimum bottom hole pressure (BHP) at 2800 psia. There is a feature in *Sensor* simulator where we can run the simulation in Black Oil (BO) model but we still can put the EOS model in the dataset. This feature basically will generate the BO tables of fluid properties based on the EOS model we specified in the dataset. This feature was used to run the radial model under BO model.

Fig. 20 - Fig. 22 show the results of the radial simulation. As shown in **Fig. 20** this simulation gives the plateau period of around 17.5 years where afterward the BHP has already reached its constraint and consequently the production gas rate decreases until it goes to zero at year 35 when the model doesn't have enough pressure to produce gas from the formation (p_R already drops to 2800 psia). **Fig. 20** also shows that the condensate rate practically decreases since the beginning because the condensation already happens at the area near wellbore (Region 1 and 2) at the beginning and once the p_R is already below the p_d initial then the condensation happens at the whole parts of the reservoir. The ultimate recovery of gas and condensate are 40% and 33% respectively as seen in **Fig. 22**. The difference between the ultimate gas recovery and oil recovery indicates how much condensate is left in the formation during the production life of the reservoir. 7 out of 40 means around 17.5% of the condensate should be produced is lost due to retrograde condensation and immobile condensate.

4.3. Observation at area near well bore

The condensate blockage happens since the beginning because the model used the BHP constraint lower than p_R . To observe this phenomenon we might choose any time we desire but probably the appropriate time to choose is at the end of the plateau period. This time basically will represent the ultimate accumulation of the condensate blockage effect in the near wellbore. The observation then was done at year 17. This observation intends to see the effect of condensate blockage near well region and also the effect of the log normal permeability distribution used in the model.

4.3.1. Gas Rate distribution

Since this radial model used the same numerical layer thickness (h) then the gas production rate, as described in Eq. (2), is proportional to the absolute permeability. Hence the distribution of the gas rate in each individual geological layer is also proportional to the permeability distribution. **Fig. 23** shows the distribution of numerical layer gas rate in K1 at year 17. There are only 5 out of 20 layers which have contribution higher than 1%. Layer 9 which is the highest k layer in K1 has the biggest contribution to the total gas rate of K1. The contribution of this layer is almost 90% which means that almost all the gas produced from K1 is produced from this layer.

Fig. 24 tells the contribution of each numerical layer in K2 which is exactly proportional to its permeability distribution as shown in **Fig. 17**. K2 has total production gas rate of 28.86 MMSCF/D. The highest k layer, layer 41, contributes around 74% of K2 total gas rate. There are only 10 out of 32 layers which have rate contribution higher than 1%. The same situation is also depicted by **Fig. 25** for K3, layer 67 as the highest k layer contributes 74% of K3 total gas rate and only few layers contribute more than 1%. Layer 98, the highest k layer in K4, contributes only 34% of total rate as shown in **Fig. 26**. This contribution is not as high as the others highest k layer because the k distribution in K4 has more high k layers as

seen in **Fig. 19** which leads the total gas production rate of K4 is not too dominated by the highest layer as in other geological layers.

All the geological layers, as explained above, are dominated by their highest k layer in term of production gas rate. The consequence of such domination is that the vertical cross flow in the formation becomes important phenomenon particularly in the highest k layer where it's surrounding layers always feeding reservoir gas to this highest k layer.

4.3.2. Capillary number profile

The gas velocity, either Darcy's velocity or pore velocity, is the main factor which determines the capillary number (N_c) profile in each geological layer as described in Eq. (11). The linear velocity itself is proportional to the gas rate since all the layers have the same cross-section area due to the uniform h used in the radial model then basically N_c profile is similar to the gas rate profile where the high k will have high N_c . **Fig. 27 - Fig. 30** show the N_c profile of K1, K2, K3 and K4 respectively. These profiles are similar to the k distribution of the geological layers as shown from **Fig. 16 - Fig. 19**. The calculated N_c for the whole layers have the N_c ranging from in the order of 10^{-8} to 10^{-4} .

4.3.3. Oil Gas Ratio (OGR) profile

The two parameters previously explained, gas rate and N_c , have explicit correlation to the permeability which then give clear analogous profile to the k distribution. OGR profiles resulted from the radial model simulation, which are presented in **Fig. 31 - Fig. 34**, do not give clear correlation particularly related to the k distribution. The highest k layers do not always have highest OGR but they still belong to the layers which have high OGR. The highest k layers which have highest OGR are only found in K1 and K3. There are other facts found in K1 and K3 that the 5 highest k layers also belong to the 5 highest OGR, but again these facts can not be seen in K2 and K4.

4.3.4. Oil Saturation profile

The oil saturation profiles as depicted in **Fig. 35 - Fig. 38** are calculated at the first radial block from the wellbore in the model. In K1 as shown in **Fig. 35** the big five of the highest k layers are also the big five of S_o , the order of the five highest S_o is also the same to the order of the five highest k layers. But this trend doesn't apply for K2, K3, and K4. Particularly in K4 there are many layers which have almost no correlation between S_o and k profile.

4.3.5. Correlations

The observations which have made to see the profile of some properties are only related to the distribution of the k , so we haven't tried yet to correlate the properties between each others. In this part the correlations between each property are studied.

The first correlation to study is between gas rate and capillary number which is shown in **Fig. 39**. This figure tells us that N_c is proportional to gas rate for all geological layers. The more gas produced from particular numerical layer will imply to have higher N_c . The plot of K1 exactly falls on the top of K4 plot, the reason of this agreement is that both layers have the same formation and fluids properties which leads giving the same gas rate and exactly the same N_c as described in Eq. (11). This condition also applies for K2 and K3 so that they also have the same Q_g vs. N_c plots.

The correlation between OGR and N_c is the second correlation to study. As explained in the part when we discussed about the OGR profile that there were only very few numerical

layers which have clear correlation to the k distribution, this also applies to the correlation of OGR and N_c . **Fig. 40** shows this correlation. From this figure it is found that K1 gives the clearest correlation that the OGR is proportional to N_c . Even though in this layer not all numerical layers give proportional correlation between OGR and N_c but it has strong proportional trend. K3 gives quite clear trend to the correlation. Basically K2 and K4 also have the same trend as K1 and K3 but there are many scattered points mainly in K4 which do not strongly support this trend.

Fig. 41 depicts the correlation between N_c and oil saturation (S_o) in all geological layers. Clearly seen that S_o is propositional to N_c for all geological layers. The more gas produced from a given layer is the more oil condensing in this layer which will lead the more condensate banking in near well region. And again it is shown that this correlation has much more agreement in K1 and K3 while K2 and K4 have many scattered points. From the second and third correlations have been developed, both show that OGR and S_o have a trend to be propositional to N_c . If then we make correlation between OGR and S_o it should have the similar trend and even be stronger than to N_c itself. The fourth correlation is developed to investigate this hypothesis.

The correlation between OGR and S_o is depicted in **Fig. 42**. This figure proves above hypothesis that in general the OGR is proportional to S_o . The higher OGR indicates the higher p^* in the given layer, and since the BHP of each perforated block could be considered as the same then the higher p^* will give more condensation in Region 1 of this layer. So in general the high OGR will contribute to the high oil saturation in Region 1. As the phenomena happened in the previous correlations that OGR- S_o correlation also has clear trend in K1 and K3 but not so in K2 and K4. We suspect that these phenomena are related to the thickness of the geological layers. As described in the reservoir model that the order of geological layer based on its thickness from the thickest to the thinnest are K4, K2, K3 and K1. There is a trend that when the formation has thick productive zone it leads to have more scattered points in the correlations between N_c , OGR, and S_o . Inversely, when the formation is not so thick then the correlation developed becomes quite clear. We suspect that the gravity contributes to the scattering because basically the gravity will give more affect in the thick formation. We did not develop further examination about the possibility of this gravity effect since we did not see essential reason so far to do so in term of improving the understanding about condensate blockage phenomenon.

4.3.6. Permeability Effect

In the previous section we have discussed about the permeability distribution effect to some property profiles at the region around the wellbore. In this section we will discuss the permeability effect along gas flow path from the outer boundary to the wellbore but only for some numerical layers. Observation at the highest k layer and its surrounding layers has been done and K3 was chosen to be geological layer to examine.

The observation then is extended to see the permeability effect when it is altered from the original model (moderate low permeability). The very low permeability is chosen to be the new case to run radial model simulation. The comparison between the simulation results for both cases will be presented in the second part of this section.

Permeability effect in pressure, oil saturation and k_{rg} profile. K3 was arbitrarily chosen as the observed geological layer. The highest k layer was examined since it is the most important layer in the geological layer production history. The surrounding layers investigated are 2

layers upper and 2 layers below the highest k. Layer 65, 66, 67, 68 and 69 are observed after simulated for 17 years. The permeability of these layers are 1 md, 6 md, 907 md, 0.33 md and 12 md respectively. The observations are done for pressure, oil saturation and gas relative permeability profile.

Fig. 44 shows the oil saturation profile for those 5 layers. Layer 67 which is the highest k layer reaches the critical oil saturation first at the radius around 100 ft. Then it is followed by layer 66 and 69 (almost at the same radius), 65 and finally 68. This order is basically proportional to the order of the k value; the highest k has the highest oil saturation. Layer 67 is where almost all the gas in K3 is produced through, the more gas flowing in this layer leads the more oil condensed along its flow path so that in the 100 ft from the wellbore after 17 years simulation it has already reached S_{oc} where the condensate starts flowing from this radius to the wellbore. Layer 68 which has the lowest k needs longer flow path to have enough condensation to reach S_{oc} and it happens at the radius 5 ft from the wellbore. The interesting fact is that layer 66 (6 md) has the same radius as layer 69 (12 md) at when they reach S_{oc} .

The k_{rg} profile is shown in **Fig. 45**. Basically this figure is similar to oil saturation profile because the k_{rg} is strongly affected by the oil saturation. Once the oil saturation already reaches S_{oc} the k_{rg} will drop sharply and the gas will loss most of its mobility. Layer 67 is the first layer which has big drop of k_{rg} and layer 68 is the last one. **Fig. 43** tells us the profile of pressure in the five interest layers. The interesting observation is only at Region 1, the region after S_o already reaches S_{oc} or higher. At Region 2, where the condensate is immobile, the pressure profile is affected by gravity where the upper layer has lower pressure and so forth. The slope of pressure becomes sharper in Region 1 due to more k_{rg} loss. Layer 67 is the first layer which has sharp drop in pressure and finally layer 68 becomes the last one. Again, layer 66 gives interesting phenomenon. This layer should have sharp pressure drop since radius 24 ft, where its S_o is higher than S_{oc} , but in fact it has the first change in pressure slope at the around 100 ft where layer 67 starts having mobile condensate. To simplify the pressure profile of layer 66 we can divide it into 3 regions as below:

- Region A ($100 \text{ ft} < r < 4140 \text{ ft}$) : slow pressure drop (Region 2)
- Region B ($24 \text{ ft} < r < 100 \text{ ft}$) : quite sharp pressure slope (Region 2)
- Region C ($0.69 \text{ ft} < r < 24 \text{ ft}$) : sharp pressure drop (Region 1)

Region A and C are not interesting to discuss because these are exactly the same as Region 1 and 2 where have been well-discussed earlier. We suspect that there is significant cross-flow in Region B from layer 66 to 67. The cross flow causes more gas produced from layer 66 which lead to have higher pressure drop than it should be. The other impact is more condensate produced in this region which implies the increasing of oil saturation is faster and even faster than layer 69 which has absolute permeability two times higher. Eventually layer 66 reaches the S_{oc} at the same radius (24 ft) as layer 69. Layer 68 doesn't have pressure drop as big as layer 66 in Region B because it only has very low permeability (0.33 md) so the cross-flow from layer 68 to layer 67 is not so significantly seen compared to layer 66.

Low permeability effect. This part will discuss about the effect of altering permeability to some properties such as oil saturation, OGR, capillary number and gas rate. The original radial model used log normal permeability distribution. The permeability magnitude and the uniformity effects are tried to analyze for the next case. The sensitivity analysis study has been done in this thesis and discussed elsewhere in this report gives result that the distribution of permeability doesn't have significant contribution to the production history. Log normal distribution and uniform distribution where both have the same average permeability will have

almost the same simulation results. Due to that result in this part we didn't compare the original case to the uniform distribution case but we directly compare to the different magnitude of the permeability used. The quite extreme case is introduced which has permeability $\frac{1}{4}$ lower than original case. To simplify the model, the uniform permeability distribution in each geological layer is used. The comparison between average permeability between original and new models is presented in **Table 7**.

The very low permeability model (new model) is simulated for 50 years period and still using the BHP constraint at 2800 psia and gas well rate at 100 MMSCF/D. The observations are done for each geological layer since the very low model uses the uniform distribution so the numerical layer based observation becomes not relevant. The new observation is also done for original case to equalize what have been done in the very low case. For oil saturation and OGR we used average value in each geological layer, and then for calculating capillary number (N_c) we used total gas rate and the overall thickness of each geological layer. Both observations are done at the end of their plateau period, the difference is that original k model is evaluated at year 17 while the very low k model is observed at year 11 since it only has around 11 years plateau period. The comparisons of the simulation result of both models are depicted in **Fig. 46 - Fig. 50**.

Fig. 46 shows the comparison between two models in term of production gas contribution. The contributions of K1/K4 become smaller in the very low k model and inversely K2/K3 give bigger contribution when simulated in the very low k. The similar phenomenon is also found in term of capillary number as shown in **Fig. 47**. Since in the very low k model K2/K3 have more gas flowing then it leads those layers to have higher N_c , while K1/K4 have lower N_c due to production gas rate reduction in the very low model. The similarity trend between K1 and K4 is not surprising because basically those layers are almost identical both in reservoir description and fluids composition. The similar reason is given for K2 and K3.

OGR profile comparison for different permeability model is shown in **Fig. 48**. There are increasing OGR for all layers when simulated in the very low k model. K1, K2 and K3 have an increasing around 3 STB/MMSCF while K4 has a bit higher at 4 STB/MMSCF. **Fig. 49** depicts the similar trend when the average oil saturation of the first radial block from the wellbore is compared. All layers have higher S_o in the very low k model, the increasing of S_o is almost same for all layers at around 0.04. Since the very low k model has to produce the gas as much as the original model, the very low model will be forced to increase its pressure drop to compensate the lack of permeability. The higher pressure drop in the very low model will lead increasing of oil condensed in the formation or the higher oil saturation in the formation. If the plot of oil saturation vs. radius is developed then it will be seen that for the very low k model S_{oc} is reached farther (from the wellbore) than in original model. Or in other word Region 1 in the very low model is larger which means the condensate blockage effect becomes more important issue in the very low k system.

From the last two observations, once again, it is found that there is close relationship between the changing of OGR and S_o . The increasing in S_o will be followed by the increasing of producing OGR. If this phenomenon is correlated to the existence of Region 1 and 2 in the flow region development theory in gas condensate well there is an explanation as follows: producing OGR is basically proportional to p^* . From **Fig. 50** it is shown that the very low k model has lower BHP in all geological layers. Higher p^* and lower BHP means bigger pressure drop, and it gives more condensation or more oil saturation in Region 1.

5. Skin Factor Prediction

Skin factor is always associated to the reduction or improvement of well productivity. By convention if the skin factor is positive then it will be considered as the productivity reduction and inversely when it is negative then the improvement of well productivity is defined. There are some factors that could be included as the parameters which will give skin factor in the well deliverability calculation such as near-well bore damaged, vertical fracture and flow improvement due to horizontal well trajectory. Condensate blockage which only happens in the gas condensate well basically also gives reduction in term of well productivity or well deliverability. So by definition condensate blockage is also able to be included as the parameter which gives contribution in skin factor calculation. However, including the condensate blockage in radial model simulation which using fine grid model is not relevant because this radial model can capture the effect of condensate blockage in the simulation which means that the productivity loss due to condensate blockage is automatically included in the simulation. In the full field simulations where usually use coarse grid model the effect of condensate blockage becomes very difficult to capture since this effect only develops in the near well region. So in order the FFM being able to include this effect in the simulation then including this effect as a skin factor would be reasonable.

In this chapter the some procedures to predict the skin factor due to condensate blockage are demonstrated. In the first part the spreadsheet calculation is done to predict the “condensate blockage skin factor” in the radial simulation. The term skin factor here is predicted by comparing the gas rate of the gas condensate reservoir to dry gas rate which is free from condensate blockage effect. In the second part the effective skin factor is predicted to generate a representation of the condensate blockage effect in the full field model simulation.

5.1. Condensate skin factor prediction

Based on the theory proposed by Fevang and Whitson¹ as discussed earlier, the spreadsheet calculation becomes possible to use to predict the gas rate of any given time when GOR/OGR is known. This part will demonstrate how to use spreadsheet to predict the production gas rate for given OGR/GOR and the improvement of gas rate due to capillary number, and finally to compare the calculated gas rate to the dry gas rate which then gives an approximation of “condensate blockage skin factor”. The predicted skin factor basically will give description about how much well productivity will loose due to condensate blockage. The procedure has been applied in this work is detailed as follows:

1. Develop radial simulation model and run simulation
2. Pick up any time step from the simulation result
3. Collect data of gas rate, GOR, BHP and average p_R
4. Predict the exact p^* for given GOR from PVT properties used in the simulation
5. Select any pressure steps for Region 1 (p^* to BHP) and Region 2 and 3, if exists, from p_R to p^*
6. Determine all PVT properties for all pressure nodes such as B_o , B_{gd} , R_s , etc
7. Calculate the k_{rg}/k_{ro} using Eq. (6) for all pressure nodes in Region 1
8. By using plot k_{rg}/k_{ro} from relative permeability correlation (e.g. Corey-like), calculate $k_{rg} = f(k_{rg}/k_{ro})$ for Region 1 and for Region 2 as approximation it may use maximum k_{rg} from the correlation
9. Since all parameters are known the pseudopressure integral can be calculated using Eq. (4).

10. Calculate gas rate using Eq. (2)

To calculate the improved gas rate due to capillary number basically we just need to modify the k_{rg} using Eqs. (10) - (15) and as an approximation we can use correlation $p_i=f(\ln r_i)$ to estimate the radius of each pressure node. Unfortunately the trial and error procedure is required to calculate the gas rate which is dependent on capillary number. Skin factor due to condensate blockage is predicted by comparing the calculated dry gas rate to the gas rate calculated from procedure (10). Again it is required to do trial and error calculation to get skin factor which will give the modified dry gas equal to the simulated gas rate.

Two radial models are prepared as presented in **Table 8** to predict condensate blockage skin factor. We only developed two models since in our reservoir model K1 is similar to K4 as K2 to K3, by predicting for K3 and K4 these will have represented the whole Khuff formation. The example of the detail spreadsheet calculation is presented in **Appendix C**.

In the calculation has been done for both models we picked data which basically have similar OGR around 22.6 STB/MMSCF. The ranges of k_{rg}/k_{ro} in Region 1 from the calculation are shown in **Fig. 51** which are between 1-100 for both models. The spreadsheet calculations show that the predicted gas rate are very similar to the simulated gas rate which only have differences around 2% as presented in **Table 9**. These similarities give good evidence that basically the gas rate of radial model simulation can be reproduced using simple spreadsheet calculation without losing the accuracy.

The pseudopressure integral, or could be termed as gas mobility, vs. pressure in K3 model calculation is depicted in **Fig. 52**. There are 2 regions exist at the given OGR, Region 1 and 2. The gas mobility shown in this figure is calculated by using rock relative permeability correlation, and this result is then compared to other cases, which are calculated using rate dependent k_{rg} and dry gas equation, as shown in **Fig. 53**. The same comparison is done for K4 model and shown in **Fig. 54**.

From both comparisons above it is seen that by including the effect of capillary number can improve the gas mobility which then gives higher gas rate. In addition, these figures also show how big the condensate blockage reduces the well deliverability in both models are. The effect of condensate blockage is shown by the differences between gas mobility of dry gas and others or could be termed as condensate blockage skin factor. The gas rate comparison and correspond predicted skin factors are presented in **Table 10**. The condensate blockage at OGR 22.6 STB/MMSCF gives well productivity loss equivalent to skin factor of 20 and 27 for K3 and K4 respectively. When including capillary number effects then the skin factors reduce to 16 and 20. Capillary number only gives considered small improvement in production gas rate for both models, which is equivalent to the range of 4 - 6 skin factor, compared to the total well productivity loss due to blockage.

We might use these range of skin factor to describe the magnitude of condensate blockage effect in Khuff formation but to include this skin factor as a representation in coarse grid reservoir simulation is not so relevant because basically the condensate blockage will vary for varying producing OGR. To include the exact effect of condensate blockage in full field model simulation we need to repeat the calculation procedure to predict gas rate (including N_c if needed) for some given OGRs and then we use these results to develop a correlation table between OGR and gas rate which then could be included in the simulation dataset as a table similar to tubing performance table. But, when the simulation applies the real tubing performance table then it becomes not possible to incorporate the condensate blockage effect table. To solve this problem in the next part there will be a discussion about a term

called effective skin factor to represent condensate blockage effect in the full field model simulation.

5.2. Effective skin factor prediction

One alternative way to include the blockage effect in the full field model is by incorporating this effect to the skin factor which then termed by effective skin factor. Radial model with fine grid model simulation is able to capture the blockage effect, so to represent this effect in the FFM it just needs to match the FFM simulation to the radial simulation by putting the effective skin factor. As mentioned earlier that the radial model has been used in Chapter 4 is a representation of one production well in the FFM. By multiplying the production rate of the radial model by factor 20 basically this will be equal to the FFM simulation result which including condensate blockage effect. Then the matching is done by adjusting the effective skin factor put in the dataset of FFM until the simulation output is equal to 20 times radial simulation result. To get the effective skin factor which includes N_c effect in the FFM, the reservoir model that uses Corey-like exponent 1.5 is introduced. Finally there are 2 reservoir models used in this effective skin factor prediction, one has Corey-like exponent 3 and the other does 1.5. The simulations are done for 50 years and with BHP constraint at 2800 psia.

The plots used to perform the matching are gas production rate, condensate production rate, GOR, gas recovery and condensate recovery plots. We didn't only examine those plots in the field level but we also did in the regional level (geological layer level) K1, K2, K3 and K4. But due to these numerous plots examined then in this report we only display some of them. **Fig. 55 - Fig. 57** show the matching plots of exponent 3 model for some effective skin factors. Those figures show that the skin factor set of 17, 13, 15, and 12 for K1, K2, K3, and K4 respectively gives the best agreement to the radial model. For exponent 1.5 the uniform skin factor of 3 is the best skin factor set to match to the radial model as shown in **Fig. 58 - Fig. 60**.

To assure that the predicted skin factors are reliable for any others simulation case then the new reservoir models with including tubing performance table of 5.5" production tubing are simulated for both exponent 3 and 1.5 cases. The plots yielded from the matching procedure for both cases are depicted in **Fig. 61 - Fig. 64**. Those figures show good agreements between the radial model and the FFM which means that the predicted effective skin factor are also reliable for other reservoir simulation cases.

The very low permeability model ($\frac{1}{4}$ lower than the original permeability set) had significant effect specifically in the production plateau period. Hence the effective skin factors of lower permeability model are also predicted. The condensate blockage effect in extreme low permeability model is studied. The matching plots of this model are presented in **Fig. 65 - Fig. 68**. The predicted effective skin factors of exponent 3 are little bit different from the original permeability model. However, the exponent 1.5 gives the same result of 3, uniform for all layers. The summary of the results of the effective skin factor prediction is presented in **Table 11**.

Even though the predicted effective skin factors are different for the two permeability models but basically those differences are not so significant when compared to the magnitude difference of the permeability models. Four times lower in permeability but only gives skin factor difference at around 3 and in addition, for exponent 1.5 the predicted skin factors are exactly the same. These results give indication that the condensate blockage is not so sensitive to the permeability model but very sensitive to the effect of capillary number where the optimistic high capillary number effect, represented by exponent 1.5, can reduce the well deliverability loss due to condensate blockage equivalent to the effective skin factor of 12

(difference between skin factor exponent 3 and 1.5). From the observations done for North Field FFM effective skin prediction we might conclude that basically the magnitude of condensate blockage in this reservoir is equivalent to effective skin factor ranges from 3 (for optimistic case or high capillary number) to 15 (for pessimistic case or neglecting high capillary number effect).

The discussion of capillary number effect from the previous section gave indication that it only contributed small improvement to the well productivity loss due to blockage, while in this section the effect of capillary number is very significant. The different approximation to represent the capillary number is the reason for this difference. The correlation proposed by Whitson et al.² seems to give pessimistic capillary number effect in radial model simulation of North Field, while the Corey-like exponent 1.5 gives optimistic effect.

6. Sensitivity Analysis

This chapter intends to see the sensitivity of some parameters either in full field model or radial model simulation. The Corey-like exponent is studied since this parameter might be used to see the effect of capillary number in term of field productivity, while production tubing size basically tells its contribution to the total pressure drop from the formation to the surface. Permeability distribution effect has been discussed earlier but those are associated to the condensate blockage effect which is mainly only in the area near wellbore. In this chapter the effect of permeability is studied in term of fluids production rate and ultimate recovery for field level.

6.1. Corey-like equation exponent and Production Tubing size

This section discusses about the effect of Corey-like exponent used in the analytical relative permeability correlation and production tubing size. The North Field FFM which including effective skin factor is used in this sensitivity analysis and there are 4 cases to run as follows:

- A. Exponent 3 and Tubing size 5.5"
- B. Exponent 3 and Tubing size 7"
- C. Exponent 1.5 and Tubing size 5.5"
- D. Exponent 1.5 and Tubing size 7"

As mentioned earlier that exponent 3 is the original Corey-like exponent used in the FFM and 1.5 is an approximation of high capillary number model. Production tubing size of 5.5" and 7" are the sizes which have been used in the actual production well in North Field for North Field Alpha (NFA) Project and North Field Bravo (NFB) Project⁷. Including the production tubing in the simulation is done by putting additional tubing performance table in the dataset and for all cases tubing head pressure constraint (THP) at 2000 psia is applied.

Fig. 69 - Fig. 73 show the simulation results of all cases. From all figures it is shown that the exponent different is not sensitive for both tubing sizes used. **Fig. 69** shows that the gas rate of exponent 3 and 1.5 for the same tubing size almost don't have any difference or the difference is not significant. It means that the capillary number is not an issue in this reservoir model because it doesn't improve the field production rate so much. The production string of 7" gives additional plateau period of 4.5 years compared to 5.5" tubing as shown in **Fig. 69**. In term of recovery both sizes have the same ultimate recovery both in gas (44%) and condensate (34%), but the 7" case has better performance since it can give shorter period to reach the ultimate recovery.

6.2. Pressure Constraints and Tubing Size

In reservoir simulation there are two types of pressure constraint usually used: bottom hole pressure (BHP) and tubing head pressure (THP). In this part the effect those pressure constraint are studied and for THP constraint production tubing sizes of 7" and 5.5" are used. So the cases to be compared are:

- A. BHP at 2800 psia.
- B. THP at 2000 psia with 5.5" tubing.
- C. THP at 2000 psia with 7" tubing.

All cases then are run in the FFM with exponent 3 and including effective skin factor. The simulation results of those cases are depicted in **Fig. 75 - Fig. 80**.

The THP 5.5" 2000 psia tubing has plateau period of 14 years. BHP 2800 psia and THP 7" 2000 psia cases give almost the same gas production plateau period at around 18 years as shown in **Fig. 75**, but after the pressure constraint is reached then 7" tubing has better gas

rate. **Fig. 76** show the similar condition for condensate rate that after the plateau period is over THP 7" 2000 psia has better rate than BHP 2800 psia. In term of GOR as shown in **Fig. 77** the THP cases (7" and 5.5") have higher GOR after the plateau period compared than BHP case. Accordingly, as shown in **Fig. 78 - Fig. 79** THP cases give the ultimate recoveries of gas and condensate 4.5% and 3% higher respectively. **Fig. 80** explains the reason why BHP case has lower recovery, the average reservoir pressure in BHP case is still 250 psia higher than THP cases.

6.3. Permeability distribution

Permeability sensitivity is studied for radial model and full field model simulation. In radial model sensitivity analysis the log normal permeability distribution is compared to the uniform distribution and $\frac{1}{4}$ lower uniform permeability distribution. In the FFM only uniform distribution is used. The original permeability model is compared to $\frac{1}{4}$ lower permeability model. Different Corey-like exponent is also introduced in the FFM simulation.

6.3.1. Radial Model Simulation

The radial model used in this sensitivity analysis is exactly the same as the radial model discussed in Chapter 4. The cases to be compared are:

- A. Log normal permeability distribution
The original permeability set with log normal permeability distribution in each geological layer.
- B. Uniform permeability distribution
The uniform permeability distribution in each geological layer, which has exactly the same average permeability as the log normal distribution case.
- C. Lower permeability model
The $\frac{1}{4}$ lower permeability model which has uniform distribution in each geological layer.

BHP constraint at 2800 psia and well production rate of 100 MMSCF/D are used.

Fig. 81 - Fig. 86 show the simulation results comparison between all cases. For the original permeability set, log normal distribution case practically has the same simulation result as the uniform permeability case. All figures show the agreement between those permeability distributions. This means that the permeability distribution is not so important in the gas condensate reservoir. But the magnitude of the permeability is an issue in this case because when the permeability is reduced until $\frac{1}{4}$ lower the plateau period becomes 7 years shorter than the original set as shown in **Fig. 81**. As shown in **Fig. 83** the very low permeability model gives higher GOR or lower OGR than the original permeability set mainly in the plateau period, it indicates that this case has more condensate left in the formation since it has bigger pressure to compensate the low permeability which will give more condensation in the formation. The very low permeability model is slower to produce both gas and oil than the original one but they have the same ultimate recovery as shown in **Fig. 84 - Fig. 85**. The consequence of faster recovering is that the original permeability cases have lower average pressure than the very low case as shown in **Fig. 86** particularly just after reaching the pressure constraint, but eventually all cases have the same average reservoir pressure.

6.3.2. Full Field Model Simulation

The FFM with including effective skin factor is used to study the sensitivity of permeability and Corey-like exponent. The cases to be compared are:

- A. Exponent 3 and Original permeability model
- B. Exponent 3 and Original permeability model
- C. Exponent 1.5 and Lower permeability model
- D. Exponent 1.5 and Lower permeability model

The simulation results of those cases are shown in **Fig. 87 - Fig. 92**.

The different results between the original and the very low permeability model are not surprising and it has been discussed in the previous sensitivity analysis for radial model. The more interesting fact to discuss is the difference between exponent 3 and 1.5 is bigger in the very low permeability model. As concluded from the previous chapter that different permeability is not as issue in condensate blockage phenomenon because both original permeability model and very low model have predicted effective skin factor 3 for exponent 1.5 and 15 for exponent 3. The gas rate equation, as described in Eqs. (2) - (3), explains that the gas rate is proportional to absolute permeability and inversely proportional to skin factor. The skin factor difference between exponent 3 and 1.5, which is equal to 12, will have bigger impact to the lower absolute permeability in term of production gas rate. It means that the high N_c case which is represented by exponent 1.5 gives better improvement in gas rate than in exponent 3 and it leads the additional plateau period in exponent 1.5 is longer than in exponent 3 as shown in **Fig. 87**. The bigger differences in other figures basically are related to the better gas rate improvement in the very low permeability model.

7. Petroleum Stream Management

Reservoir simulation produces hundreds or thousands or even millions streams where each stream contains the quantity of the reservoir fluids either in black oil or compositional description. The streams produced from simulation will be much more numerous when the simulation uses the complicated reservoir model such as including multiple reservoirs description, using single reservoir description but there are many regions or sub-regions in this reservoir, and etc. Usually the streams resulted from simulator are generated in the simulation output file. Having defined the regions or sub-regions in the simulation dataset leads the reservoir simulator to be able to generate the streams of any well connections (perforated blocks), sub-regions, regions, well or field levels. Some difficulties might come up when it is desired to filter some streams with quite complicated specification, for instance the streams of some production wells which are the contribution of particular region. We might use the North Field FFM to give real example. This reservoir model has specified 4 regions to represent the geological layer K1, K2, K3 and K4. Each region is defined by connecting the corresponding numerical layers to each geological layer. In the simulation output file the streams of each region is clearly presented in all specified time steps, so it readily shows how much the gas production rate of Region K1 at any time step is. However, when it is desired to get information about how much gas production rate of well P-0203 which is produced from K1 is then the simulation output file can not give immediate data. The extra filtering procedure is needed to do to get such information. Moreover, the extra work will be more complicated when the field has complex production line structure such as subsea manifolds (which cover some production wells), surface manifold (which covers some subsea manifolds), and etc. Obtaining information how much gas rate of a given subsea manifold which is produced from Region K1 becomes really need an extra time-consuming work.

There are some others issue, besides **filtering**, in the petroleum streams management which are basically beyond the ability of reservoir simulator to handle. Those issues are **aggregation**, **averaging**, and **optimization**. Hoda in his dr.ing. thesis¹⁴ explained about the engineering of petroleum streams including discussion about those important issues except optimization. This thesis has studied about three out of four main issues in the petroleum stream management. Streams management procedure including filtering, aggregation, and averaging operations are developed for the North Field FFM to give the early step of complicated work of petroleum streams management in such huge gas condensate reservoir which will be basically dealing with millions of streams if the whole North Field reservoir is modeled.

7.1. Petroleum streams management in North Field

Petroleum streams management mainly consists of 4 main issues as discussed earlier: averaging, filtering, aggregation and optimization. Petroleum streams used in this streams management usually are produced from reservoir simulation but these may be collected from the real field stream data. The streams generated from the reservoir simulation are used in this thesis to develop a petroleum streams management procedure in North Field or specifically in one block concession of North Field.

The study of petroleum management in this thesis is based on the ability of streams management software developed by PERA a/s. called PetroStream Management (*PSM*) which has internal “engine” software developed by Zick Technologies named *Streamz* to handle some streams operations such as filtering or aggregation. The FFM with effective skin factor is used to run the simulation to generate the streams. The procedure of streams management

proposed in this thesis basically includes the main operations (filtering, averaging and aggregation). Optimization operation is not performed in this thesis but discussed as a part of petroleum streams management procedure so then this operation is recommended to do in the next step of the streams management in North Field following this thesis work.

The main idea to develop stream management in North Field is that the limitation of reservoir simulation to satisfy complicated production constraints which might exist in such huge gas condensate reservoir. To satisfy some production constraints such as field plateau rates, well rates or well bottom hole pressure the reservoir simulation is still able to handle, but when the constraints is growing to the specific and complicated constraints such as maximum H₂S contents or minimum heating value of produced gas then the simulator might have some limitations to do so.

The first step to develop petroleum streams management is setting up the complete production aggregation level from the lowest up to the highest level in our production line structure. This thesis proposes a simple production line structure from the well connection level to the surface process level, the schematic of this structure is presented in **Fig. 93 - Fig. 95**. The production line structure from well connection to well level is shown in **Fig. 93** and then from the well connection (in this case represented by geological layers) up to the sub sea manifold is depicted in **Fig. 94**. **Fig. 95** shows the higher level from well level to the surface process as the highest level. From these three figures we can get clear description about the production nodes in each aggregation level. The production node is basically the node where it has petroleum streams either black oil or compositional streams.

The second step is running the North Field FFM simulation to produce streams for the well connections level, well level, and field level. In the simulation dataset some regions which are related to the geological layers (K1, K2, K3, and K4) have been introduced to get streams based on those regions. But unfortunately in the simulation output files those streams can not be used directly to give detail description about the regional contribution in the well level because those streams are based on field level, which means that the produced streams are the streams produced from given region in the whole reservoir.

The third step is completing all production nodes of the developed production line structure as described in **Fig. 93 - Fig. 95** with its the petroleum streams. So far what we have had are the petroleum streams produced from the reservoir simulation. From *Sensor* we have well connections streams, well streams and field streams. But to get the streams in Subsea manifold and Surface manifold level, the filtering and aggregation operations are needed to apply. The additional filtering operation has to perform when we want to put regional contribution in each production line level (e.g. the gas rate in well P-0203 which is produced from K1). Finally what produced from this third step are the streams of all developed production line structure which include the regional contribution streams.

The fluids rate in the database streams generated from the third step is still similar to what have been produced by the simulation. It means that those streams have flow rate at every time step as used in the simulation. Then *the forth step* is done by performing aggregation and averaging operations in the streams database generated from the previous step to get average flow rate in a given time period (e.g. average flow rate of H₂S in the first month of the simulation period). This procedure is very useful to give the description of the average production when the production rate is highly varied for given period.

The fifth step is determining how many constraints (with its constraint value) needed during the reservoir production life and in which production nodes those constraints are applied. There are some constraints which might be applied for North Field such as:

1. Field gas plateau rate.
2. Gas sales rate.
3. H₂S contents of produced gas.
4. Heating value of produced gas.
5. Water production rate.

The final step is performing optimization based on the streams of all the production nodes to satisfy the developed constraints. This final step is probably the most difficult and complicated step during applying the petroleum streams management of North Field.

The procedure from the first until the fourth steps have been done in this thesis but the last two steps which are mainly dominated by optimization operation are not done yet. Those four steps will be discussed further in the following part.

7.2. Generating streams database of North Field

The first step of the petroleum streams management has been discussed and done earlier. **Fig. 93 - Fig. 95** are the result of this step. The second step has a sequence work as presented in **Fig. 96**. The FFM simulation which has been run to generate the streams is a compositional simulation and accordingly gives the compositional streams in well connection level, well level and field level. The output streams from *Sensor* have different format with the streams file could be read by *PSM*. Then the format conversion needs to perform in this second step, this operation is handled by one feature in *PSM* called *Sen2Str*. The result of this step is the big streams file (termed as Main Stream File) which contains all the streams information of each well connection of all production wells of the North Field FFM for all time steps. In the well connection level stream there is additional data about the pressure of each individual perforated grid block.

In this section, the third and fourth steps are demonstrated, **Fig. 97 - Fig. 102** show the sequences used in *PSM* to generate streams database of North Field FFM including the average flow rate for monthly based. The Main stream file generated from the second step is the main source to generate the streams in all production nodes. **Fig. 97** explains the sequence to generate the streams in well level. The Main stream file is being filtered based on a given well name to get only the streams related to this well name. All of these streams then are copied in the well stream file which means that all information from the Main stream file are saved including the pressure of each perforated block of the given well name. The pressure needs to keep because it becomes important data when we want to convert the streams into volumetric rate format which is dealing with formation volume factor dependent on pressure. The well stream file has the stream rate for every time step used in the simulation, to get average stream rate these streams needs to be aggregated for some time period and the divided by that time period. The time period used in this thesis is monthly basis. The well stream file then is tabulated into monthly time step by aggregating the streams in each monthly time step, afterward the averaging is done for those monthly basis streams to get average stream rate in the given well name. The final result of this well sequence is the average well stream file which contains the average streams rate of all 24 components in monthly time step for given well name. This sequence is repeated for some other production wells in the North Field production line structure.

Fig. 98 tells the similar sequence as described earlier for the subsea manifold level. As shown in **Fig. 94** that one subsea manifold covers five production wells which mean that the streams of one subsea manifold are the aggregation of the streams of the five wells covered by. Again, as the starting point, the Main stream file is being filtered based on the five given

wells name which are covered by the given subsea manifold. The filtered streams are stored in the subsea manifold streams file. The same tabulating and averaging operations as applied in well sequence are done to get the average subsea manifold stream file which contains the average streams rate of all 24 components in monthly time step for given subsea manifold name. This sequence is repeated for three other subsea manifolds in the North Field production line structure.

The slight different sequence is developed for generating the streams of surface manifold. Since the surface manifold is exactly the same as the field level then the filtering is not needed to perform. **Fig. 99** shows the sequence used in this case. The Main stream file is only tabulated into the daily time step instead of being filtered, and then saved into surface manifold stream file. The same tabulating and averaging operations as applied in well sequence are done to get the average surface manifold stream file which contains the average streams rate of all 24 components in monthly time step for given surface manifold name.

Fig. 100 shows the sequence to generate the regional contribution streams for given production well name. This procedure uses the well stream file, which is produced from the filtering step in the well streams generation procedure, as the source stream file. The well stream file is being filtered based on a given geological layer name and then tabulated into daily time step. The result of this step is stored in well layer stream file. The same tabulating and averaging operations as applied in the well streams generation procedure are done to get the average regional well stream file (average well layer stream file) which contains the average streams rate of all 24 components in monthly time step for given geological layer and well name. The daily tabulating, monthly tabulating and averaging operations are repeated to generate the same well layer stream file and average well layer stream file for different regional contribution (e.g. K2, K3 or K4). The whole sequence is again repeated for some other production wells in the North Field production line structure. The similar sequence as shown in **Fig. 101** is developed for subsea manifold level to generate the regional contribution stream file and average stream file. For surface manifold the developed sequence is depicted in **Fig. 102** which is similar to the sequence applied in the well and subsea manifold level.

Having done all the sequences as explained above then the streams database of the developed production line structure in North Field FFM is completed. All the production nodes have own compositional streams description both in actual rate (as produced from the simulation) and average rate based on monthly time step. In addition, the regional contribution streams rates from all geological layers are also ready for all production nodes in both actual rate and average rate.

7.3. Some applications in streams database

There are many possibilities to do after getting the streams database of a production line structure. The most common and important further step to follow the generation of streams database is by conducting the optimization to satisfy some production constraints as explained at the earlier section. Since in this thesis the optimization is not performed than the advantages of having streams database related to the optimization step can not be presented. However, there are still some other applications to do to use this streams database to describe the result of the North Field FFM simulation. This section demonstrates how easy to make analysis in any production nodes after the streams database is completed.

Supposed we want to have description about how much methane and H₂S are produced from well P-1003 and also how much the regional contribution rates for those components in the same production well are. The streams database easily gives those expected plots as shown

in **Fig. 103 - Fig. 104**. The methane (C_1) molar rates for the whole simulation period are presented in four different plots; one is the total rate in P-1003 and the others are regional contribution rate from K1, K2, K3 and K4. **Fig. 104** tells the same plots for H_2S molar rate. From those figures it is found that the C_1 production rate in well P-1003 is dominated by the C_1 rate from K4, while for H_2S production rate K2 gives the biggest contribution for the total H_2S well rate. So when the production constraint used in the optimization is the maximum H_2S contents of the produced gas then the production rate from both K2 and K3 need to be controlled carefully. **Fig. 105** shows the molar rate of some heavy components ($C_6 - C_{10}$) in well P-1003, it shows that C_7 gives the highest rate compared than the others. Those heavy components molar rate from Region K4 are plotted in **Fig. 106**. The orders of those components molar rate are still the same for both total well rate and regional rate which give C_7 as the highest production rate.

The total rate and regional rate of methane and H_2S in subsea manifold (SSM) A are depicted in **Fig. 107 - Fig. 108**. K2 and K3 are still the regions which give the biggest contribution in H_2S production rate while K4 which has the thickest formation still gives the biggest methane production rate in SSM A. Some heavy components production rates are plotted in **Fig. 109**. **Fig. 110** gives regional molar rate contribution of those components from Region K4. Both figures basically have the similar result in term of the rate contribution of individual components where C_7 has the highest production rate. **Fig. 111 - Fig. 114** show the similar observation results, as yielded in SSM A, for surface manifold (SFM). From the similarity of the observations done for well level, SSM level and SFM level then we might conclude that the uniformity model set for each geological layer (i.e. permeability, porosity, fluids composition) and the uniformity of the plateau well rate and well completion for all production wells lead the streams rate in all the production nodes have the similar trends almost for all cases. K2 and K3 which has initial H_2S content higher than K1/K4 give the biggest contribution of H_2S production rate in all production line nodes.

8. Conclusions

Condensate blockage phenomenon in North Field and Petroleum Streams Management have been studied and based on these works there are some conclusions can be drawn as follows:

1. Radial model simulation can give description about blockage phenomenon around the wellbore. Almost in the whole production history of North Field only Regions 1 and 2 are developed.
2. The region near the well (Region 1), where both gas and condensate are flowing, is the most important region in gas condensate reservoir simulation since it strongly affects the well deliverability.
3. The $k_{rg}(k_{rg}/k_{ro})$ and $k_{rg}/k_{ro}(p)$ are the key correlations to observe the condensate blockage phenomenon in Region 1. The ratio k_{rg}/k_{ro} in North Field ranges from 1 - 100 during the reservoir production life.
4. There are strong correlations between the permeability distribution, oil saturation and OGR profile. The very low permeability model gives higher oil saturation and OGR.
5. Spreadsheet calculation can reproduce accurately the production gas rate of radial model simulation when OGR data are given. The condensate blockage skin factor is also can be predicted by this calculation.
6. The condensate blockage near-well phenomenon might be captured in the full field model by including the predicted effective skin factor. The range of this skin factor is from 3 – 15 and independent the permeability distribution.
7. In the moderate low permeability model the capillary number effect is not so significant to improve the production gas rate. In the very low permeability model (1/4 lower than the moderate low model), the capillary number effect becomes more significant and hence lengthens the plateau period.
8. The BHP constraint at 2800 psia and the 7" THP constraint at 2000 psia have almost the same plateau period at 18 years but the THP constraint has higher ultimate recovery both for gas and condensate. The 5.5" THP constraint at 2000 psia give 4 years shorter plateau period that the 7" one but both have almost the same ultimate recovery.
9. There is almost no difference between the simulation result of log normal and uniform permeability distribution.
10. Petroleum streams management gives a streams database which contains complete description of the compositional streams in all production line nodes including the regional contribution for both production rate and monthly average production rate.

Nomenclature

Δp_p	=	total pseudopressure, psi/cp
B_{gd}	=	dry gas formation volume factor
BHP	=	bottom hole flowing pressure, psia or pa
BIP	=	binary interaction parameter
B_o	=	oil formation volume factor
C	=	gas rate constant
CCE	=	Constant Composition Expansion experiment
CVD	=	Constant Volume Depletion experiment
D	=	day
DX	=	length of grid blocks respect to x-axis
DY	=	length of grid blocks respect to y-axis
DZ	=	height of grid blocks
EOS	=	equation of state
$EOS24$	=	the equation of state model developed for North Field
f_i	=	immiscibility factor
FVF	=	formation volume factor
$GASREC$	=	gas recovery, %
GOR	=	gas oil ratio, SCF/STB
h	=	formation thickness, ft or m
k	=	absolute permeability, md
k_{rg}^o	=	gas relative permeability at S_{wi}
k_{rg}	=	gas relative permeability
k_{rgI}	=	immiscible gas relative permeability
k_{rgM}	=	miscible gas relative permeability
k_{rgro}	=	relative permeability of gas at $S_w=S_{wi}$, $S_o=S_{org}$
k_{ro}	=	oil relative permeability
k_{rocw}	=	relative permeability of oil at $S_w=S_{wi}$, $S_g=0$
k_{rwro}	=	relative permeability of water at $S_w=1-S_{orw}$, $S_g=0$
k_x	=	horizontal permeability respect to x-axis
k_y	=	horizontal permeability respect to y-axis
k_z	=	vertical permeability
md	=	mili Darcy
M_g	=	gas molecular weight
$MMSCF$	=	million standard cubic feet
$MMSTB$	=	million stock tank barrels
M_o	=	oil molecular weight
$MSCF$	=	thousand standard cubic feet
$MSTB$	=	thousand stock tank barrels
N_c	=	capillary number
N_{cg}	=	capillary number based on gas velocity
n_w, n_{ow}, n_g, n_{og}	=	exponents for analytical k_r
OGR	=	oil gas ratio, STB/MMSCF
$OILREC$	=	condensate recovery, %
p^*	=	pressure at outer boundary of Region 1, psia or Pa
$PAVGHC$	=	hydrocarbon pore volume average pressure, psia
PBH	=	well bottom hole pressure, psia

P_c	=	capillary pressure
P_c	=	critical pressure
P_{chor}	=	parachor
p_d	=	dew point pressure, psia or Pa
PI	=	productivity index
p_R	=	average reservoir pressure
p_{SC}	=	standard condition pressure, 1 atm
PSM	=	PetroStream Management software
P_v	=	viscous (Dracy) pressure drop
p_{wf}	=	well flowing pressure
q_g	=	surface gas rate, SCF/D
R	=	gas constant
RB	=	reservoir barrels
r_e	=	outer drainage radius, ft
R_p	=	producing GOR, SCF/STB
R_s	=	solution GOR, SCF/STB
r_s	=	solution OGR, STB/SCF
r_w	=	well radius, ft
s	=	dimensionless volume translation, skin factor
SCF	=	standard cubic feet
S_{gc}	=	critical gas saturation
S_{oc}	=	critical oil saturation = S_{org}
S_{org}	=	residual oil saturation to gas
S_{orw}	=	residual oil saturation to water
SRK	=	Soave-Redlich-Kwong
STB	=	stock tank barrels
S_{wi}	=	irreducible water saturation
T_b	=	boiling point temperature
T_c	=	critical temperature
THP	=	tubing head pressure, psia or pa
T_{SC}	=	standard condition temperature, 60 F
V_d	=	dewpoint volume, ft ³ or m ³
v_g	=	Darcy gas velocity
V_o	=	CVD oil relative volume, V_o/V_d
v_p	=	pore velocity
v_{pg}	=	pore gas velocity
V_{ro}	=	CCE oil relative volume, $V_o/(V_g+V_o)$
V_{ro}	=	CVD oil relative volume, V_o/V_d
y_i	=	molar fraction of component i
Z_c	=	critical Z-factor
z_i	=	mole fraction of the ith fraction or component
α	=	scaling parameter for N_c
β_{SC}	=	surface gas mole fraction in wellstream
ρ_g	=	gas density, lb/cuft or kg/m ³
ρ_o	=	oil density, lb/cuft or kg/m ³
σ_{go}	=	interfacial tension (IFT)
ω	=	acentric factor

$\Omega a, \Omega b$ = constant in cubic EOS
 ϕ = porosity
 μ_g = gas viscosity, cp
 μ_o = oil viscosity, cp

References

1. Fevang, Ø., and Whitson, C.H.: "Modeling Gas Condensate Well Deliverability" paper SPE 30714 presented at the SPE Annual Technical Conference & Exhibition held in Dallas, U.S.A., 22-25 October, 1995.
2. Whitson, C.H., Fevang, Ø., Sævareid, A.: "Gas Condensate Relative Permeability for Well Calculations" *Transport in Porous Media* 52: 279–311, 2003.
3. Kuntadi, A.: North Field Qatar: Fluids Characterization and Reservoir Modeling, Semester Project Report, Dept. of Petroleum Engineering and Applied Geophysics, Norwegian University of Science and Technology (NTNU), (Dec 2003).
4. Whitson, C.H. and Fevang, Ø.: "Generalized Pseudopressure Well Treatment in Reservoir Simulation" in Proc. IBC Conference on Optimization of Gas Condensate Fields, 1997.
5. Mott, R.: "Engineering Calculations of Gas Condensate Well Productivity" paper SPE 77551 presented at the SPE Annual Technical Conference & Exhibition held in San Antonio, Texas, 29 September-2 October, 2002.
6. Almarr, J.A, and Al-Saadoon, F.T.: "Prediction of Liquid Hydrocarbon Recovery from a Gas Condensate Reservoir", paper SPE 13715 presented at the SPE 1985 Middle East Oil Technical Conference and Exhibition held in Bahrain, March 11-14.
7. Martin, B.L., III: " 7" Monobore Completion Design for Qatar's Offshore North Field", paper SPE/IADC 39272 presented at the 1997 SPE/IADC Middle East Drilling Technology Conference held in Bahrain, November 23-25.
8. Al-Shiddiqi, A., Dawe, R.A.: "Qatar's Oil and Gas Reservoirs" (2003).
9. Al-Maslamani, M.: "Performance of (UNS 8028) Production Tubing Material in Sour Service Environment of Khuff Gas Formation", paper SPE 29785 presented at the SPE 1995 Middle East Oil Show held in Bahrain, March 11-14.
10. Khalaf, A.S.: "Prediction of Flow Units of The Khuff Gas Formation", paper SPE 37739 presented at the SPE 1997 Middle East Oil Show held in Bahrain, March 15-18.
11. Martin Jr., T.B., McKinnell, D., Labrugere, P., Besson, A.: "Optimization of Bit Performance for Qatar's Offshore North Field", paper SPE 39253 presented at the 1997 SPE/IADC Middle East Drilling Technology Conference held in Bahrain, November 23-25.
12. The U.S. Energy Administration Information: "Qatar, A Country Analysis Briefs" (November 2003).
13. Whitson, C.H., and Brule, M.R.: Phase Behavior, SPE Monograph Volume 20, Henry L. Doherty Series (2000).
14. Hoda, M.F.: The Engineering of Petroleum Streams, Dr. Ing Thesis, Dept. of Petroleum Engineering and Applied Geophysics, NTNU, (June 2002).
15. Whitson, C.H.: Petroleum Engineering Fluid Properties Data Book, Dept. of Petroleum Engineering and Applied Geophysics, NTNU, (May 1994).
16. Coats Engineering, Inc.: Sensor Manual (March 2001).
17. Zick, A.A.: "PhazeComp: Zick Technologies' program for compositional phase behavior computations using equation of state (EOS)" (2003)
18. Coats Engineering, Inc.: SensorPlot Manual (March 2001).
19. TotalFinaElf: " SOUTH PARS: A giant gas field off the Iranian coast ", a project description from www.total.com (2003).
20. Hoda, M.F.: PetroStream Management - Getting Started with PSM Toolkit, Pera a/s. (June 2001).

Tables

Table 1 – FINAL SRK EOS CHARACTERIZATION FOR K4 FORMATION FLUID (EOS 24)											
Comp	M	Tc	Pc	ω	s	Tb	γ	Zc	Pchor	Ω_a	Ω_b
		R	psia			R					
N2	28.01	227.16	492.84	0.0370	-0.0009	139.41	0.2724	0.2918	59.10	0.4275	0.0866
CO2	44.01	547.42	1069.5	0.2250	0.2175	333.32	0.7510	0.2743	80.00	0.4275	0.0866
H2S	34.08	672.12	1300	0.0900	0.1015	382.35	0.8085	0.2829	80.10	0.4275	0.0866
C1	16.04	343.01	667.03	0.0110	-0.0025	201.57	0.1398	0.2862	71.00	0.4275	0.0866
C2	30.07	549.58	706.62	0.0990	0.0589	332.71	0.3101	0.2792	111.00	0.4275	0.0866
C3	44.10	665.69	616.12	0.1520	0.0908	416.24	0.4990	0.2763	151.00	0.4275	0.0866
i-C4	58.12	734.13	527.94	0.1860	0.1095	471.08	0.5726	0.2820	188.80	0.4275	0.0866
n-C4	58.12	765.22	550.56	0.2000	0.1103	491.14	0.5925	0.2739	191.00	0.4275	0.0866
i-C5	72.15	828.7	490.37	0.2290	0.0977	542.37	0.6312	0.2723	227.40	0.4275	0.0866
n-C5	72.15	845.46	488.78	0.2520	0.1195	557.04	0.6375	0.2684	231.00	0.4275	0.0866
C6	82.32	924.21	491.32	0.2373	0.1341	606.17	0.7036	0.2703	232.57	0.4275	0.0866
C7	95.36	988.34	457.18	0.2714	0.1429	658.66	0.7367	0.2659	263.86	0.4275	0.0866
C8	108.77	1043.9	422.82	0.3094	0.1522	707.45	0.7594	0.2614	296.05	0.4275	0.0866
C9	121.90	1094.1	389.97	0.3500	0.1697	754.04	0.7761	0.2571	327.55	0.4275	0.0866
C10	134.78	1138.6	361.66	0.3900	0.1862	796.85	0.7896	0.2533	358.48	0.4275	0.0866
C11	147.59	1178.9	336.95	0.4295	0.2018	836.84	0.8009	0.2499	389.21	0.4275	0.0866
C12	160.30	1215.6	315.31	0.4684	0.2165	874.32	0.8107	0.2466	419.72	0.4275	0.0866
C13	172.91	1249.4	296.27	0.5067	0.2302	909.51	0.8193	0.2435	449.99	0.4275	0.0866
C14	185.42	1280.6	279.43	0.5444	0.2430	942.65	0.8270	0.2406	480.01	0.4275	0.0866
C15	197.82	1309.5	264.48	0.5814	0.2548	973.9	0.8340	0.2377	509.77	0.4275	0.0866
C16	210.11	1336.3	251.14	0.6178	0.2657	1003.4	0.8404	0.2349	539.27	0.4275	0.0866
C17-19	233.39	1383.1	229.29	0.6857	0.2843	1055.8	0.8513	0.2298	595.13	0.4275	0.0866
C20-29	299.51	1493.7	184.6	0.8712	0.3239	1183.8	0.8764	0.2161	753.83	0.4275	0.0866
C30+	477.34	1616.9	167.56	1.0411	0.1154	1309.7	0.9215	0.2058	1180.62	0.4275	0.0866

Comp	N2	CO2	H2S	C1	C2	C3	i-C4	n-C4	i-C5	n-C5	C6	C7
N2	0	0	0.12	0.02	0.06	0.08	0.08	0.08	0.08	0.08	0.08	0.08
CO2	0	0	0.12	0.12	0.15	0.15	0.15	0.15	0.15	0.15	0.15	0.15
H2S	0.12	0.12	0	0.07	0.06	0.06	0.06	0.06	0.06	0.06	0.05	0.03
C1	0.02	0.12	0.07	0	0	0	0	0	0	0	0	0
C2	0.06	0.15	0.06	0	0	0	0	0	0	0	0	0
C3	0.08	0.15	0.06	0	0	0	0	0	0	0	0	0
i-C4	0.08	0.15	0.06	0	0	0	0	0	0	0	0	0
n-C4	0.08	0.15	0.06	0	0	0	0	0	0	0	0	0
i-C5	0.08	0.15	0.06	0	0	0	0	0	0	0	0	0
n-C5	0.08	0.15	0.06	0	0	0	0	0	0	0	0	0
C6	0.08	0.15	0.05	0	0	0	0	0	0	0	0	0
C7	0.08	0.15	0.03	0	0	0	0	0	0	0	0	0
C8	0.08	0.15	0.03	0	0	0	0	0	0	0	0	0
C9	0.08	0.15	0.03	0	0	0	0	0	0	0	0	0
C10	0.08	0.15	0.03	0	0	0	0	0	0	0	0	0
C11	0.08	0.15	0.03	0	0	0	0	0	0	0	0	0
C12	0.08	0.15	0.03	0	0	0	0	0	0	0	0	0
C13	0.08	0.15	0.03	0	0	0	0	0	0	0	0	0
C14	0.08	0.15	0.03	0	0	0	0	0	0	0	0	0
C15	0.08	0.15	0.03	0	0	0	0	0	0	0	0	0
C16	0.08	0.15	0.03	0	0	0	0	0	0	0	0	0
C17-19	0.08	0.15	0.03	0	0	0	0	0	0	0	0	0
C20-29	0.08	0.15	0.03	0	0	0	0	0	0	0	0	0
C30+	0.08	0.15	0.03	0.06887	0	0	0	0	0	0	0	0

Comp	C8	C9	C10	C11	C12	C13	C14	C15	C16	C17-19	C20-29	C30+
N2	0.08	0.08	0.08	0.08	0.08	0.08	0.08	0.08	0.08	0.08	0.08	0.08
CO2	0.15	0.15	0.15	0.15	0.15	0.15	0.15	0.15	0.15	0.15	0.15	0.15
H2S	0.03	0.03	0.03	0.03	0.03	0.03	0.03	0.03	0.03	0.03	0.03	0.03
C1	0	0	0	0	0	0	0	0	0	0	0	0.06887
C2	0	0	0	0	0	0	0	0	0	0	0	0
C3	0	0	0	0	0	0	0	0	0	0	0	0
i-C4	0	0	0	0	0	0	0	0	0	0	0	0
n-C4	0	0	0	0	0	0	0	0	0	0	0	0
i-C5	0	0	0	0	0	0	0	0	0	0	0	0
n-C5	0	0	0	0	0	0	0	0	0	0	0	0
C6	0	0	0	0	0	0	0	0	0	0	0	0
C7	0	0	0	0	0	0	0	0	0	0	0	0
C8	0	0	0	0	0	0	0	0	0	0	0	0
C9	0	0	0	0	0	0	0	0	0	0	0	0
C10	0	0	0	0	0	0	0	0	0	0	0	0
C11	0	0	0	0	0	0	0	0	0	0	0	0
C12	0	0	0	0	0	0	0	0	0	0	0	0
C13	0	0	0	0	0	0	0	0	0	0	0	0
C14	0	0	0	0	0	0	0	0	0	0	0	0
C15	0	0	0	0	0	0	0	0	0	0	0	0
C16	0	0	0	0	0	0	0	0	0	0	0	0
C17-19	0	0	0	0	0	0	0	0	0	0	0	0
C20-29	0	0	0	0	0	0	0	0	0	0	0	0
C30+	0	0	0	0	0	0	0	0	0	0	0	0

Table 3 – CALCULATED INITIAL GAS COMPOSITION OF KHUFF FORMATION		
Component	K1/K4	K2/K3
	%mol	%mol
N2	3.35	3.35
CO2	1.76	1.76
H2S	0.53	3.03
C1	83.27	80.77
C2	5.16	5.16
C3	1.91	1.91
i-C4	0.41	0.41
n-C4	0.70	0.70
i-C5	0.28	0.28
n-C5	0.28	0.28
C6	0.39	0.39
C7	0.49	0.49
C8	0.36	0.36
C9	0.27	0.27
C10	0.20	0.20
C11	0.15	0.15
C12	0.12	0.12
C13	0.09	0.09
C14	0.07	0.07
C15	0.05	0.05
C16	0.04	0.04
C17-19	0.07	0.07
C20-29	0.06	0.06
C30+	0.01	0.01
TOTAL	100.00	100.00

Table 4 – FULL FIELD RESERVOIR MODEL DESCRIPTION			
<u>GEOMETRY</u>			
Surface Area		10 km x 10 km	
Gridding of Cartesian Model		20 x 20 x 17	
Size of total reservoir, cuft		32808 x 32808 x 1721	
DX = DY, ft		1640 (500 m)	
Depth to top of formation, ft		8050	
<u>ROCK AND FLUIDS PROPERTIES</u>			
Porosity K1/K4		10 %	
K2/K3		15 %	
Permeability	<u>Layer</u>	<u>kx=ky, md</u>	<u>kz, md</u>
	K1	15	1.5
	K2	45	4.5
	K3	45	4.5
	K4	15	1.5
Rock Compressibility, 1/psi		5.0E-06	
Reservoir Temperature, F		220	
Water compressibility, 1/psi		2.64E-06	
Water FVF, RB/STB		1.0375	
Water density, lbs/cuft		62.37	
Water viscosity, cP		0.65	
<u>INITIAL CONDITION</u>			
<u>K4 Layer</u>			
Initial Pressure, psig		5300	
Reference Depth, ft		9600	
Dew point pressure, psig		5120	
<u>K3 Layer</u>			
Initial Pressure, psig		5180	
Reference Depth, ft		8500	
Dew point pressure, psig		4930	
<u>RELATIVE PERMEABILITY ANALYTICAL DATA</u>			
Connate water saturation (Swi)		0.2	
Residual oil saturation to water (Sorw)		0.2	
Residual oil saturation to gas (Sorg)		0.2	
Critical gas saturation (Sgc)		0.1	
Relative permeability of water at Sw=1-Sorw, Sg=0 (krwro)		0.5	
Relative permeability of gas at Sw=Swi, So=Sorg (krgro)		0.33	
Relative permeability of oil at Sw=Swi, Sg=0 (krocw)		0.9	
Exponent for krw curve (nw)		3	
Exponent for krow curve (now)		3	
Exponent for krg curve (ng)		3	
Exponent for krog curve (nog)		3	

Table 5 – RADIAL MODEL RESERVOIR DESCRIPTION

GEOMETRY									
Surface Area, sq.km	5								
Gridding Model	25 x 1 x 145								
Well radius (rw), ft	0.583								
Outer boundary radius (re), ft	4140								
Radial coordinates, ft	0.69	0.99	1.41	2.01	2.86	4.08	5.82	8.29	
	11.83	16.86	24.04	34.28	48.87	69.68			
	99.35	141.65	201.96	287.96	410.56				
	585.37	834.62	1189.98	1696.65	2419.06				
	3449.05								
Average DZ, ft	10								
Depth to top of formation, ft	8050								
ROCK AND FLUIDS PROPERTIES									
Porosity K1/K4	10 %								
K2/K3	15 %								
Rock Compressibility, 1/psi	5.0E-06								
Reservoir Temperature, F	220								
Water compressibility, 1/psi	2.64E-06								
Water FVF, RB/STB	1.0375								
Water density, lbs/cuft	62.37								
Water viscosity, cP	0.65								
INITIAL CONDITION									
<u>K4 Layer</u>									
Initial Pressure, psig	5300								
Reference Depth, ft	9600								
Dew point pressure, psig	5120								
<u>K3 Layer</u>									
Initial Pressure, psig	5180								
Reference Depth, ft	8500								
Dew point pressure, psig	4930								
RELATIVE PERMEABILITY ANALYTICAL DATA									
Connate water saturation (Swi)	0.2								
Residual oil saturation to water (Sorw)	0.2								
Residual oil saturation to gas (Sorg)	0.2								
Critical gas saturation (Sgc)	0.1								
Relative permeability of water at Sw=1-Sorw, Sg=0 (krwro)	0.5								
Relative permeability of gas at Sw=Swi, So=Sorg (krgro)	0.33								
Relative permeability of oil at Sw=Swi, Sg=0 (krocw)	0.9								
Exponent for krw curve (nw)	3								
Exponent for krow curve (now)	3								
Exponent for krg curve (ng)	3								
Exponent for krog curve (nog)	3								

Table 6 – PERMEABILITY DISTRIBUTION FOR RADIAL MODEL			
Geological Layer	Permeability, md		
	Average	Minimum	Maximum
K1	16.7	0.1	299
K2	52.43	0.22	1295
K3	46.77	0.1	907
K4	17.7	0.1	429

Table 7 – PERMEABILITY DISTRIBUTION COMPARISON		
Geological Layer	Average Permeability, md	
	Moderate Low Model	Very Low Model
K1	16.7	4.2
K2	52.43	13.11
K3	46.77	11.7
K4	17.7	4.43

Table 8 – RADIAL MODEL DESCRIPTION FOR CONDENSATE SKIN PREDICTION		
Description	K3	K4
Gridding Model	25 x 1 x 1	25 x 1 x 1
Well radius (rw), ft	0.583	0.583
Outer boundary radius (re), ft	4140	4140
Thickness, ft	170.07	160.71
Porosity	0.15	0.10
Permeability, md	46.77	17.70
Gas plateau rate, MMSCF/D	30	30

Table 9 – GAS RATE COMPARISON					
Geological Layer	Time	OGR	Gas Rate, MMSCF/D		
	days	STB/MMSCF	Simulation	Calculated	%Diff
K3	2735	22.54	30	30.62	2.1
K4	1825	22.72	17.12	17.43	1.8

Table 10 – CONDENSATE SKIN PREDICTION RESULT							
Geological Layer	Time	OGR	Gas Rate, MMSCF/D			Skin factor	
	days	STB/MMSCF	Simulation	Rate Dependent	Dry Gas	Simulation	Rate Dependent
K3	2735	22.54	30	34.93	102.7	19.7	15.8
K4	1825	22.72	17.12	21.15	73.11	26.5	20

Table 11 – EFFECTIVE SKIN PREDICTION RESULT								
Exponent	Moderate Low Permeability Case				Very Low Permeability Case			
	K1	K2	K3	K4	K1	K2	K3	K4
3	17	13	15	12	16	18	18	16
1.5	3	3	3	3	3	3	3	3

Figures

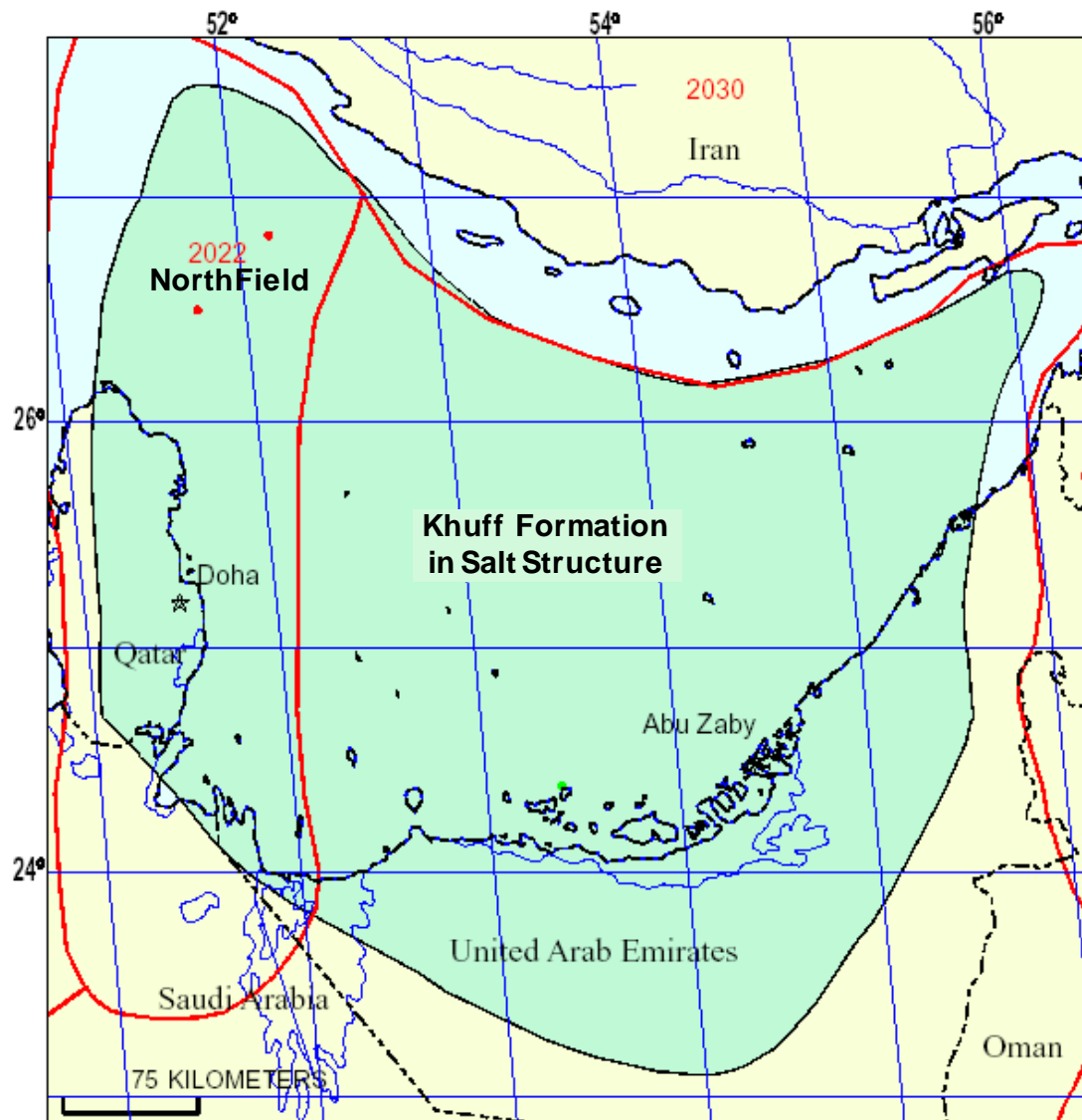


Fig. 1– Khuff Formation and North Field Map

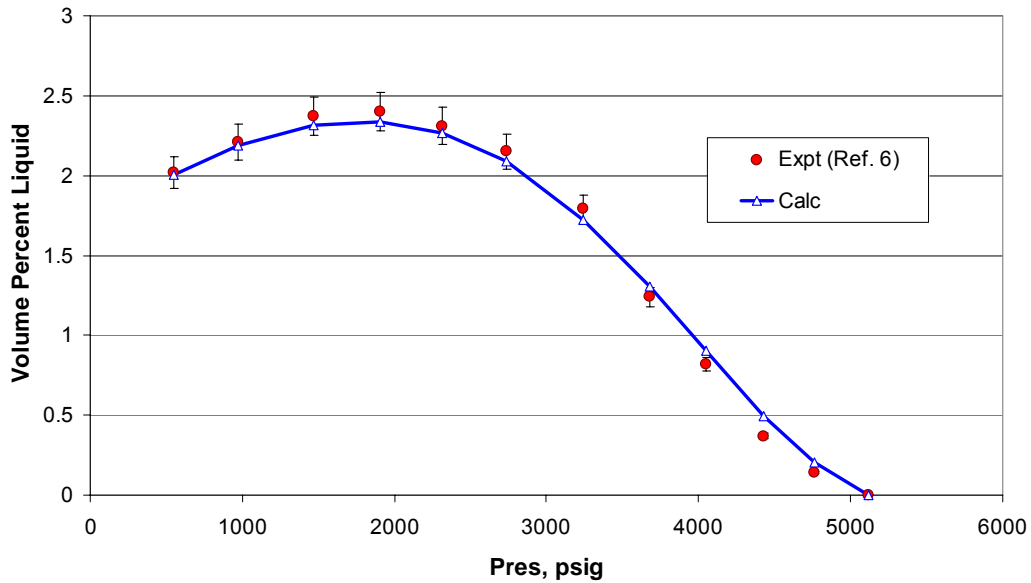


Fig. 2– Comparison volume percent liquid during Constant Volume Depletion at 220 F

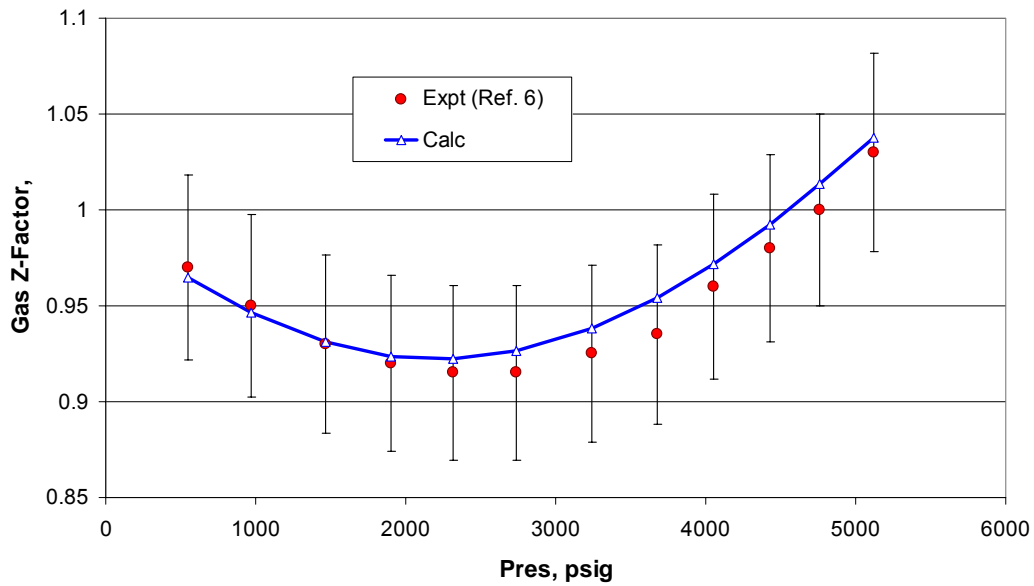


Fig. 3 – Comparison gas Z-factor during Constant Volume Depletion at 220 F

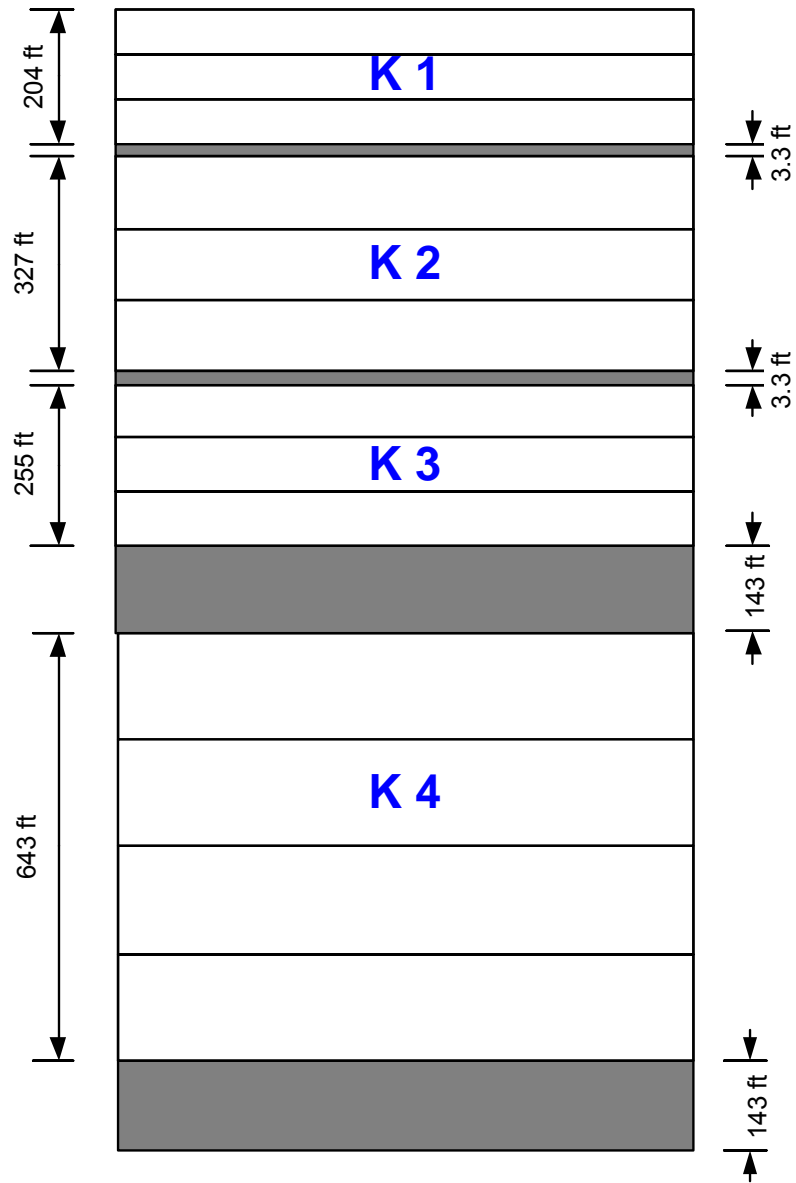


Fig. 4 – Khuff formation layering system

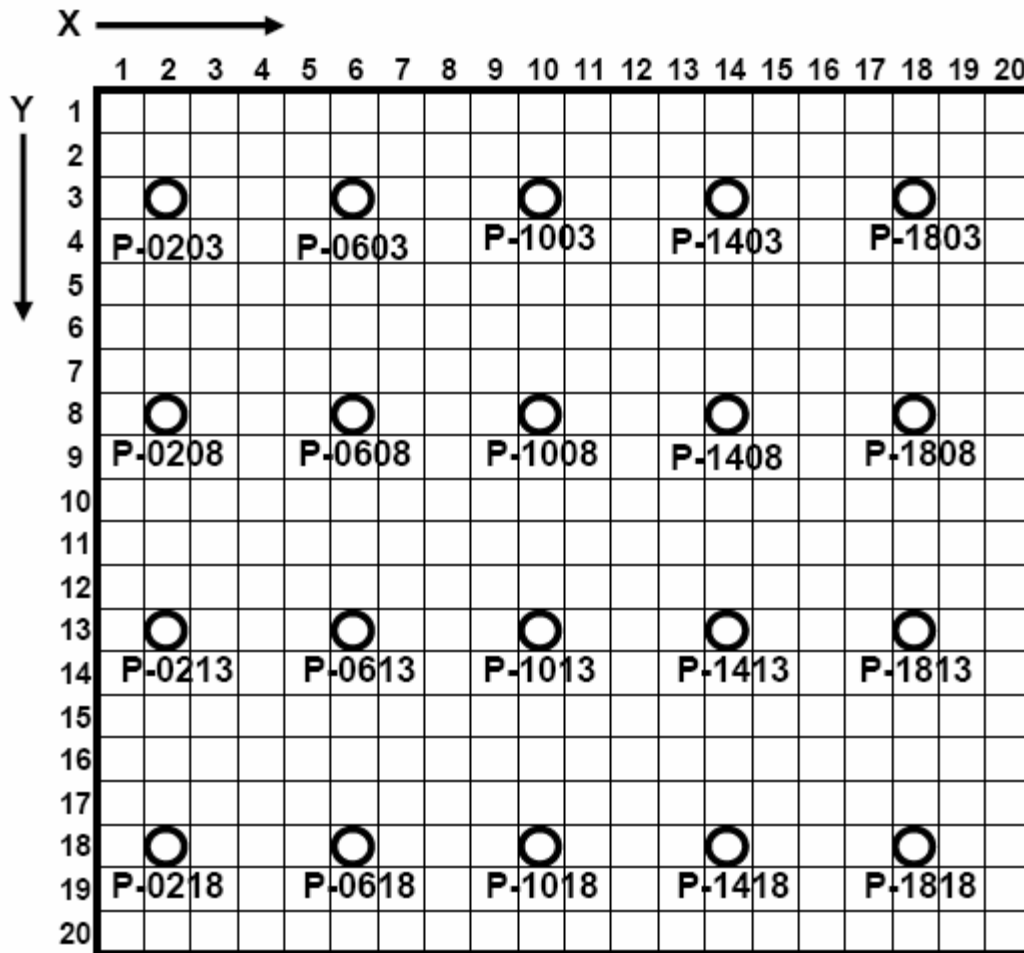


Fig. 5 – North Field Production Well Position

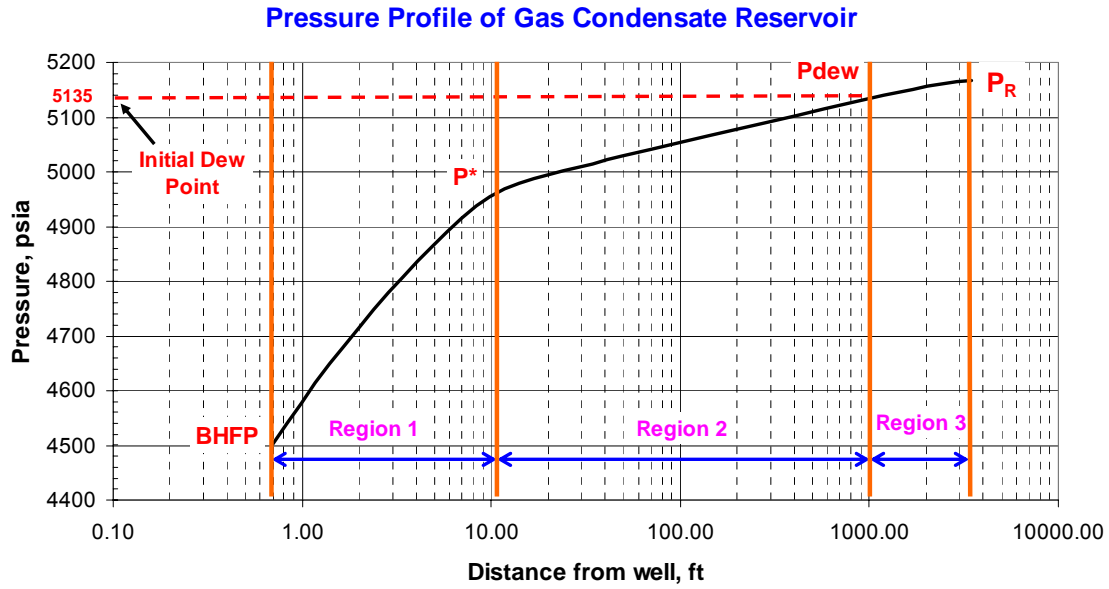


Fig. 6 – Pressure and regions profile at a given time of gas condensate reservoir simulation

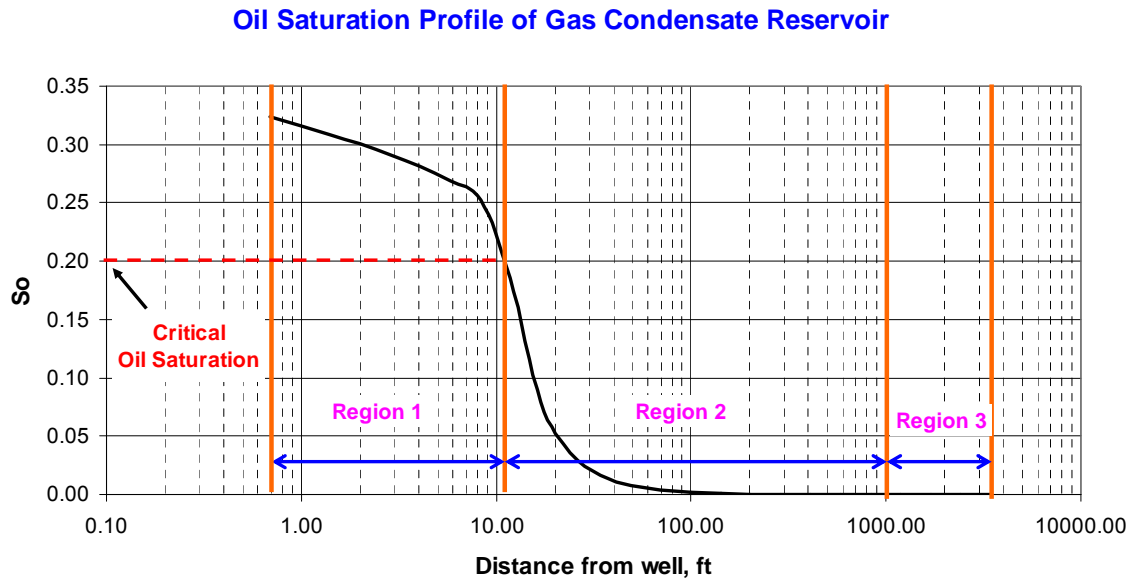


Fig. 7 – Oil saturation and regions profile at a given time of gas condensate reservoir simulation

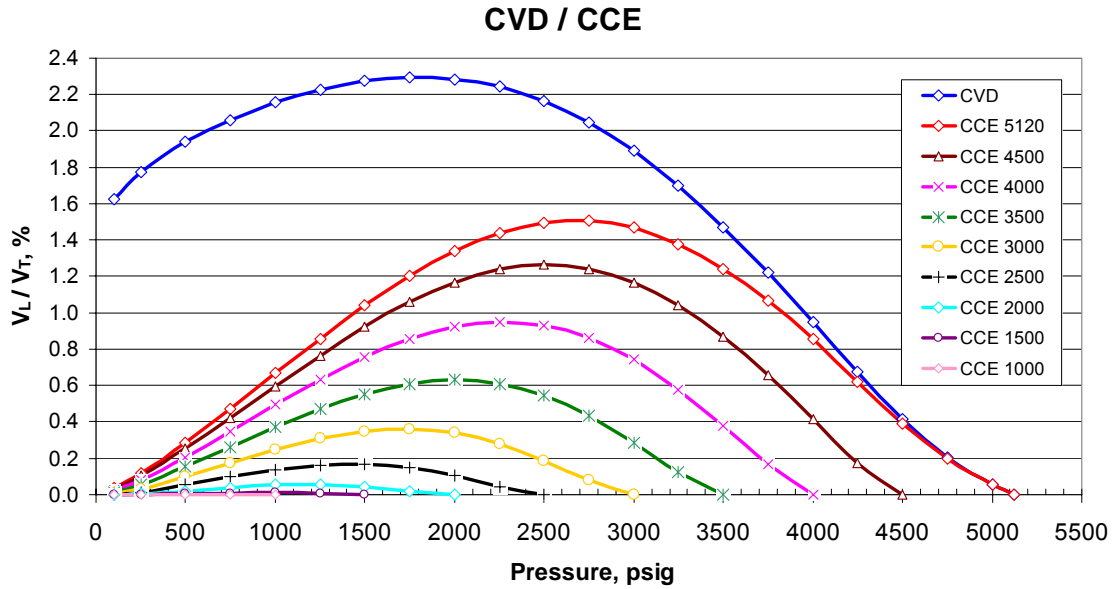


Fig. 8 – Liquid relative volume of CVD and CCE experiments which were conducted for the reservoir fluids of Layer K4

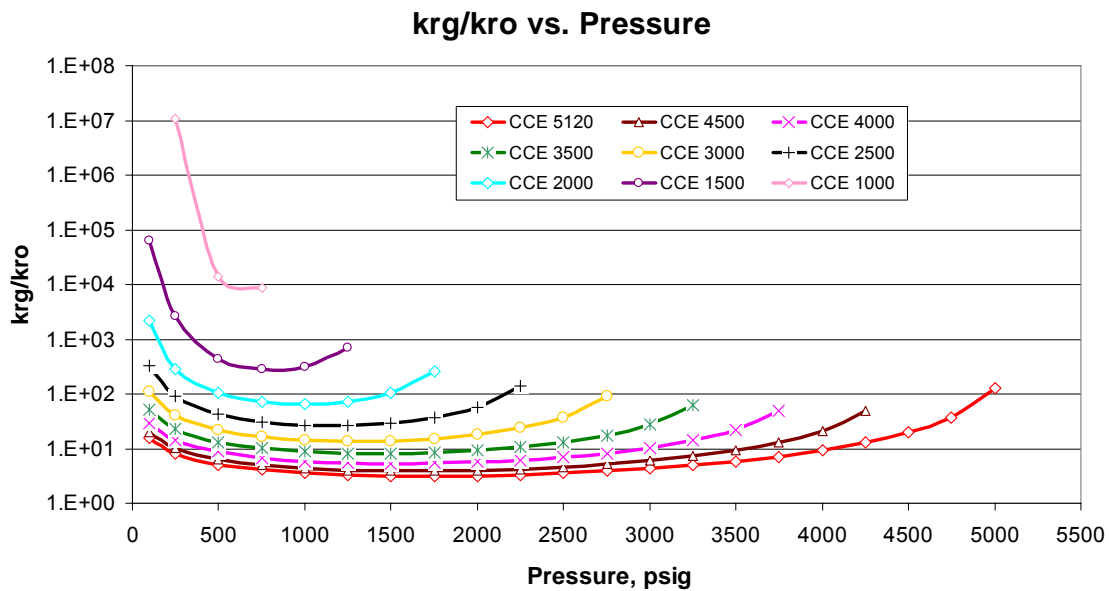


Fig. 9 – K_{rg}/K_{ro} range of the reservoir fluids of Layer K4

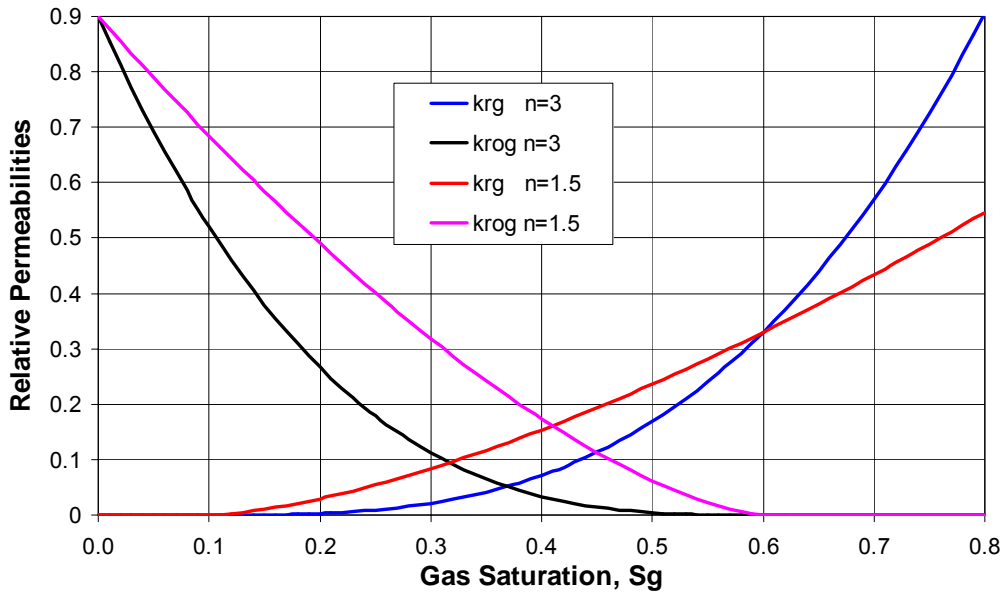


Fig. 10 – Gas Saturation (S_g) vs. k_{rg} and k_{rog} of the analytical relative permeability model used in North Field reservoir model for different Corey-like exponent

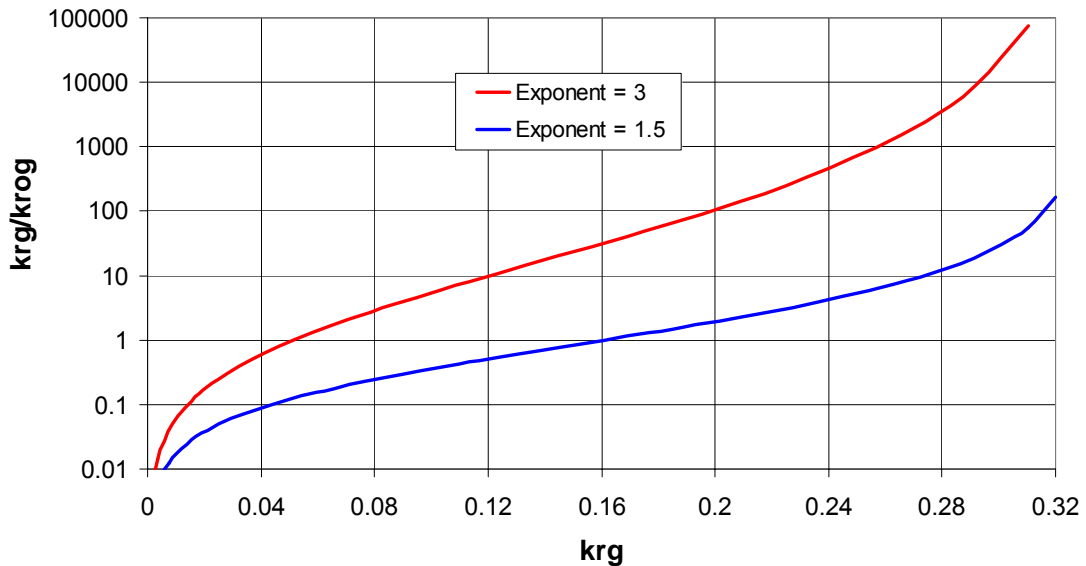


Fig. 11 – k_{rg} vs. k_{rg}/k_{rog} of the analytical relative permeability model used in North Field reservoir model for different Corey-like exponent

Pressure Profile in Radial Simulation

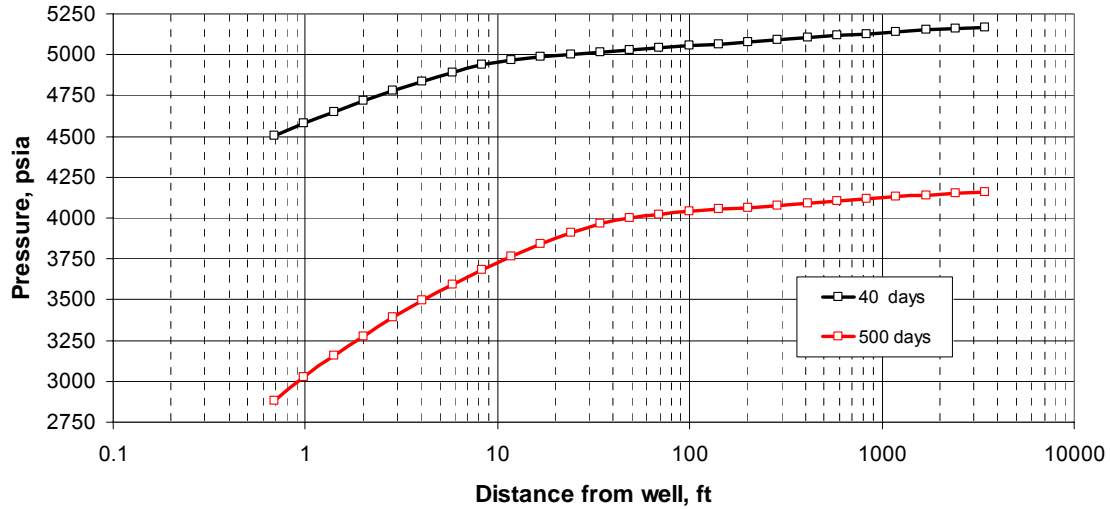


Fig. 12 – Pressure profile at Layer K4 when simulated in radial model

Oil Saturation Profile in Radial Simulation

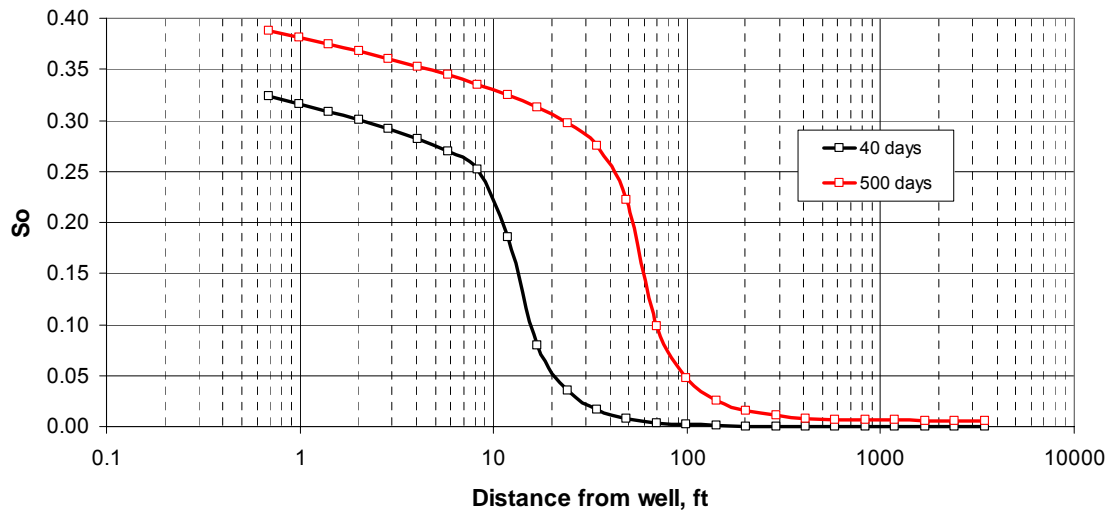


Fig. 13 – Oil saturation profile at Layer K4 when simulated in radial model

Krg Profile in Radial Simulation

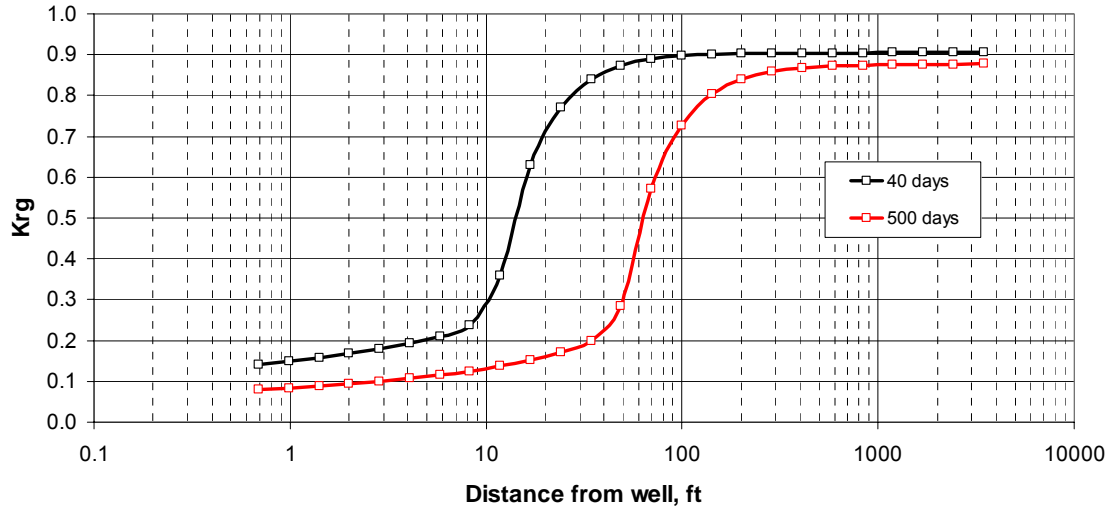


Fig. 14 – Gas relative permeability profile at Layer K4 when simulated in radial model

Kro Profile in Radial Simulation

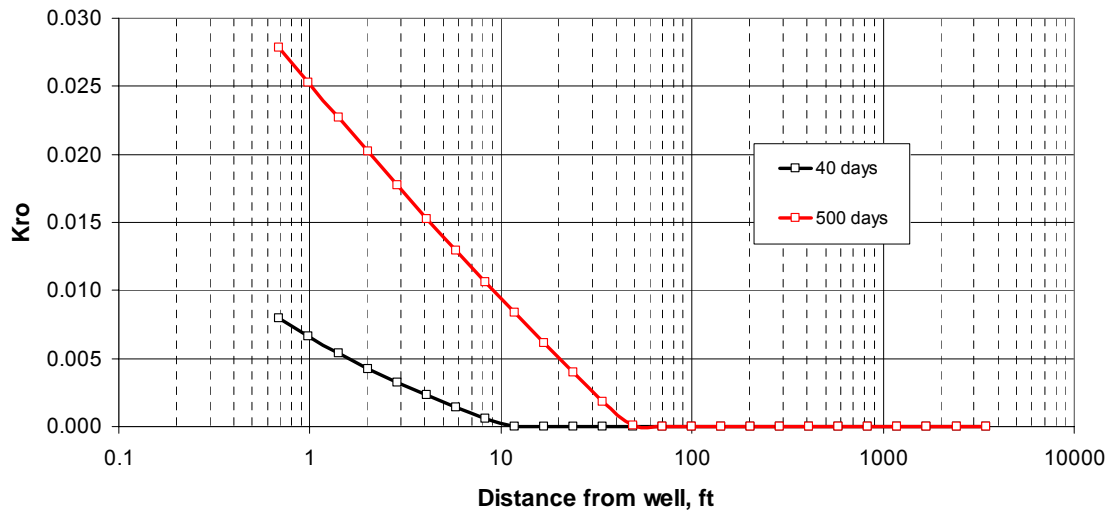


Fig. 15 – Oil relative permeability profile at Layer K4 when simulated in radial model

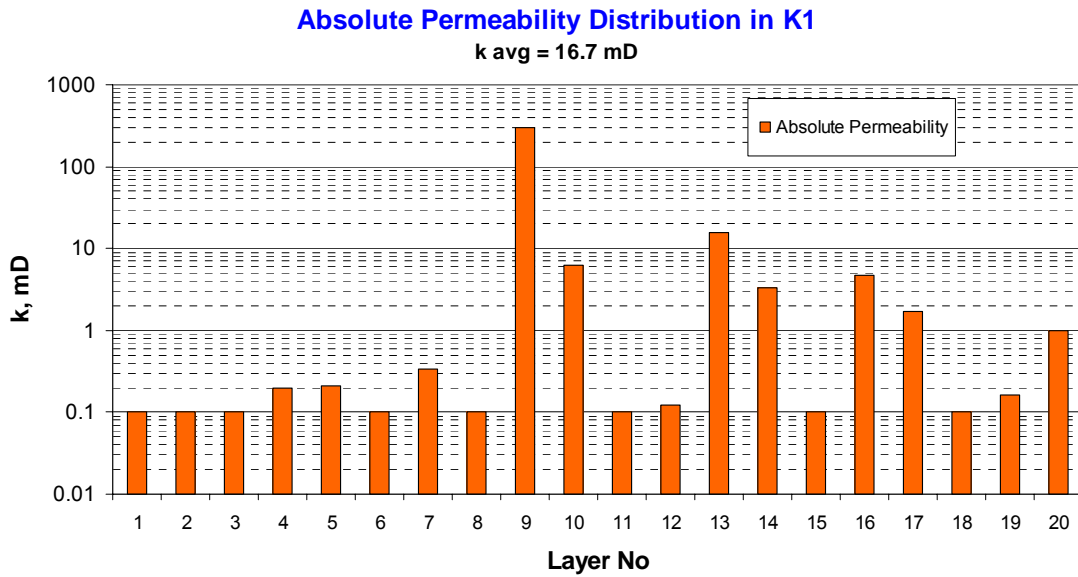


Fig. 16 – Absolute Permeability Distribution in K1

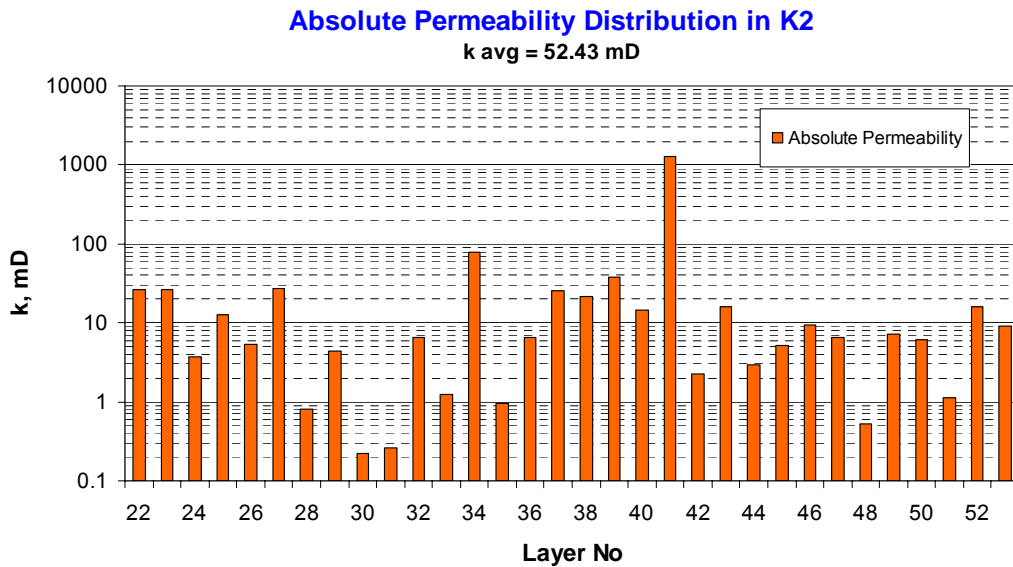


Fig. 17 – Absolute Permeability Distribution in K2

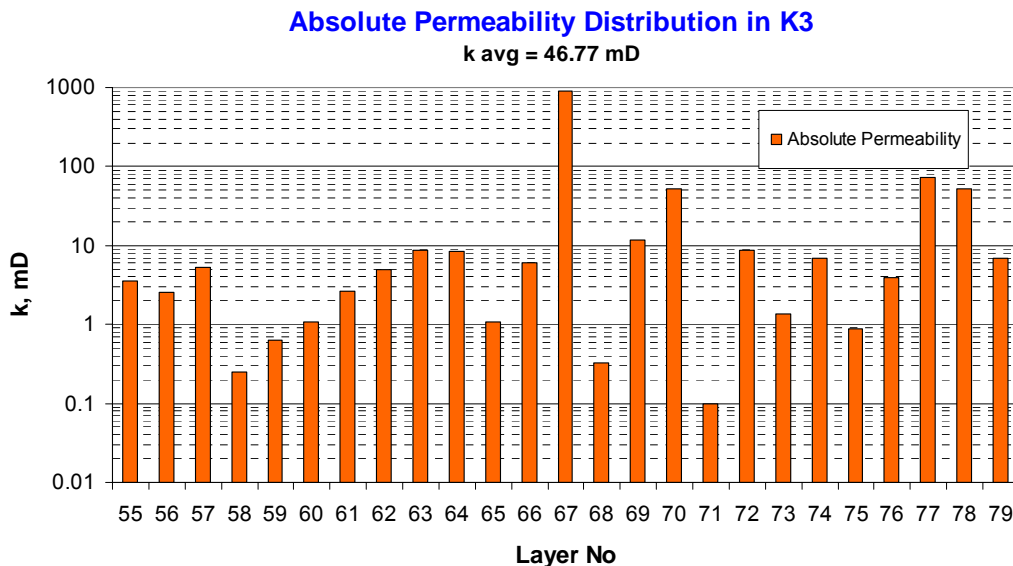


Fig. 18 – Absolute Permeability Distribution in K3

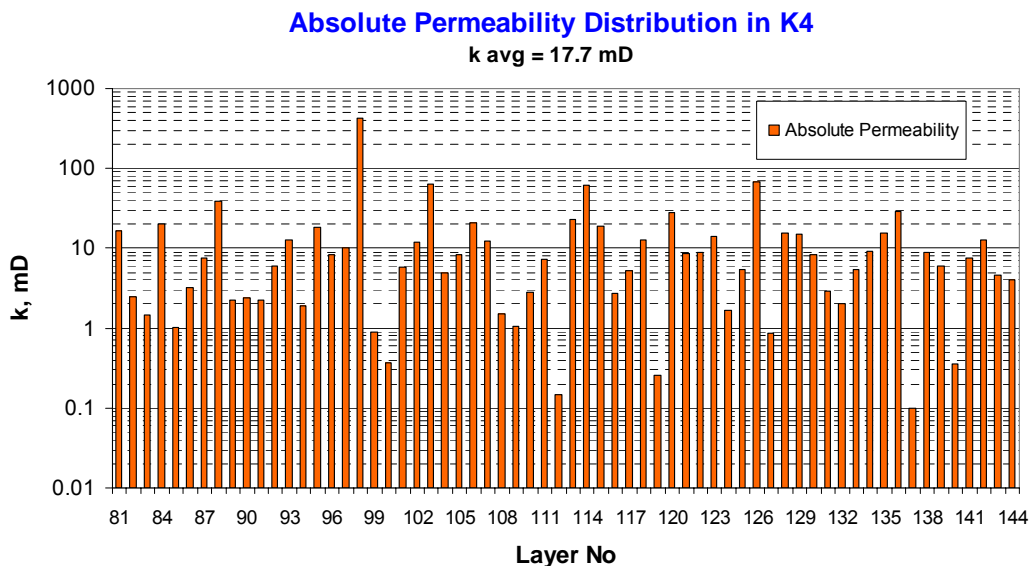


Fig. 19 – Absolute Permeability Distribution in K4

Field Gas and Condensate Production Rate

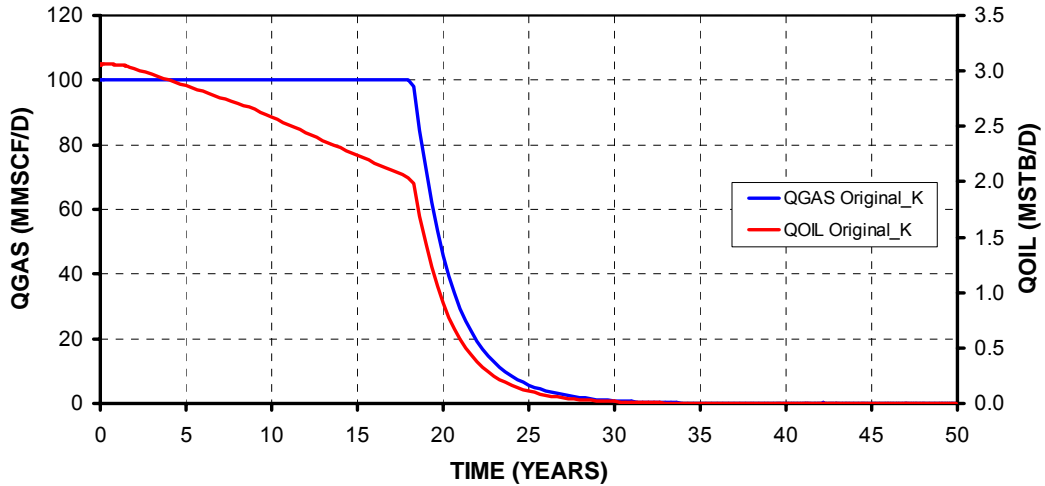


Fig. 20 – Radial Simulation Result Plots of Fluids Production Rate

Field GOR and Field Average Pressure

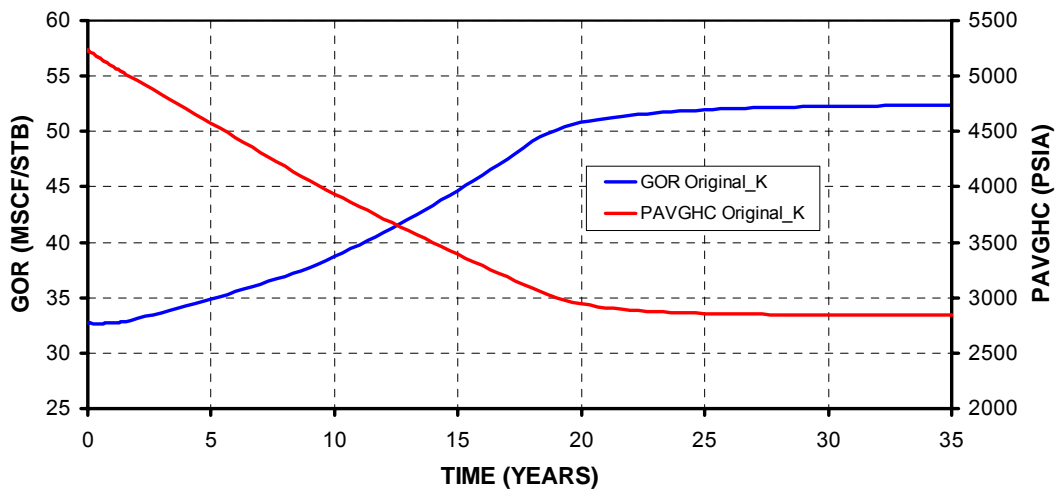


Fig. 21 – Radial Simulation Result Plots of Gas Oil Ratio and Average Pressure

Field Gas and Condensate Recovery

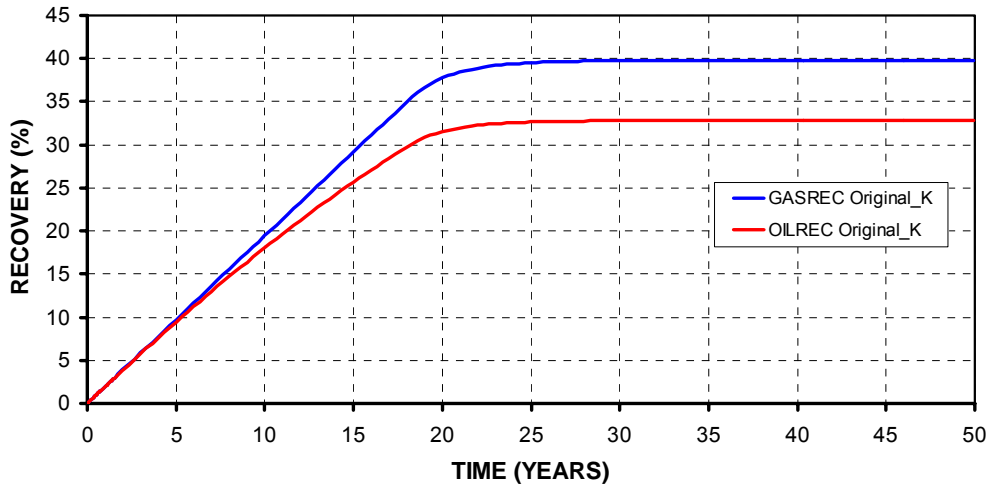


Fig. 22 – Radial Simulation Result Plots of Fluids Recovery

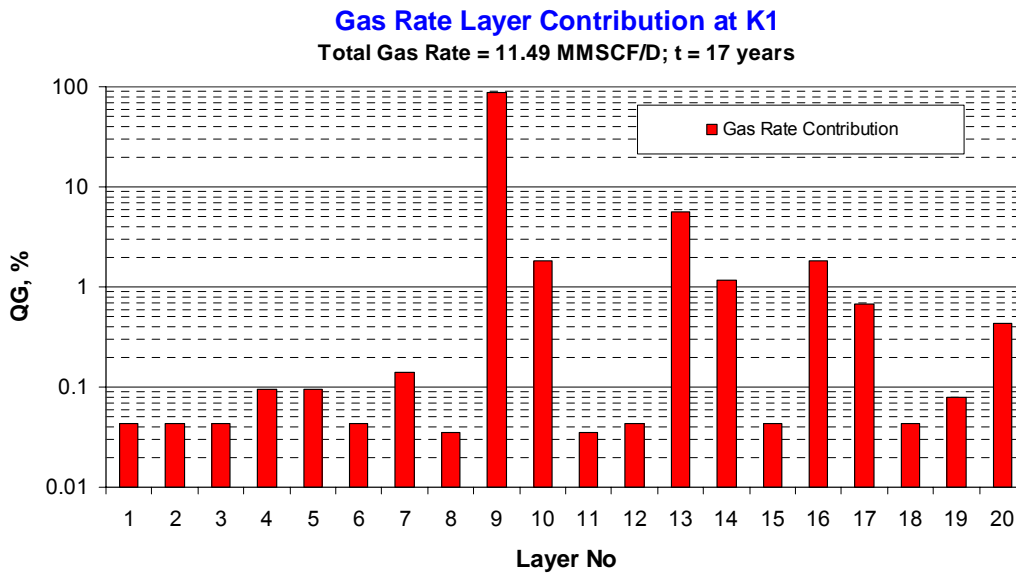


Fig. 23 – Gas Rate Layer Contribution in K1 at t =17 years

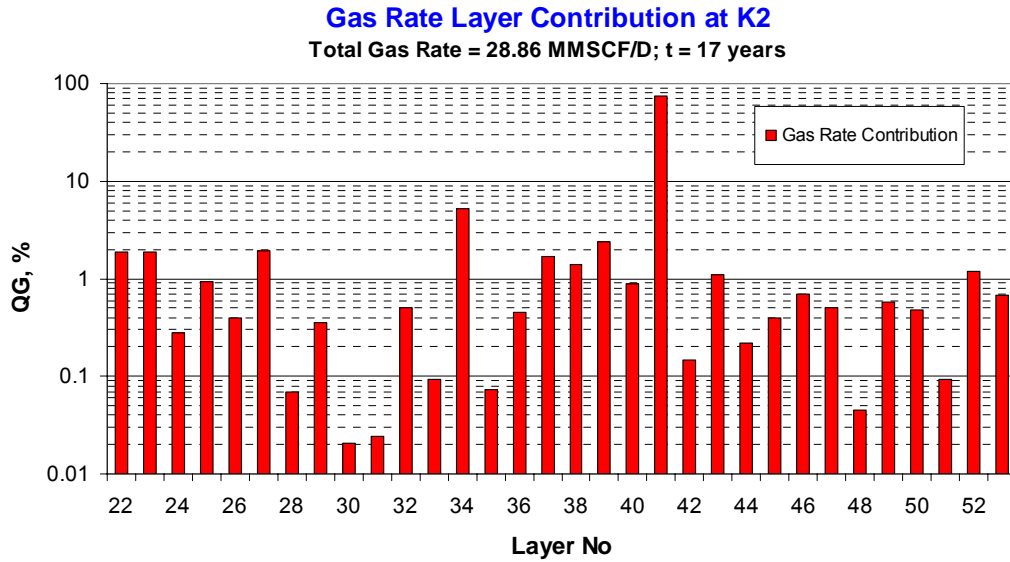


Fig. 24 – Gas Rate Layer Contribution in K2 at t =17 years

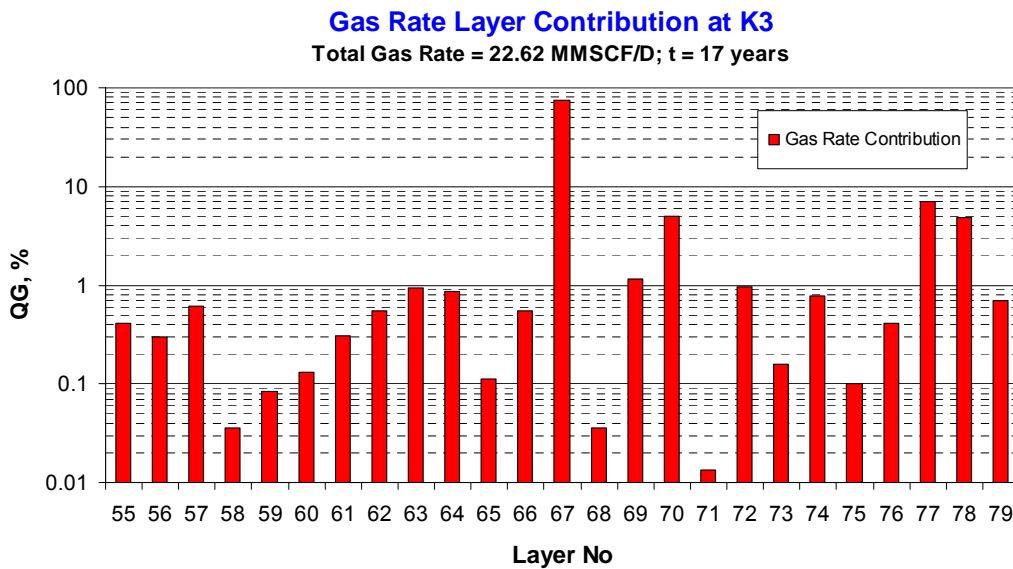


Fig. 25 – Gas Rate Layer Contribution in K3 at t =17 years

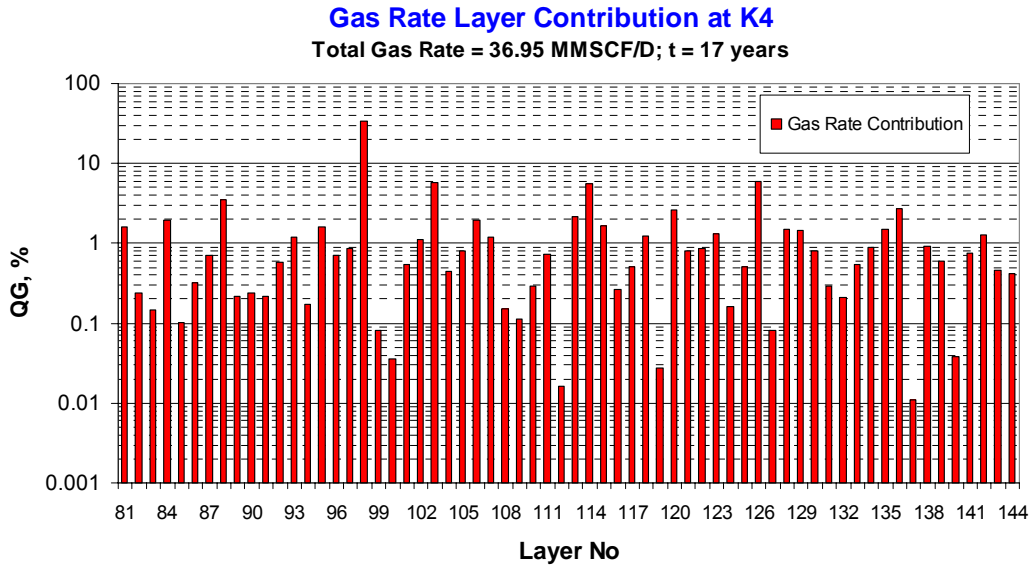


Fig. 26 – Gas Rate Layer Contribution in K4 at t =17 years

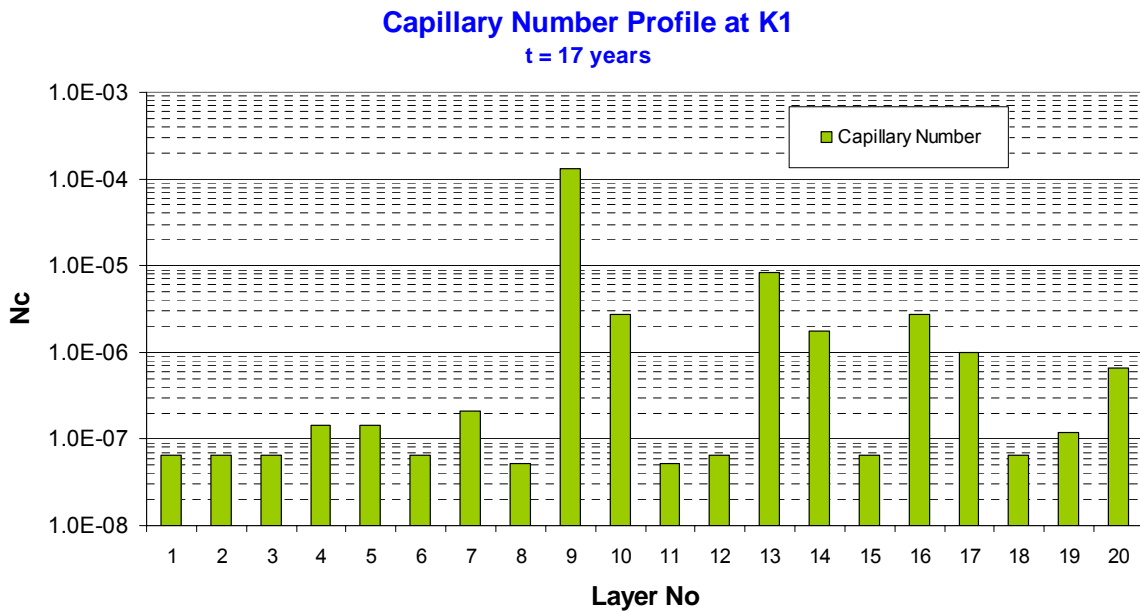


Fig. 27 – Capillary Number Profile in K1 at t =17 years

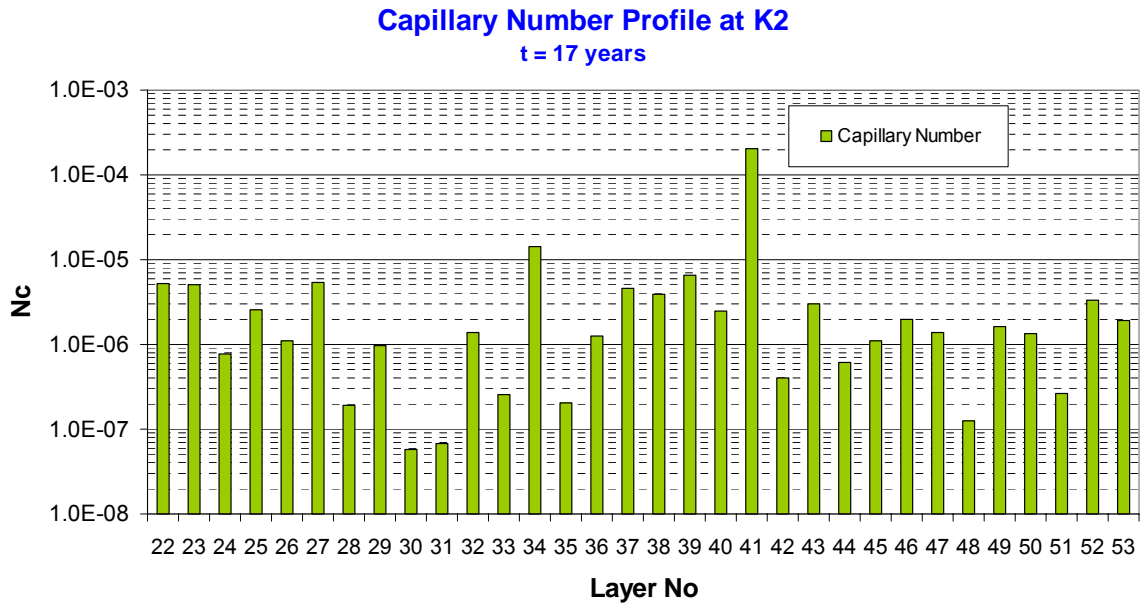


Fig. 28 – Capillary Number Profile in K2 at t =17 years

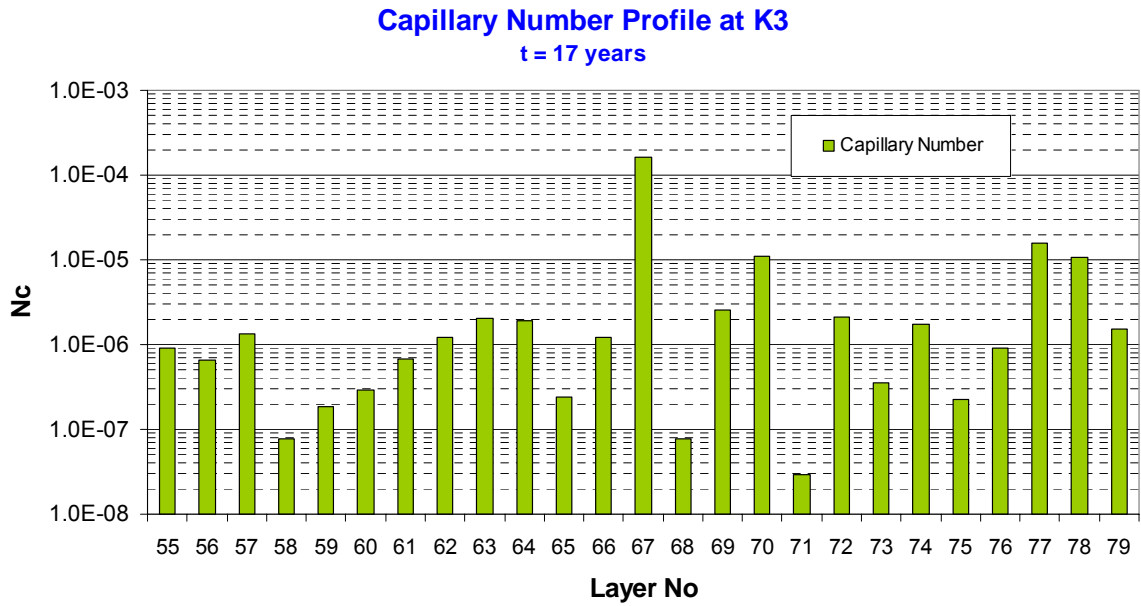


Fig. 29 – Capillary Number Profile in K3 at t =17 years

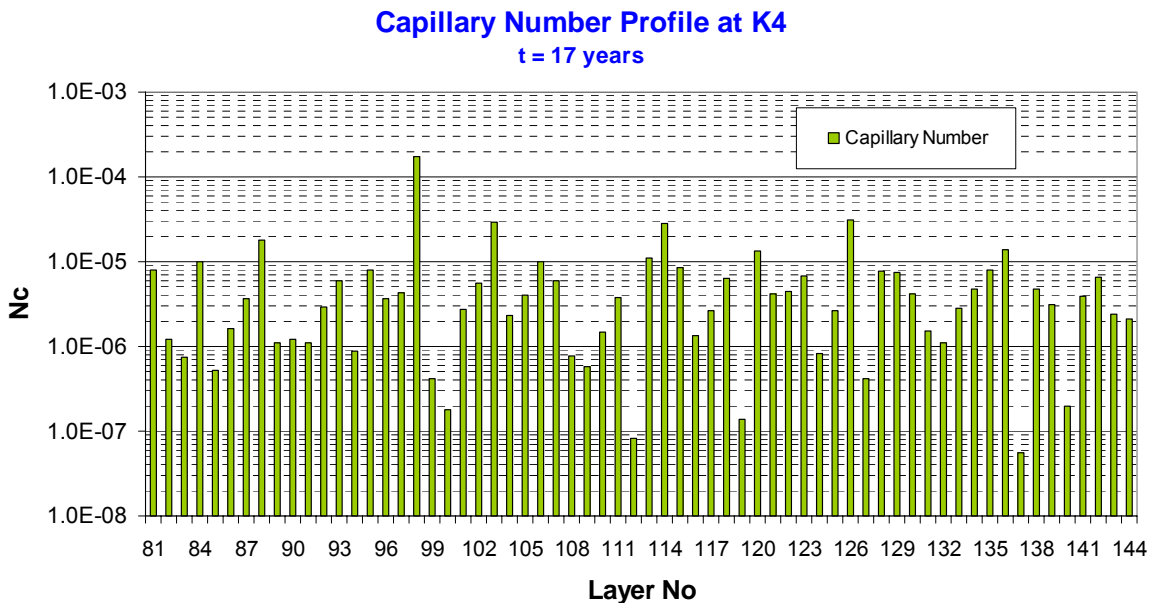


Fig. 30 – Capillary Number Profile in K4 at t =17 years

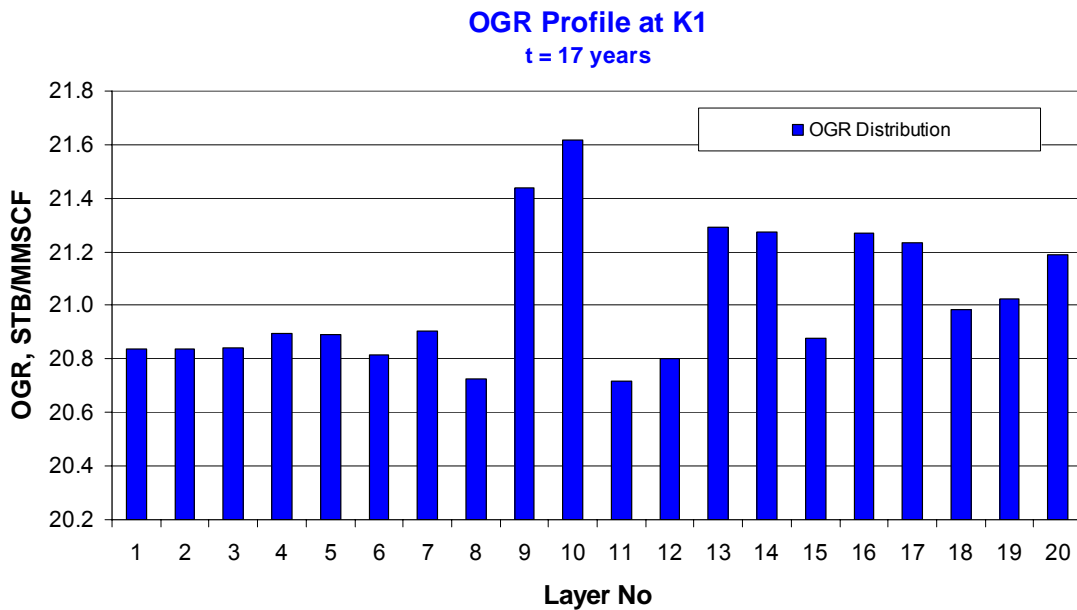


Fig. 31 – Oil Gas Ratio (OGR) Profile in K1 at t =17 years

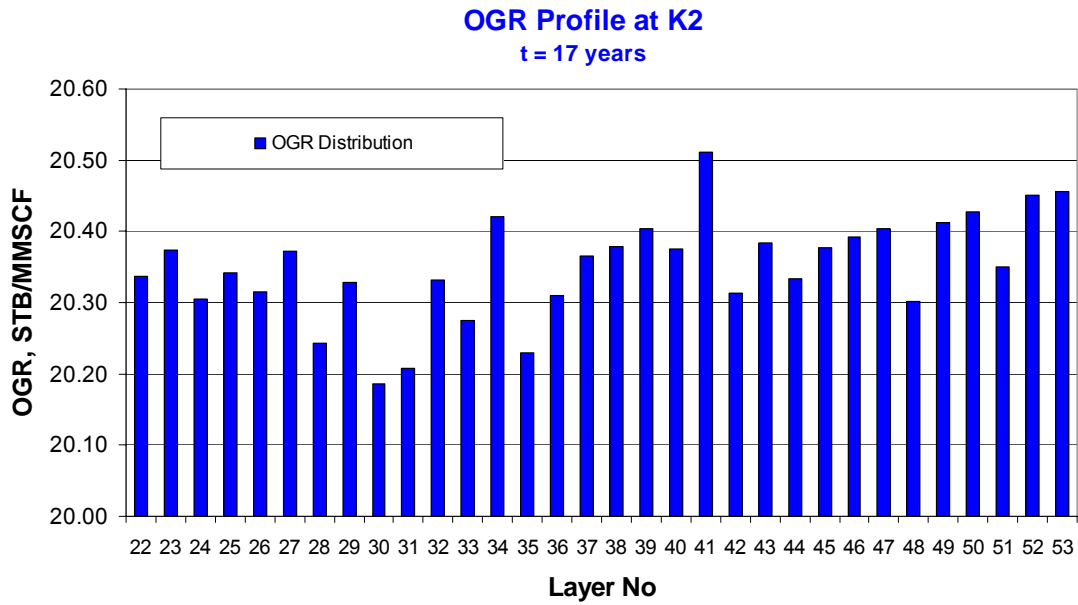


Fig. 32 – Oil Gas Ratio (OGR) Profile in K2 at t =17 years

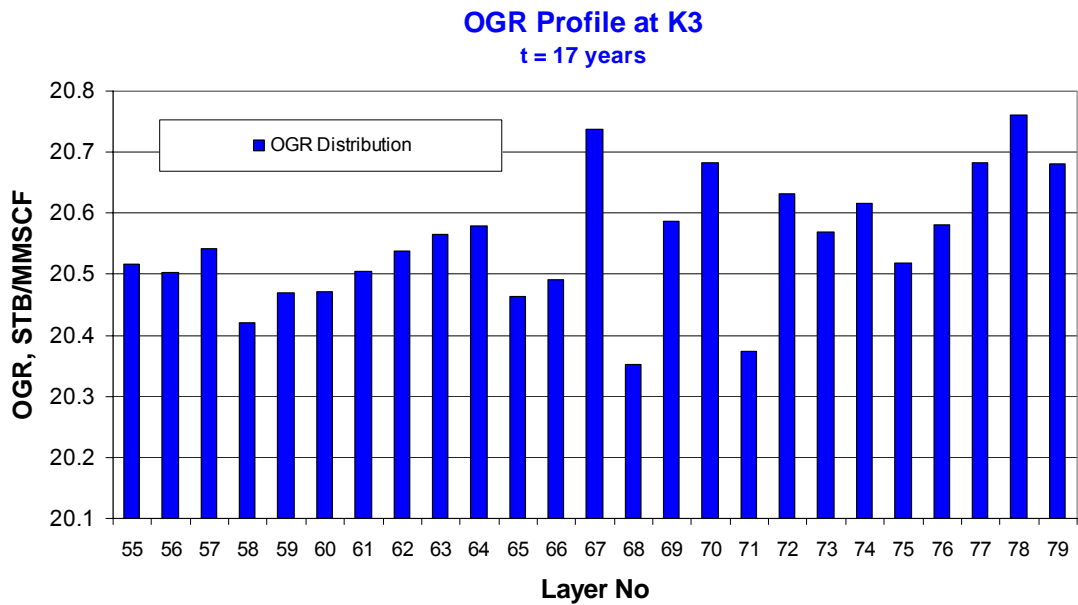


Fig. 33 – Oil Gas Ratio (OGR) Profile in K3 at t =17 years

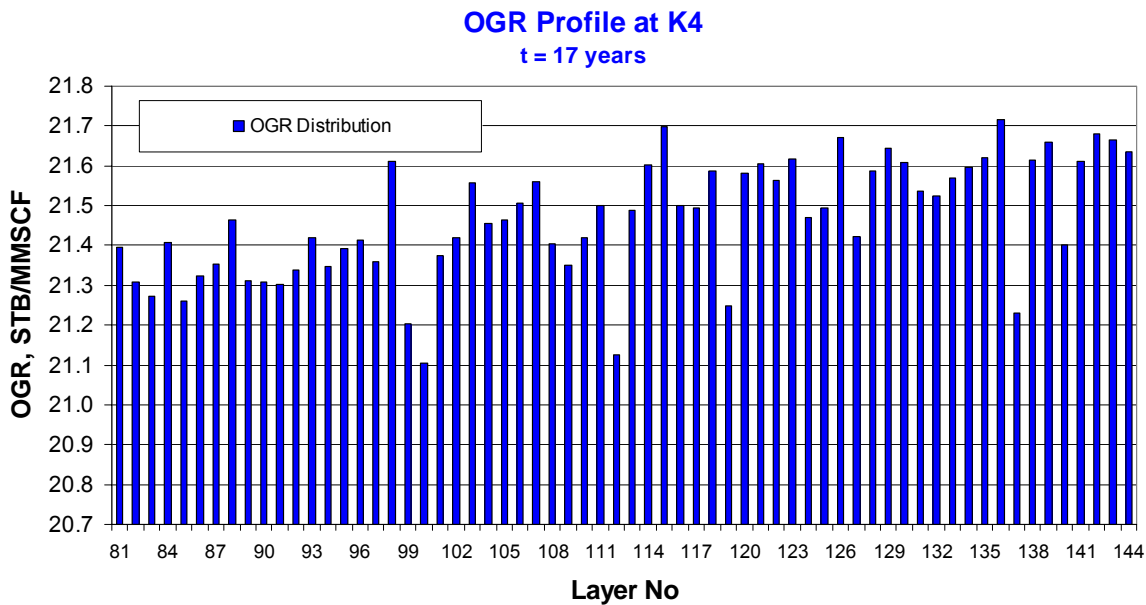


Fig. 34 – Oil Gas Ratio (OGR) Profile in K4 at t =17 years

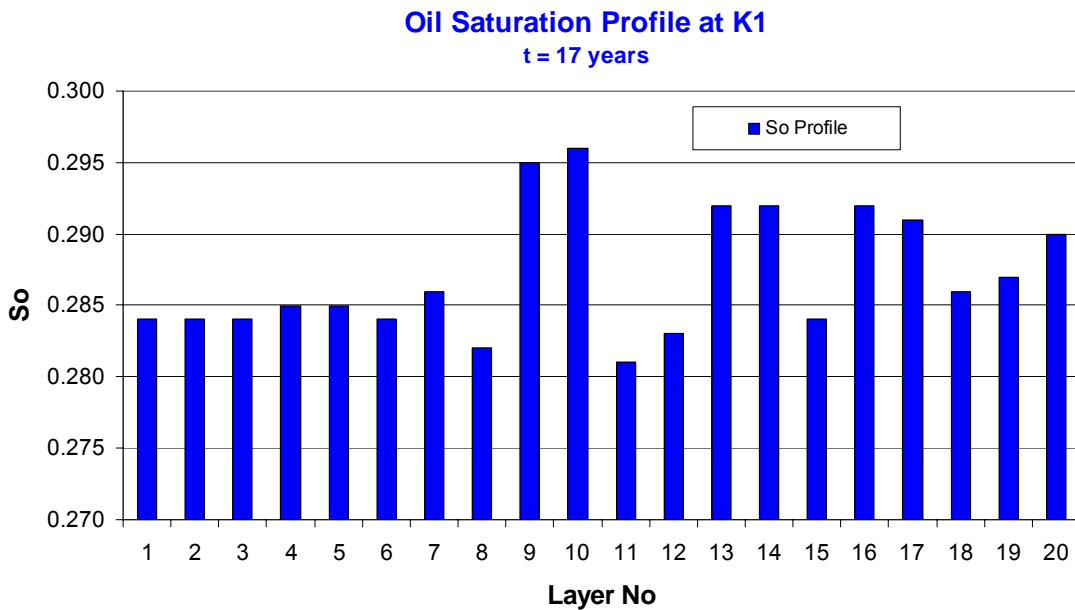


Fig. 35 –Oil Saturation of the first radial block profile in K1 at t =17 years

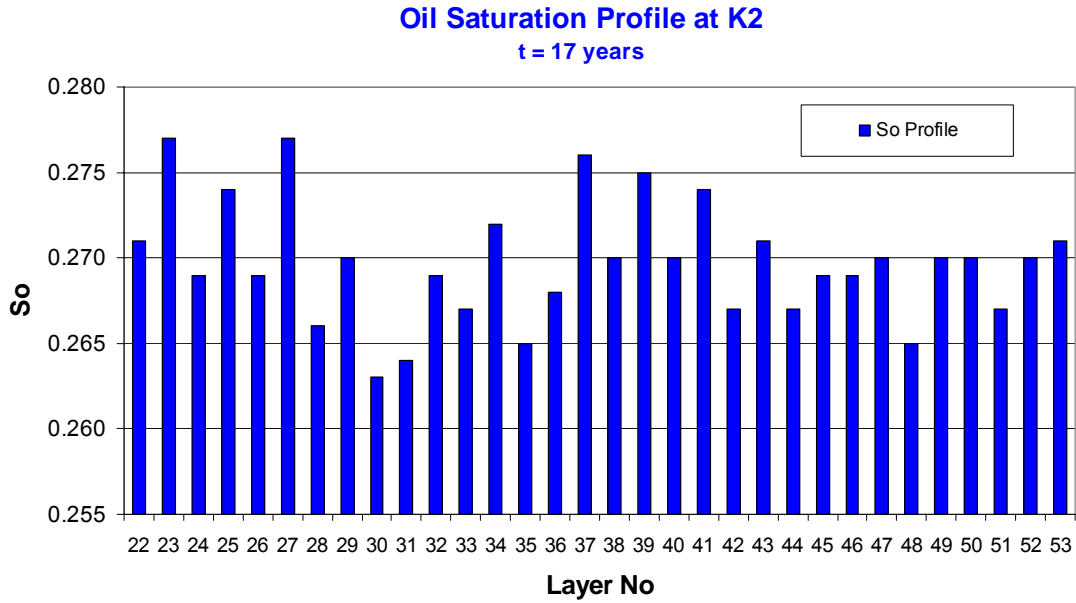


Fig. 36 –Oil Saturation of the first radial block profile in K2 at t =17 years

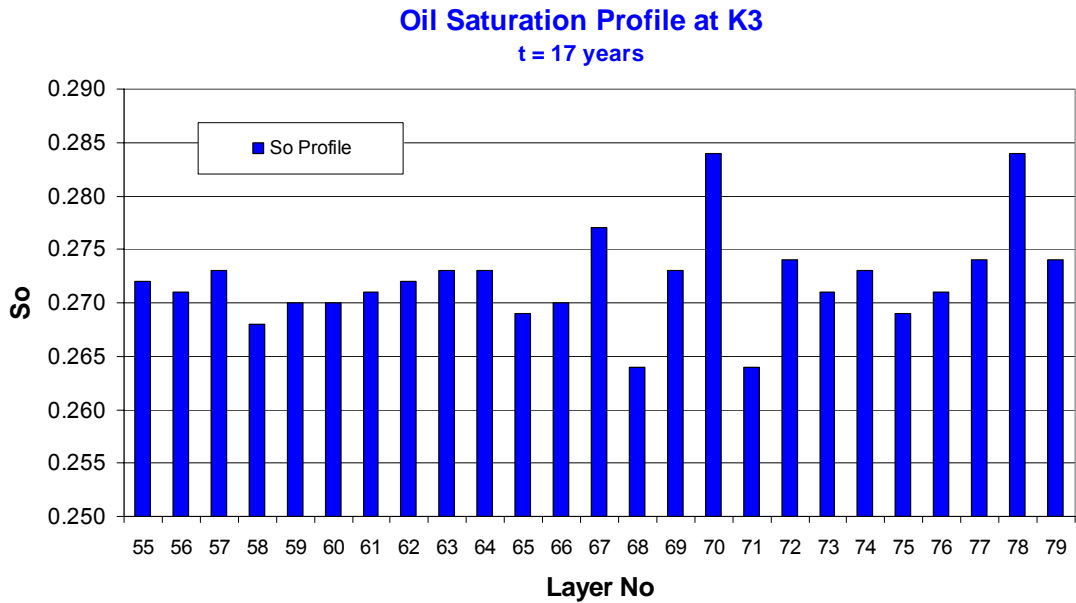


Fig. 37 –Oil Saturation of the first radial block profile in K3 at t =17 years

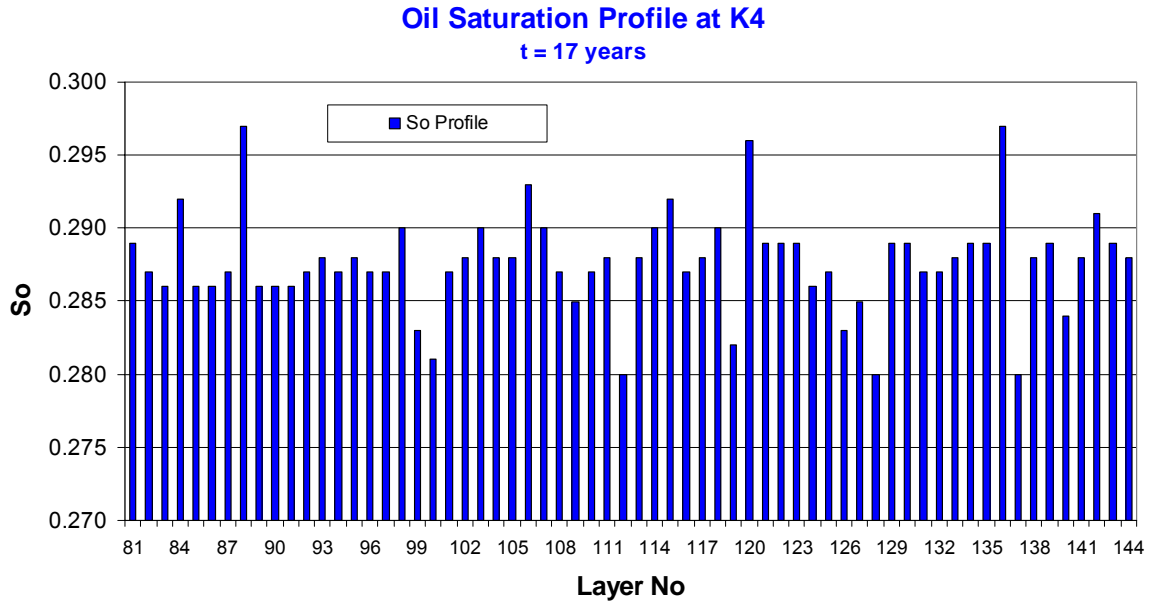


Fig. 38 –Oil Saturation of the first radial block profile in K4 at t =17 years

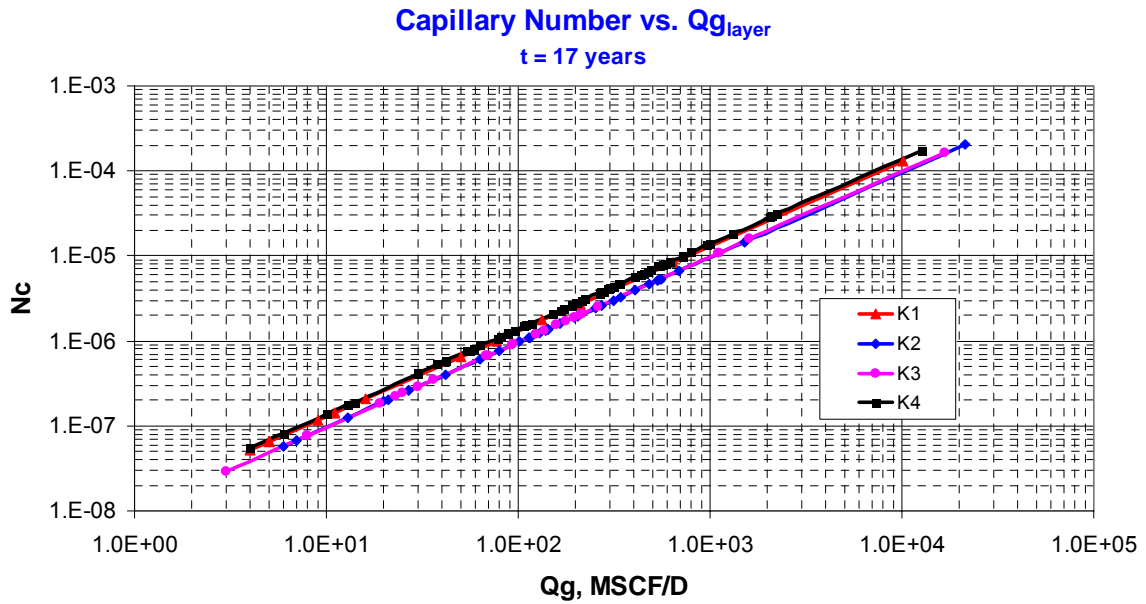


Fig. 39 – Capillary number vs. Gas Rate at t =17 years

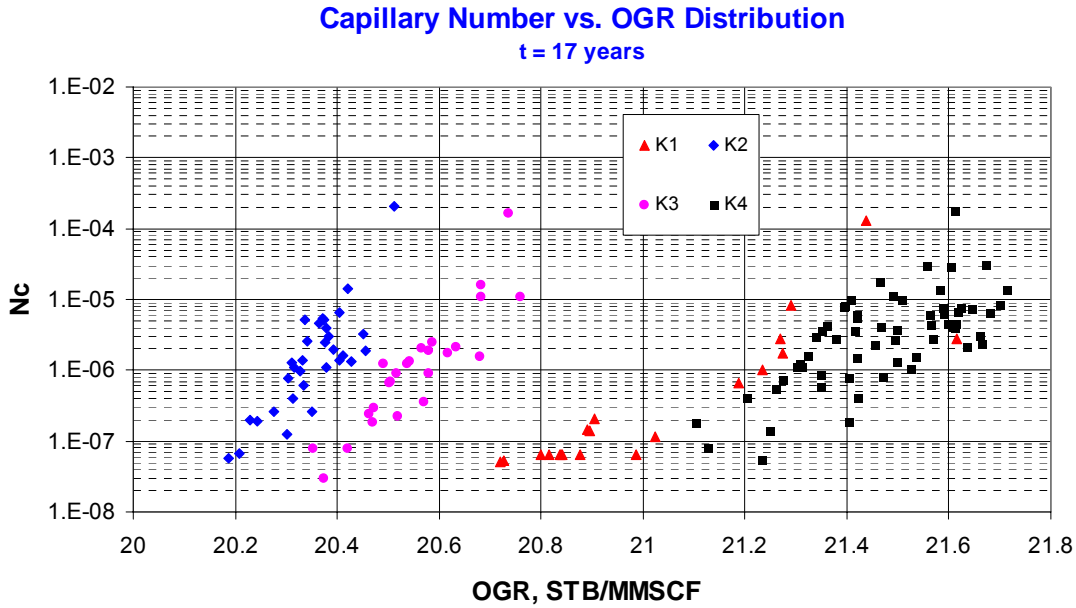


Fig. 40 – Capillary number vs. Oil Gas Ratio (OGR) at $t = 17$ years

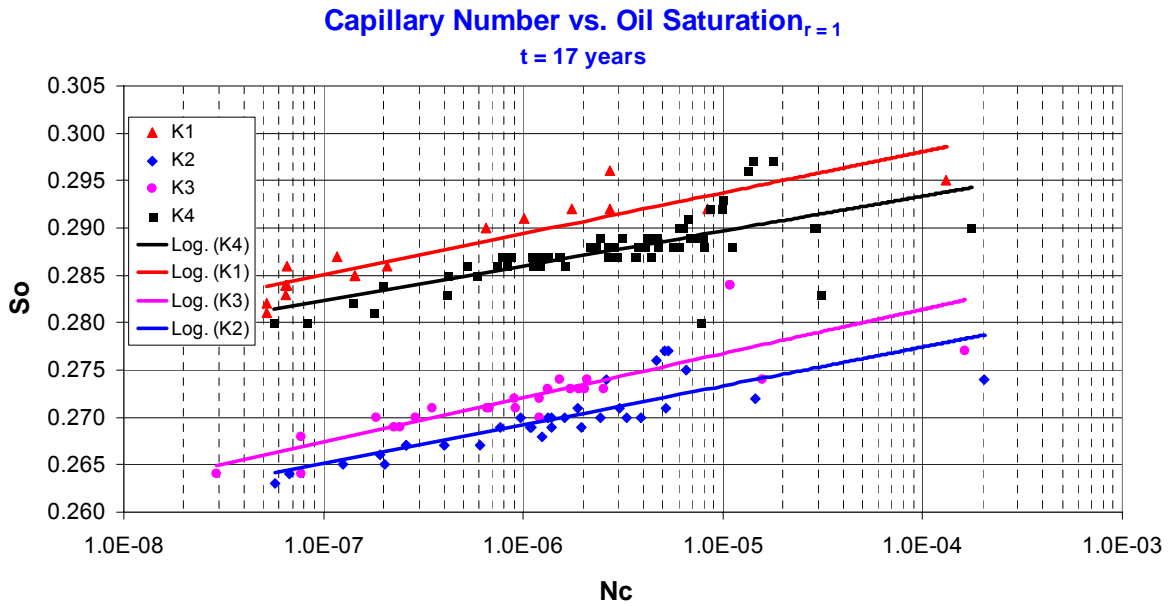


Fig. 41 – Capillary number vs. Oil Saturation of the first radial block at $t = 17$ years

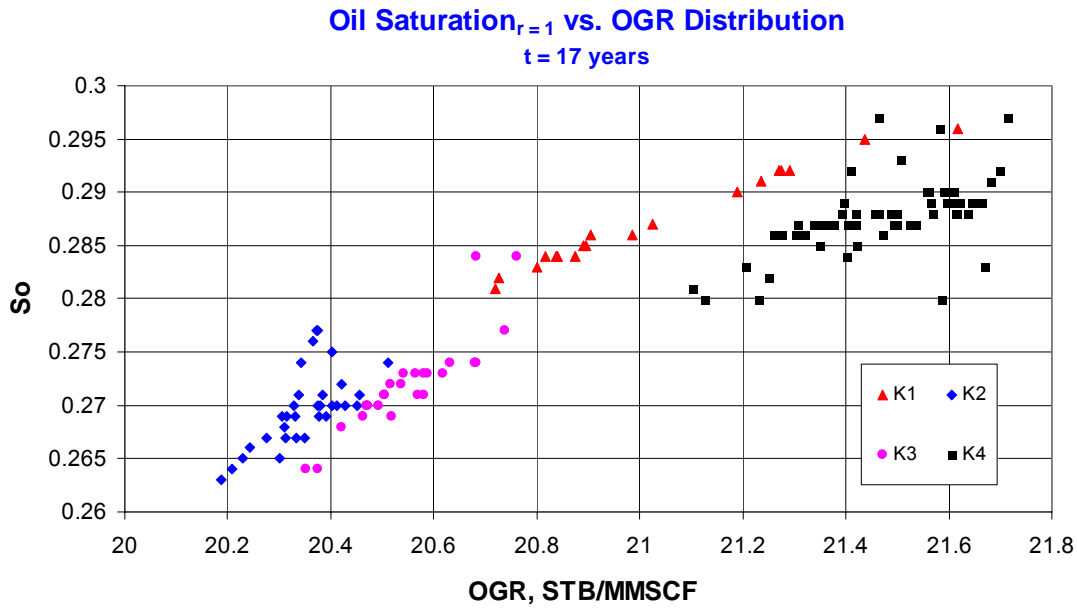


Fig. 42 – Oil Saturation of the first radial block vs. Oil Gas Ratio (OGR) at t =17 years

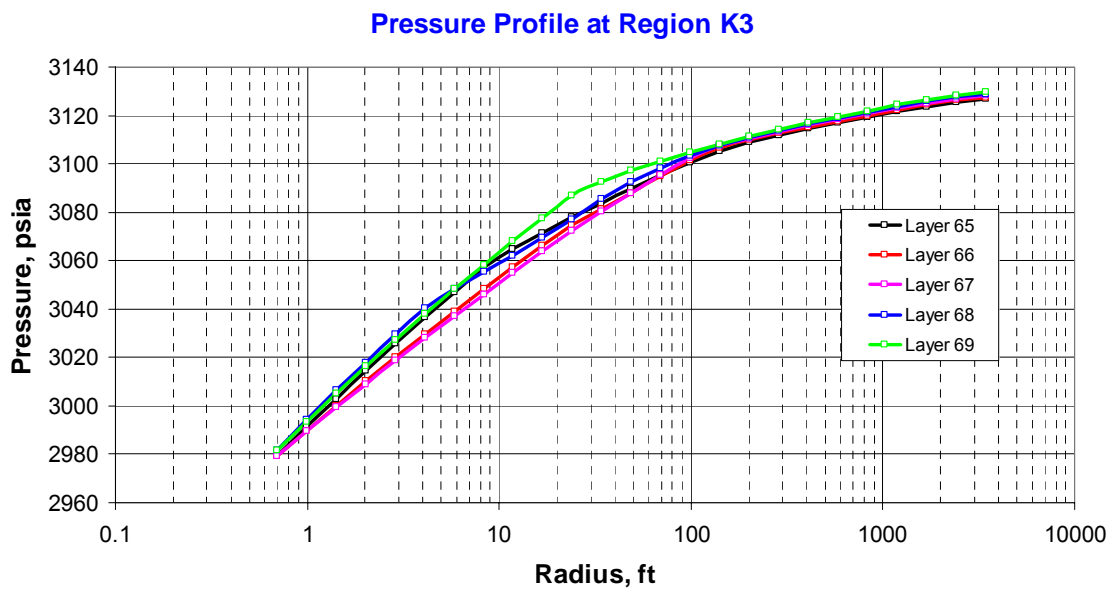


Fig. 43 – Pressure profile of the highest k layer and its surrounding layers in K3 at t =17 years

Oil Saturation Profile at Region K3

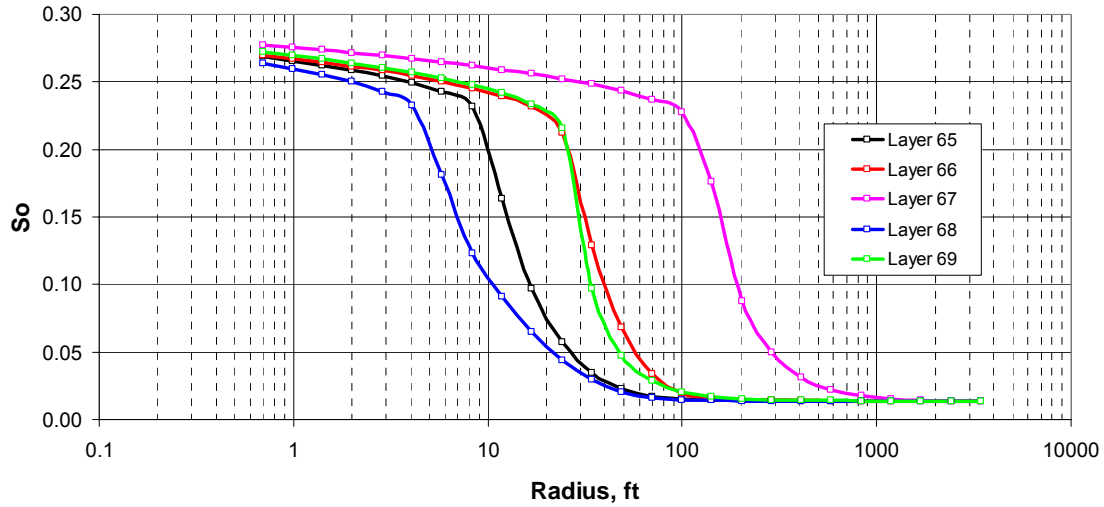


Fig. 44 – Oil saturation profile of the highest k layer and its surrounding layers in K3 at t=17 years

Krg Profile at Region K3

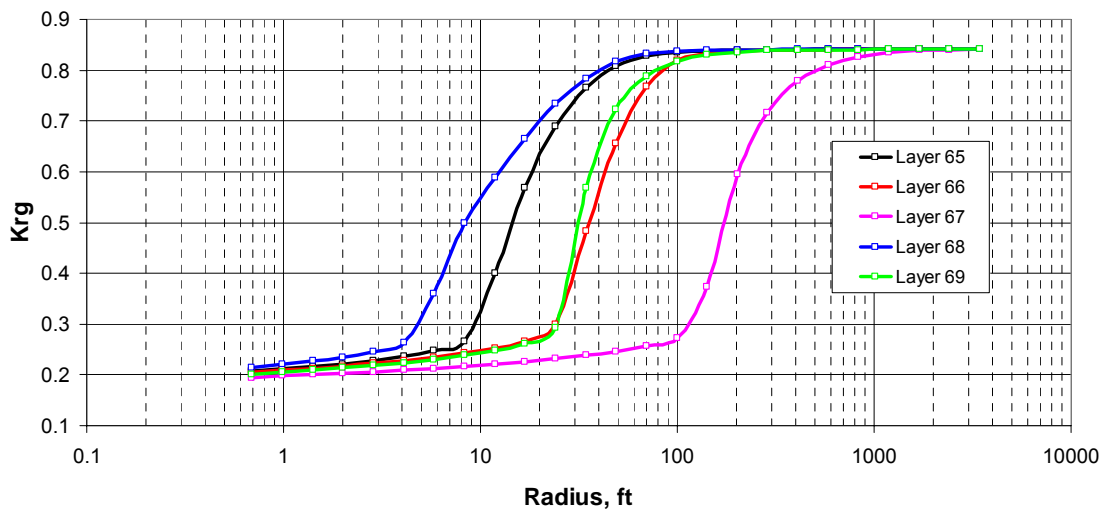


Fig. 45 – Gas relative permeability (k_{rg}) profile of the highest k layer and its surrounding layers in K3 at t =17 years

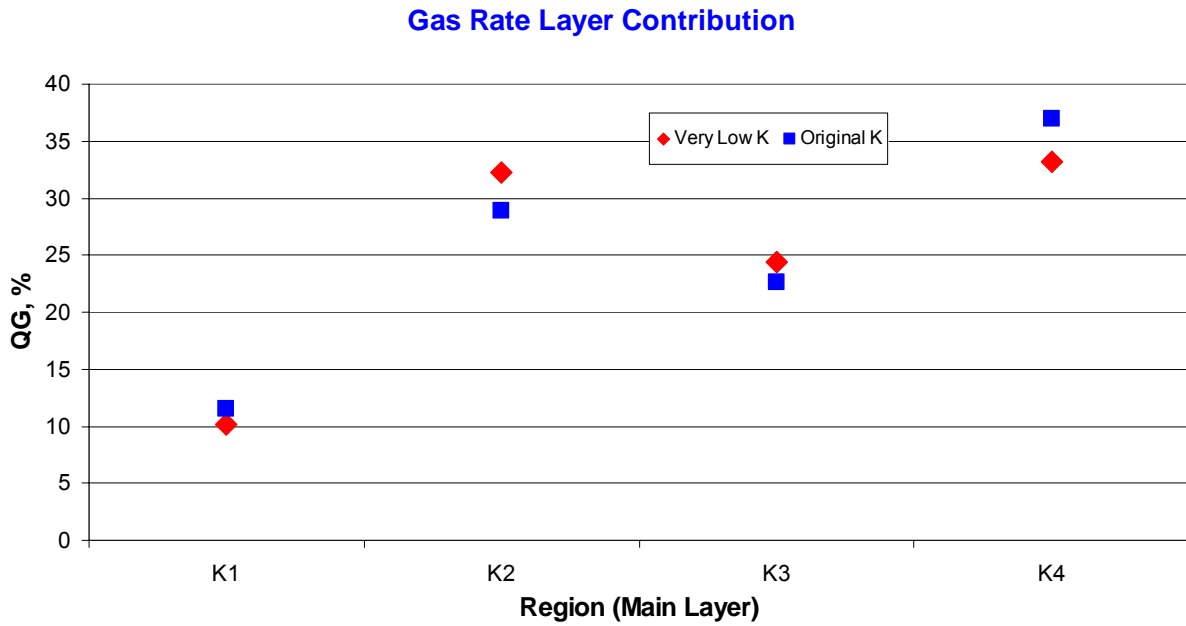


Fig. 46 – Permeability effect on Gas Rate Contribution

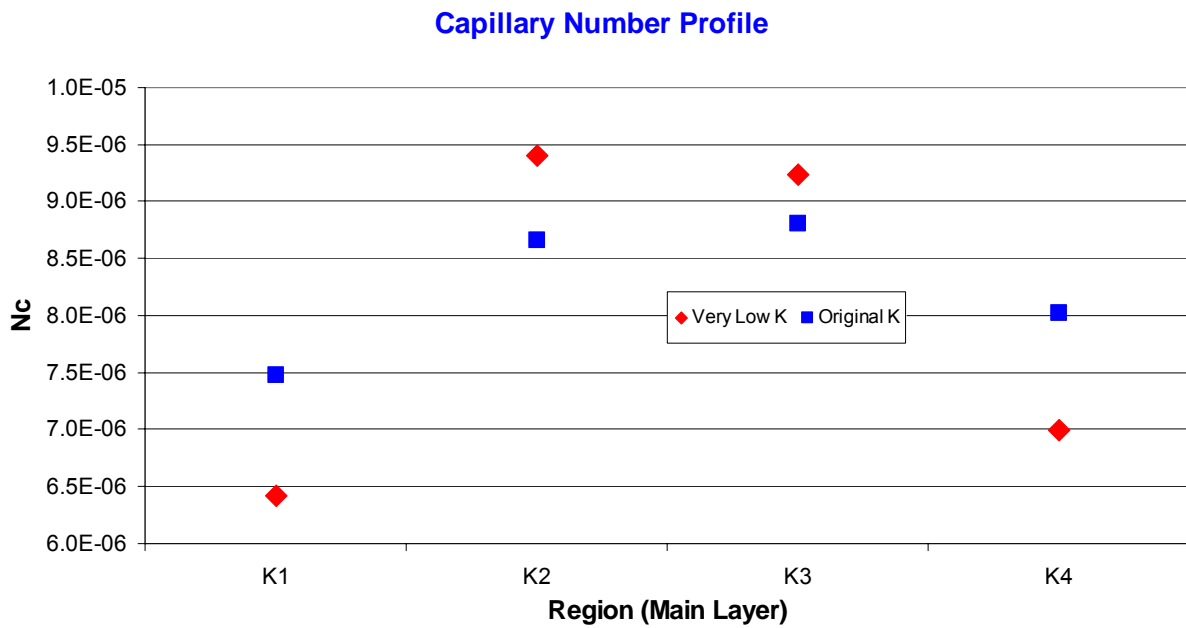


Fig. 47 – Permeability effect on Capillary Number profile

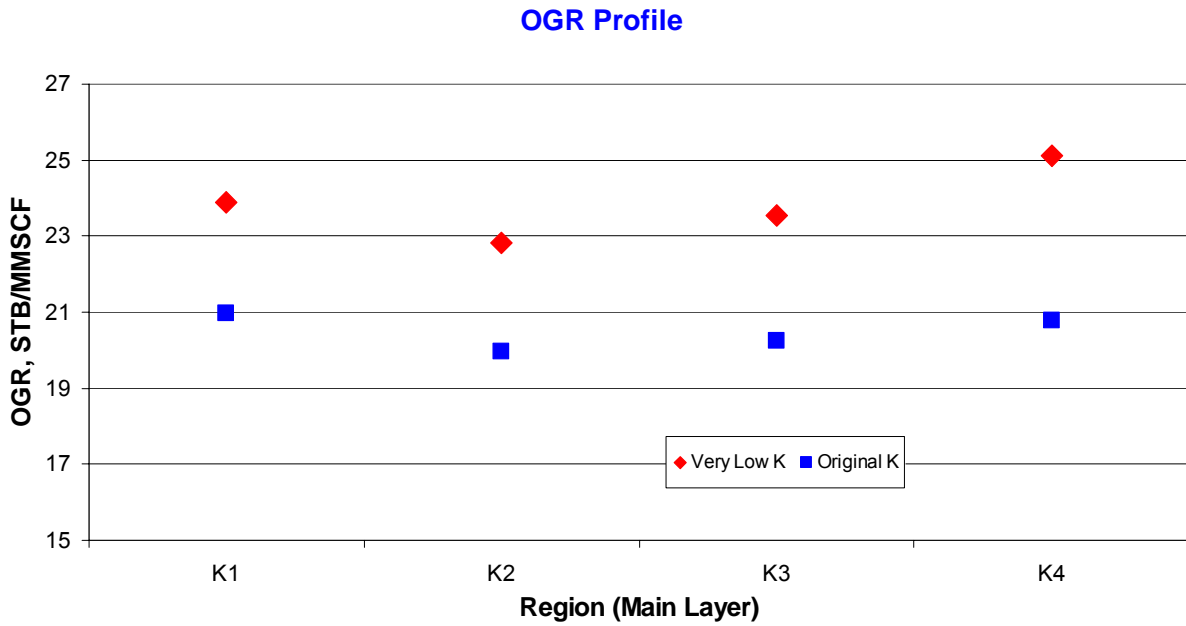


Fig. 48 – Permeability effect on OGR profile

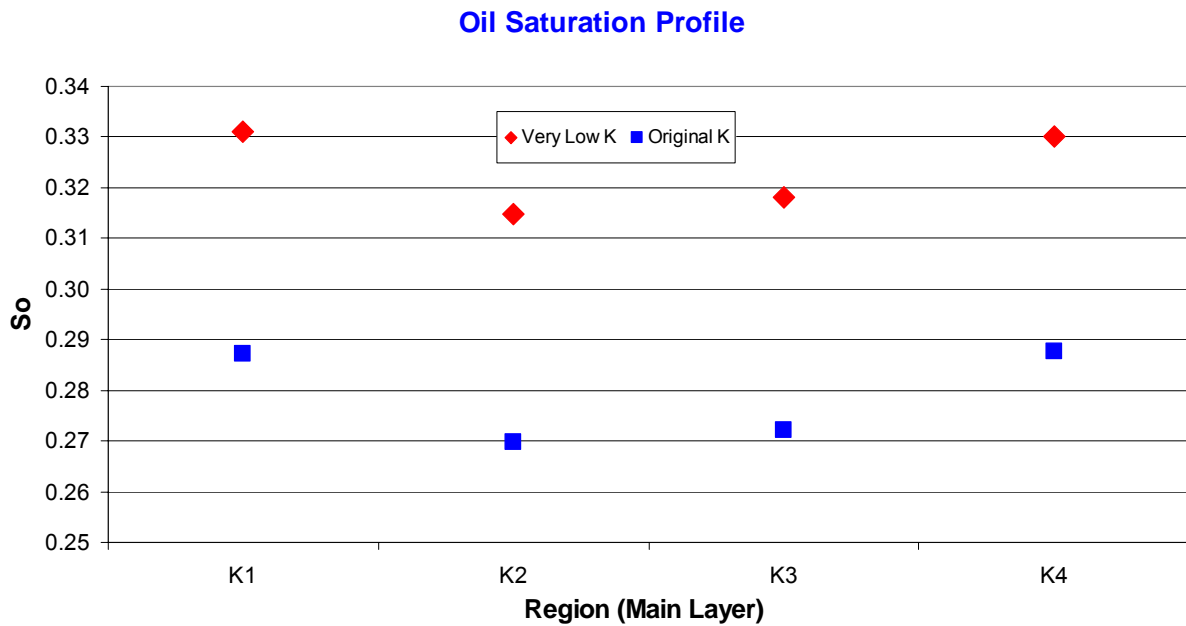


Fig. 49 – Permeability effect on Oil Saturation profile

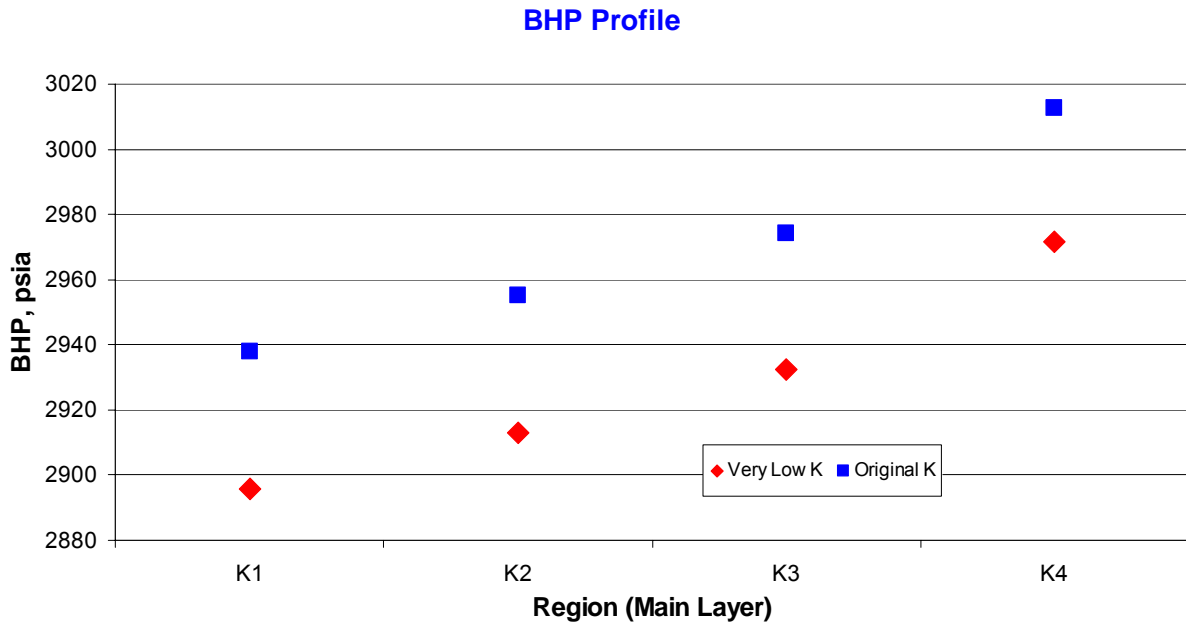


Fig. 50 – Permeability effect on BHP profile

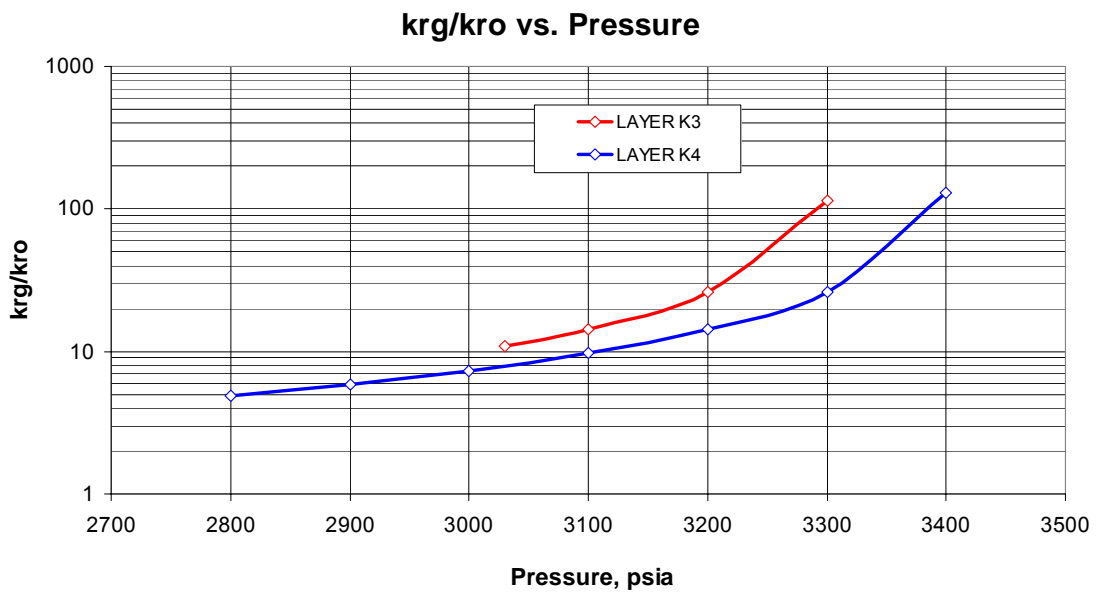


Fig. 51 – k_{rg}/k_{ro} profile at OGR = 22.6 STB/MMSCF for K3 and K4

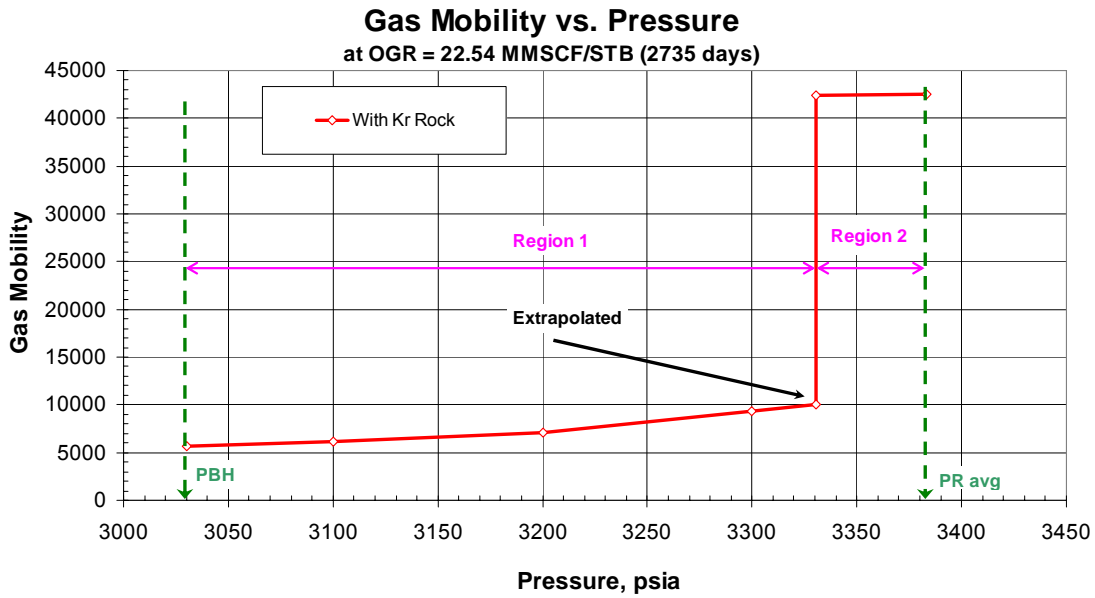


Fig. 52 – Gas mobility vs. Pressure in K3 at OGR= 22.54 STB/MMSCF (calculated by applying rock relative permeability)

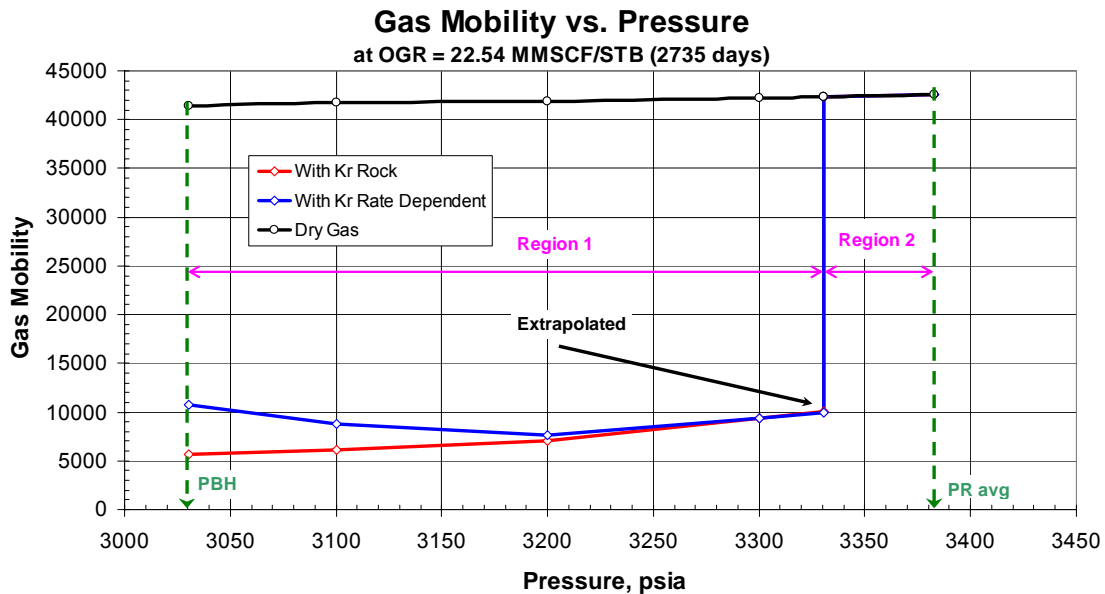


Fig. 53 – Gas mobility vs. Pressure Comparison in K3 at OGR= 22.54 STB/MMSCF

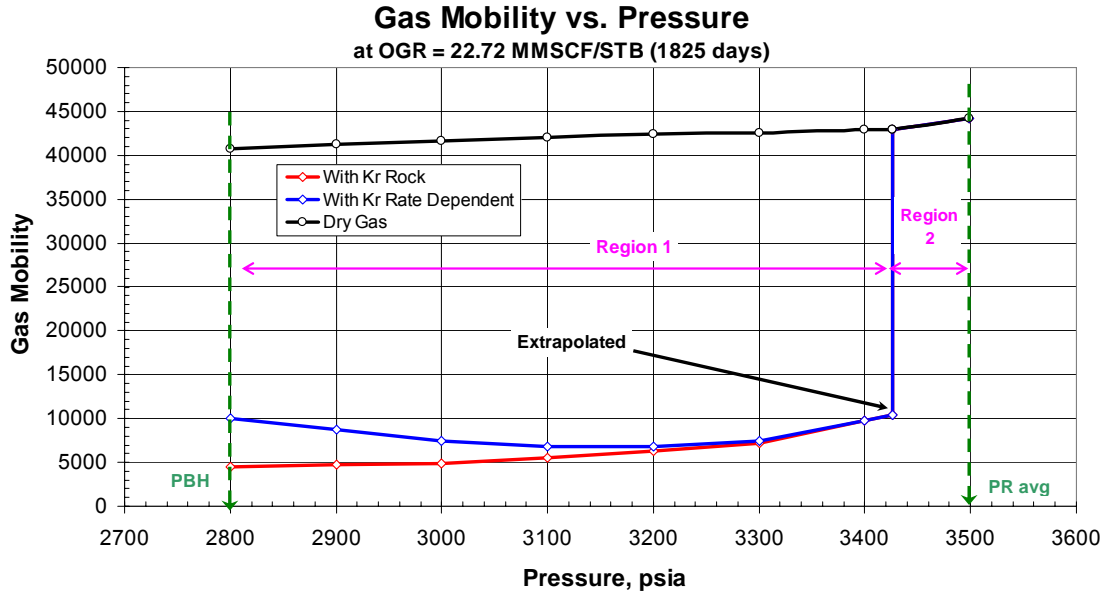


Fig. 54 – Gas mobility vs. Pressure Comparison in K4 at OGR= 22.72 STB/MMSCF

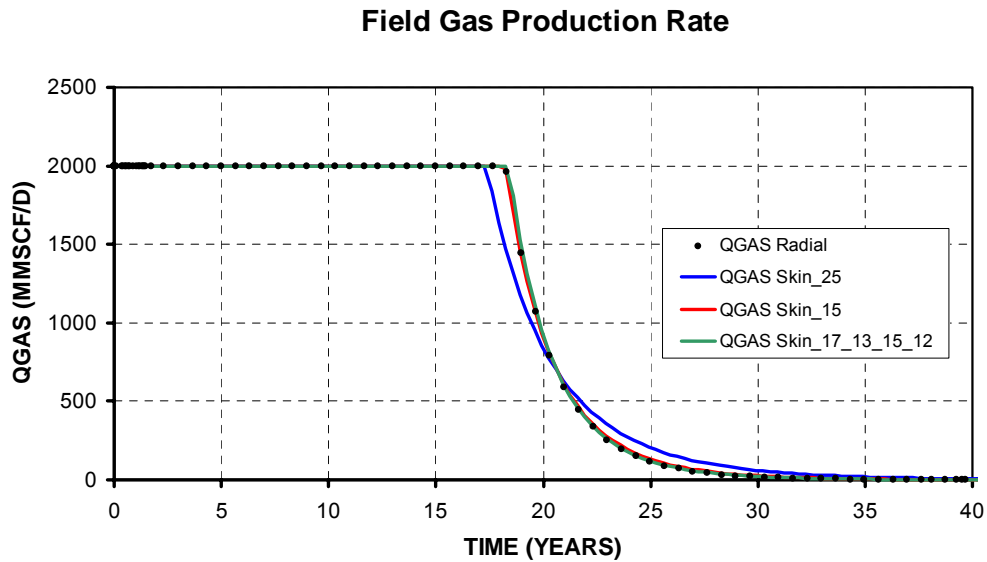


Fig. 55 – Field Gas Production Rate Matching Plots for Corey-like Exponent = 3

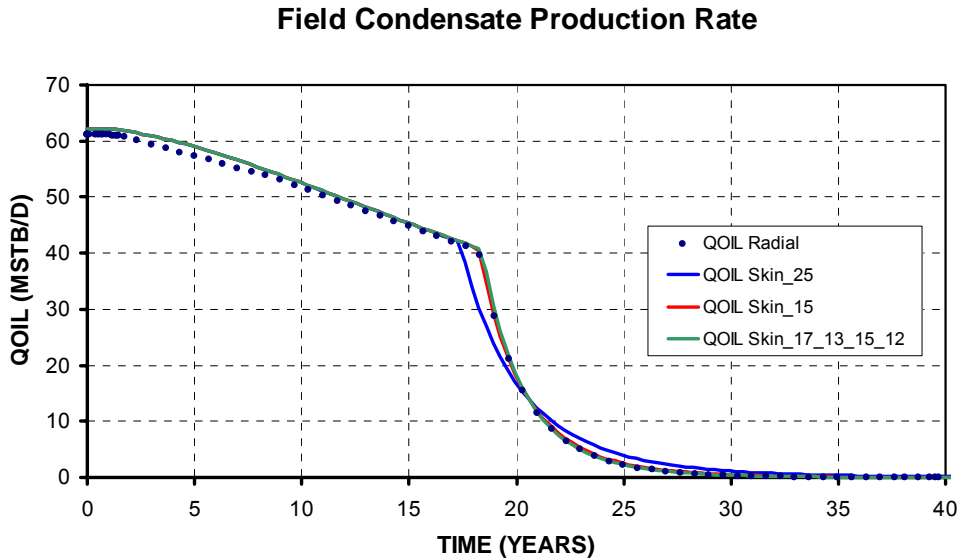


Fig. 56 – Field Condensate Production Rate Matching Plots for Corey-like Exponent = 3

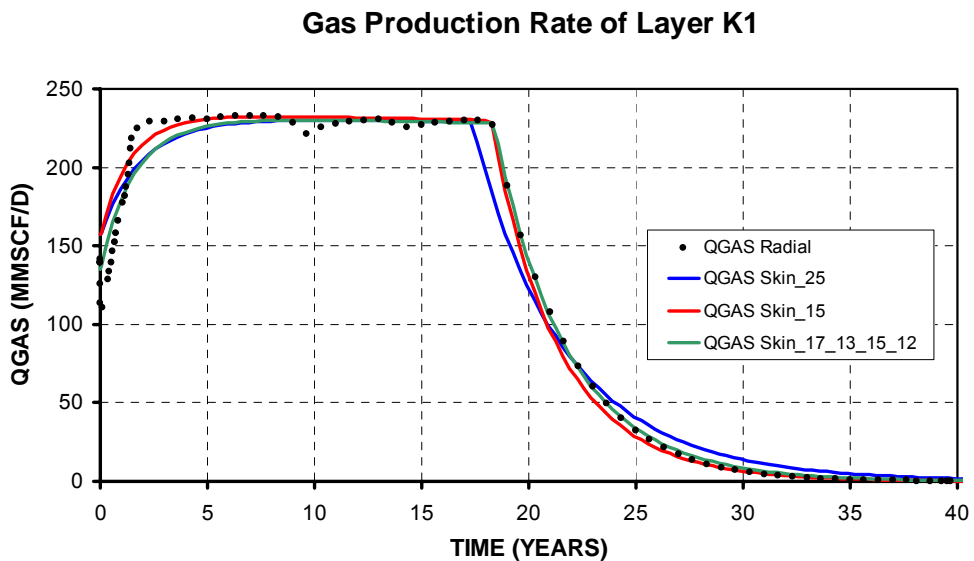


Fig. 57 – K1 Gas Production Rate Matching Plots for Corey-like Exponent = 3

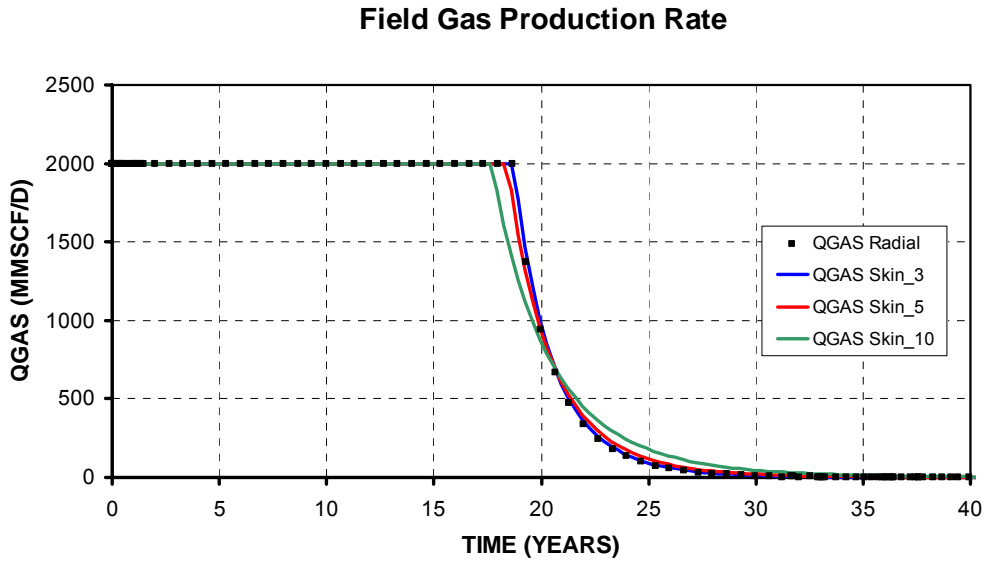


Fig. 58 – Field Gas Production Rate Matching Plots for Corey-like Exponent = 1.5

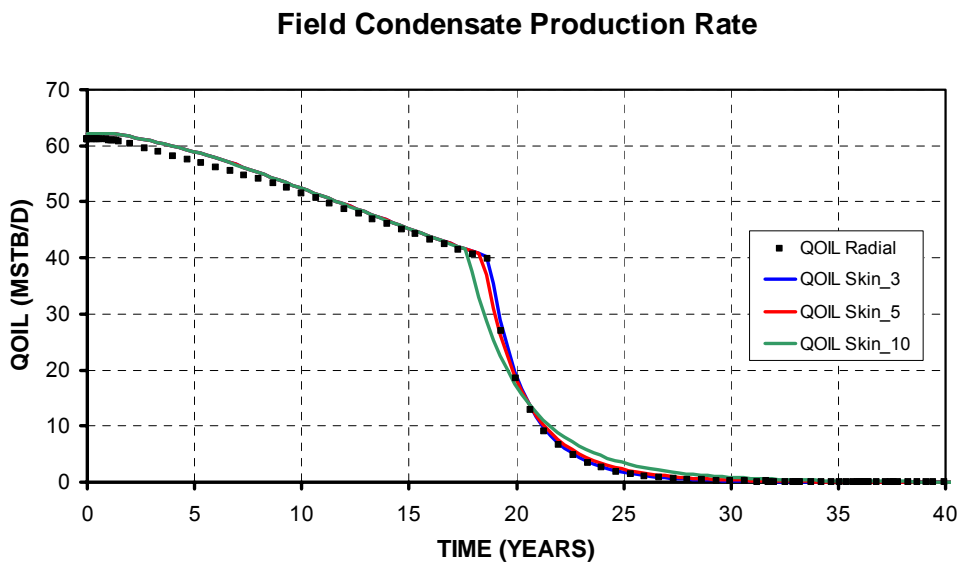


Fig. 59 – Field Condensate Production Rate Matching Plots for Corey-like Exponent = 1.5

Gas Production Rate of Layer K2

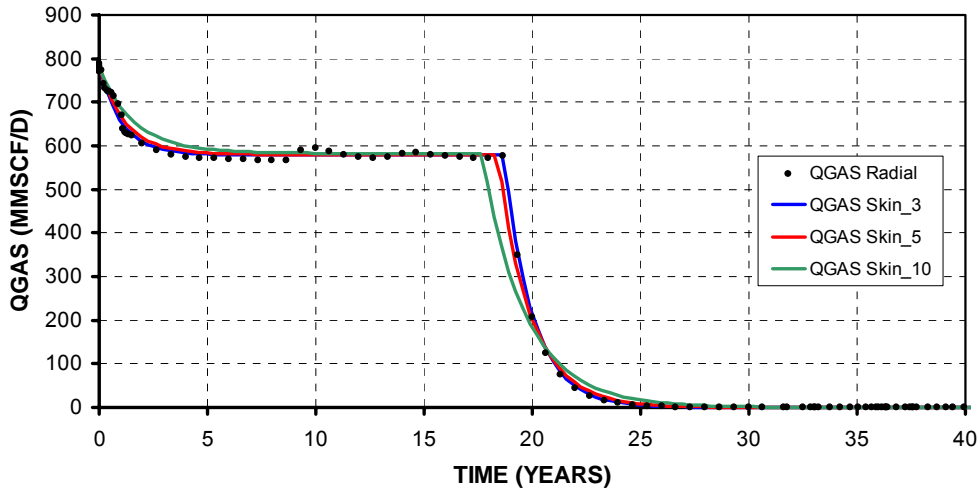


Fig. 60 – K2 Gas Production Rate Matching Plots for Corey-like Exponent = 1.5

Field Gas Production Rate

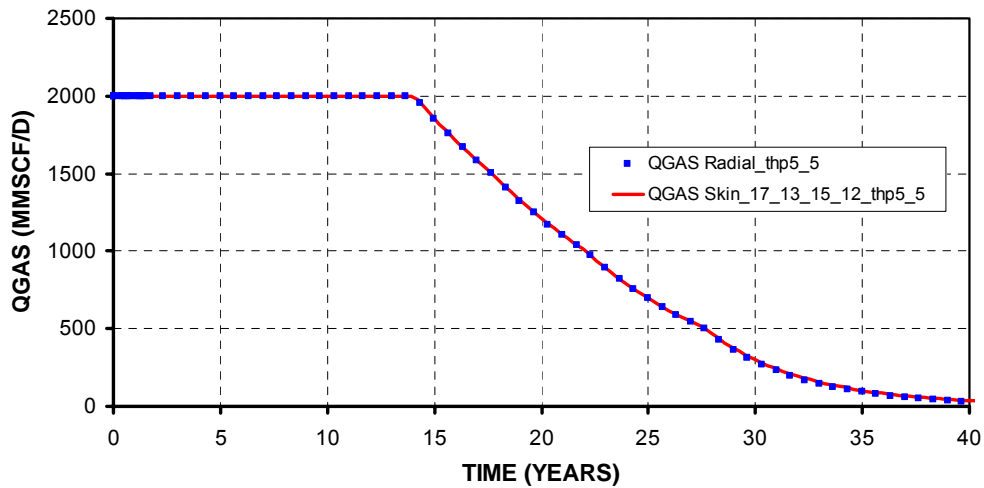


Fig. 61 – Field Gas Production Rate Matching Plots for Corey-like Exponent = 3 and production tubing size 5.5”

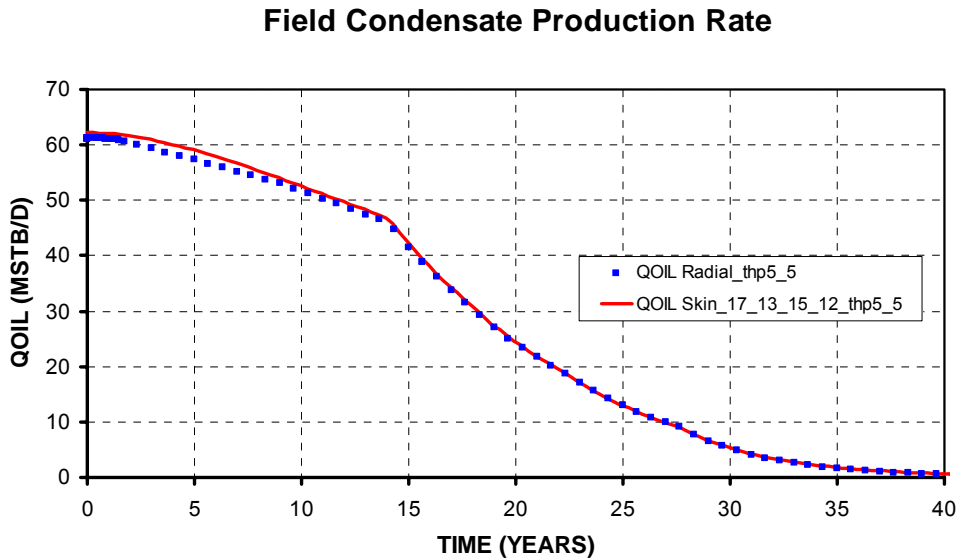


Fig. 62 – Field Condensate Production Rate Matching Plots for Corey-like Exponent = 3 and production tubing size 5.5”

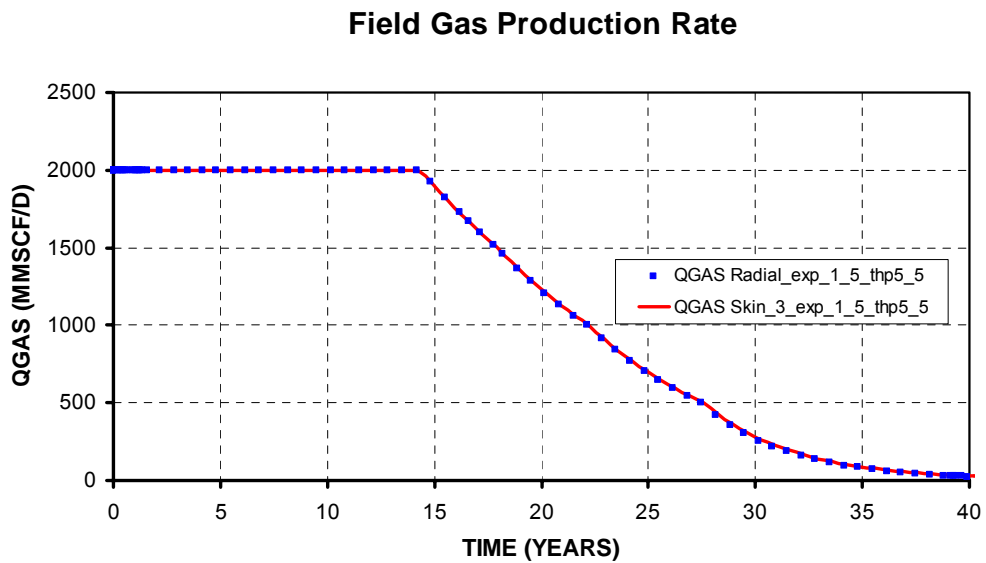


Fig. 63 – Field Gas Production Rate Matching Plots for Corey-like Exponent = 1.5 and production tubing size 5.5”

Field Condensate Production Rate

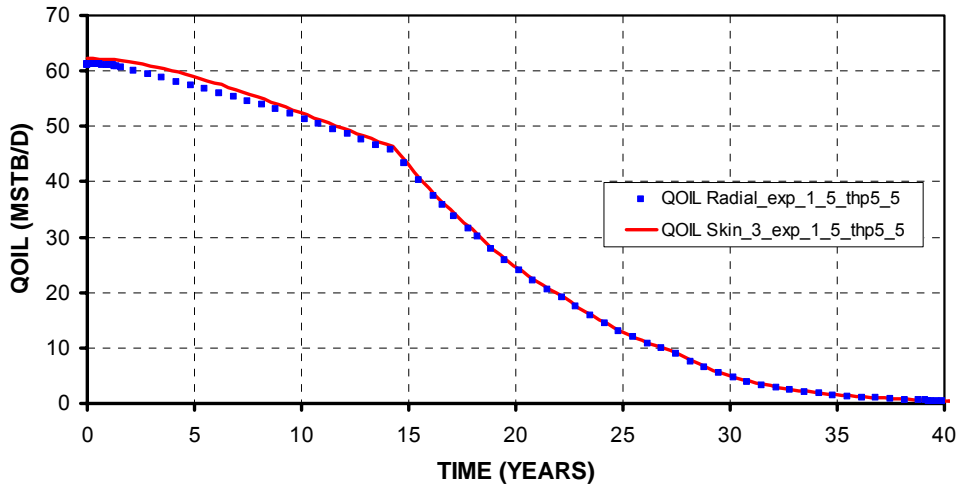


Fig. 64 – Field Condensate Production Rate Matching Plots for Corey-like Exponent = 1.5 and production tubing size 5.5”

Field Gas Production Rate

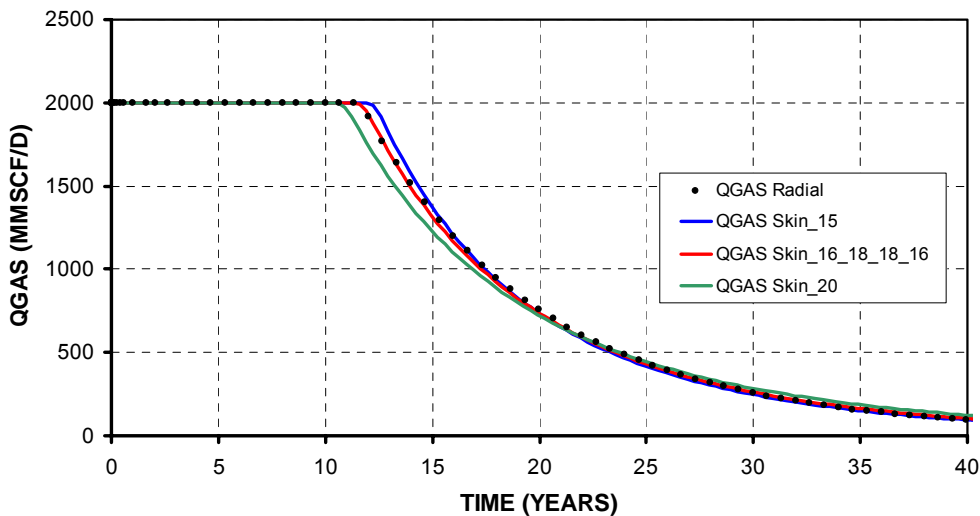


Fig. 65 – Field Gas Production Rate Matching Plots for Lower Permeability Model with Corey-like Exponent = 3

Field Condensate Production Rate

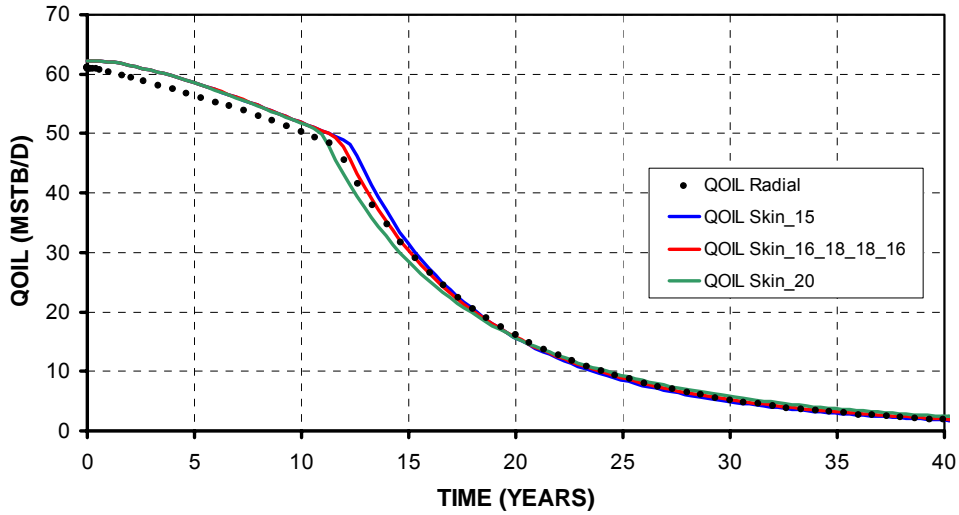


Fig. 66 – Field Condensate Production Rate Matching Plots for Lower Permeability Model with Corey-like Exponent = 3

Field Gas Production Rate

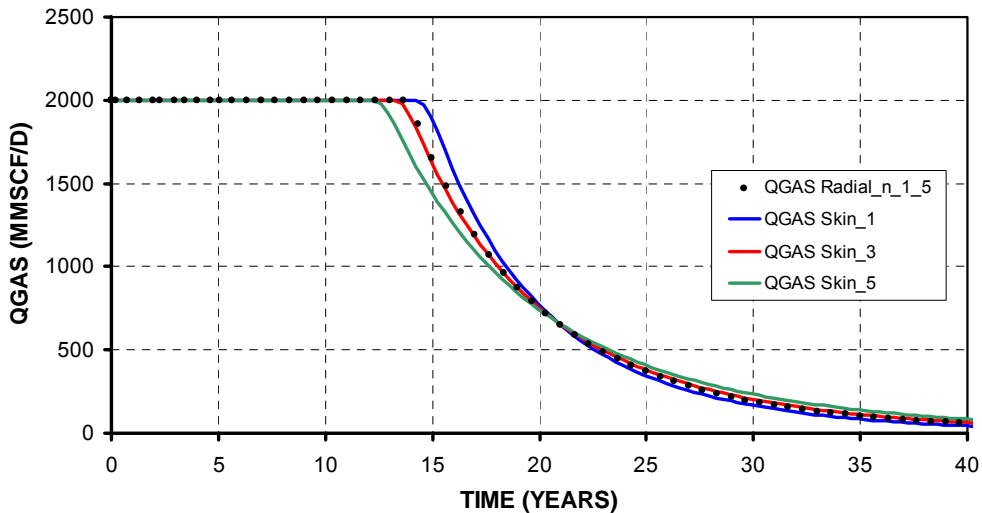


Fig. 67 – Field Gas Production Rate Matching Plots for Lower Permeability Model with Corey-like Exponent = 1.5

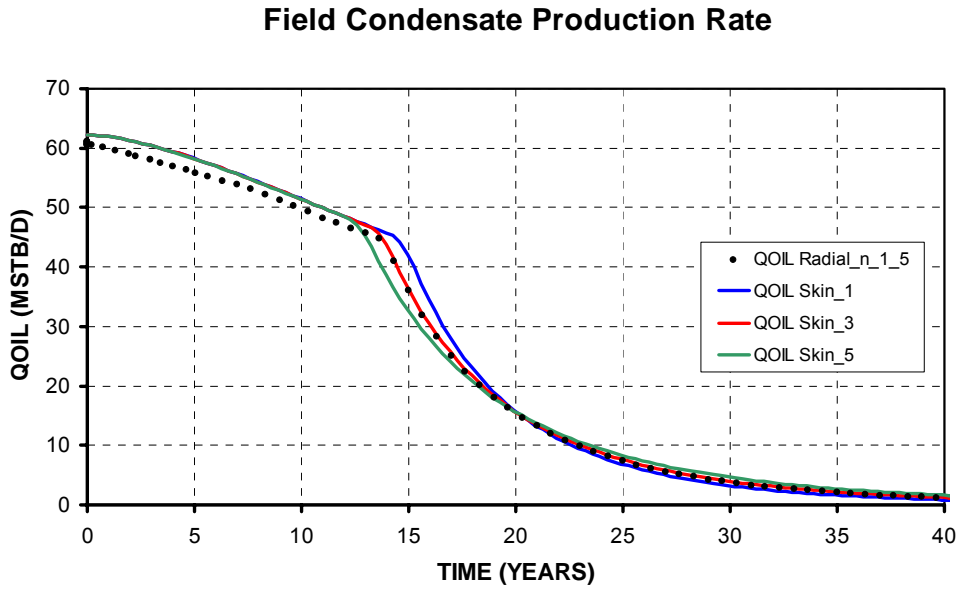


Fig. 68 – Field Condensate Production Rate Matching Plots for Lower Permeability Model with Corey-like Exponent = 1.5

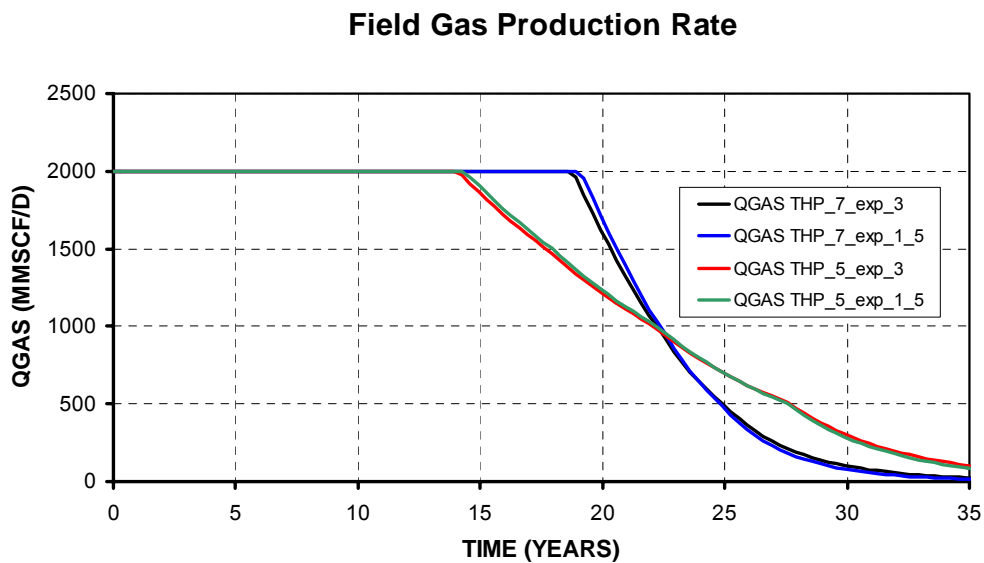


Fig. 69 – Field Gas Production Rate for different Corey-like exponent and Production tubing size

Field Condensate Production Rate

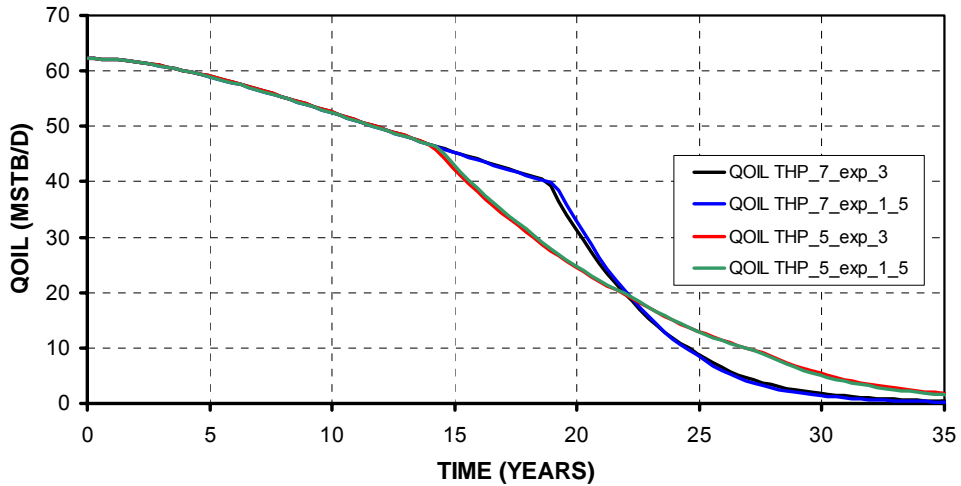


Fig. 70 – Field Condensate Production Rate for different Corey-like exponent and Production tubing size

Field GOR

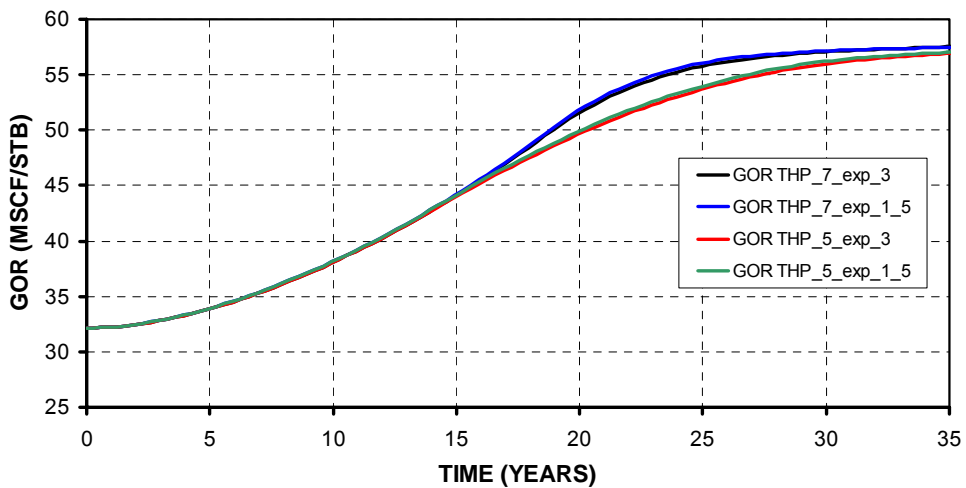


Fig. 71 –Gas Oil Ratio for different Corey-like exponent and Production tubing size

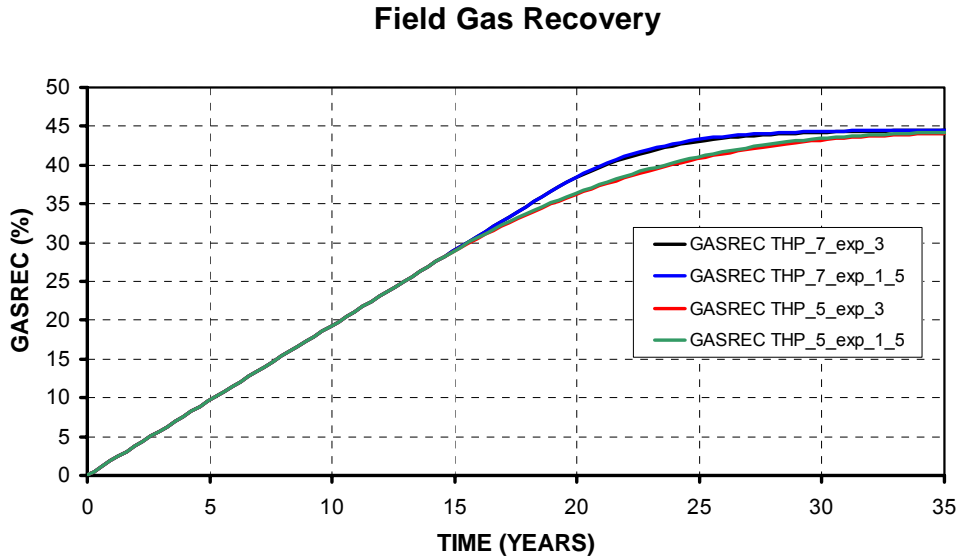


Fig. 72 – Field Gas Recovery for different Corey-like exponent and Production tubing size

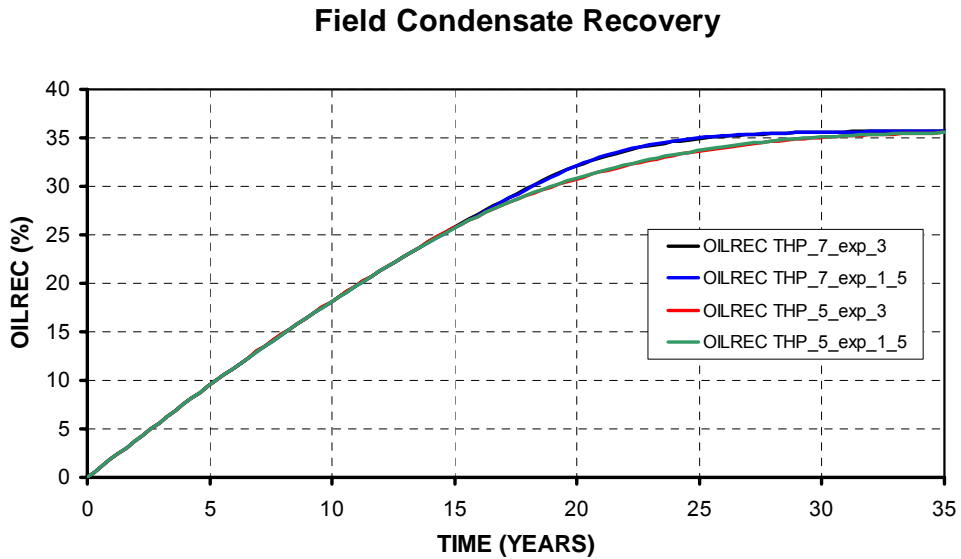


Fig. 73 – Field Condensate Recovery for different Corey-like exponent and Production tubing size

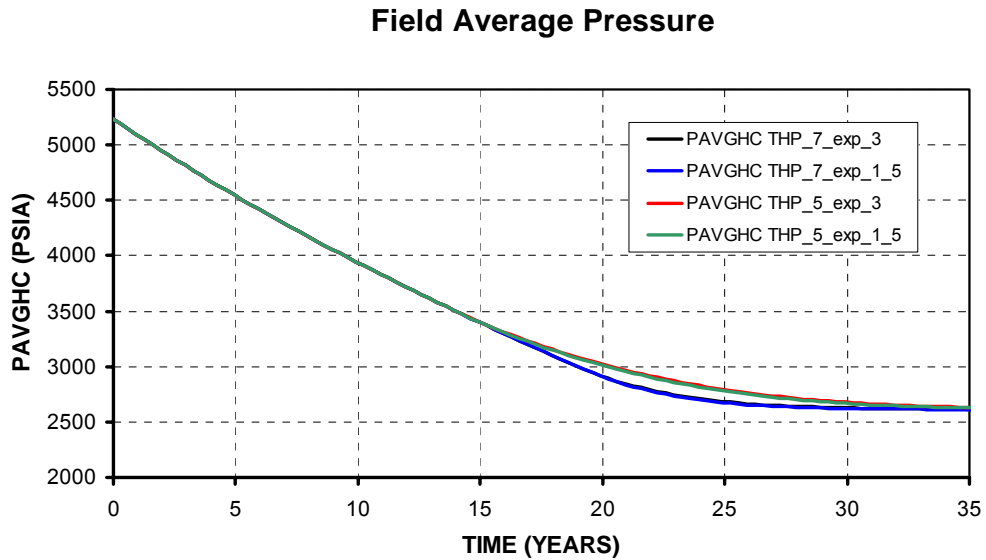


Fig. 74 – Field Average Pressure for different Corey-like exponent and Production tubing size

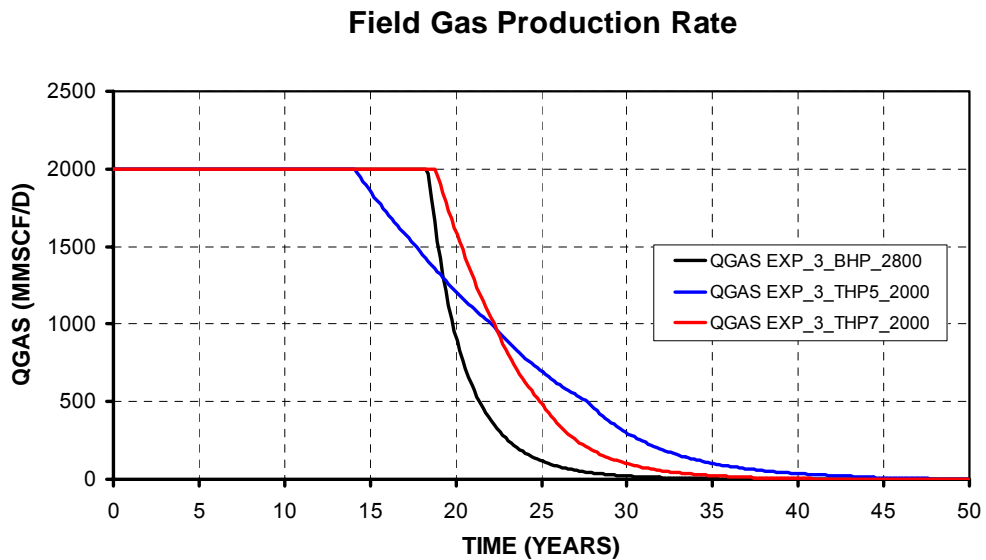


Fig. 75 – Field Gas Production Rate for different pressure constraints

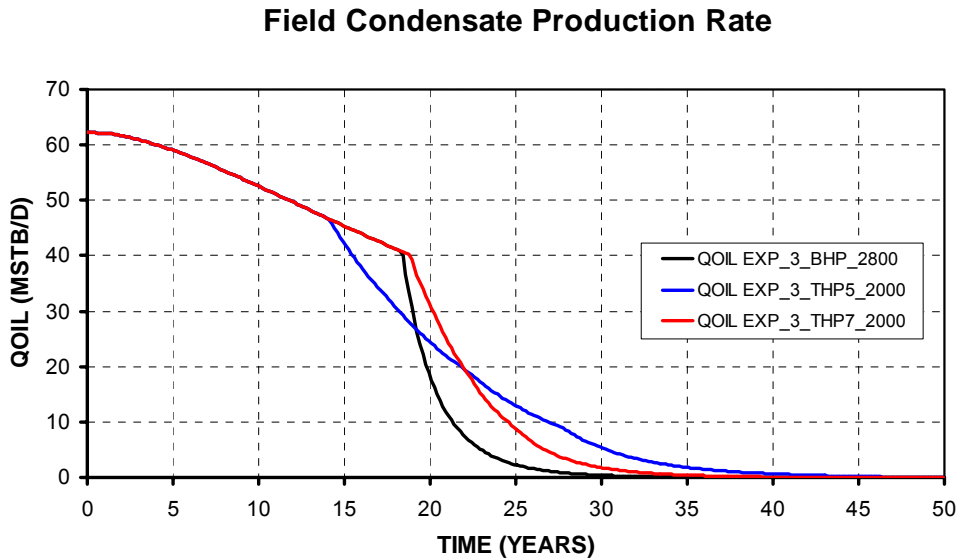


Fig. 76 – Field Condensate Production Rate for different pressure constraints

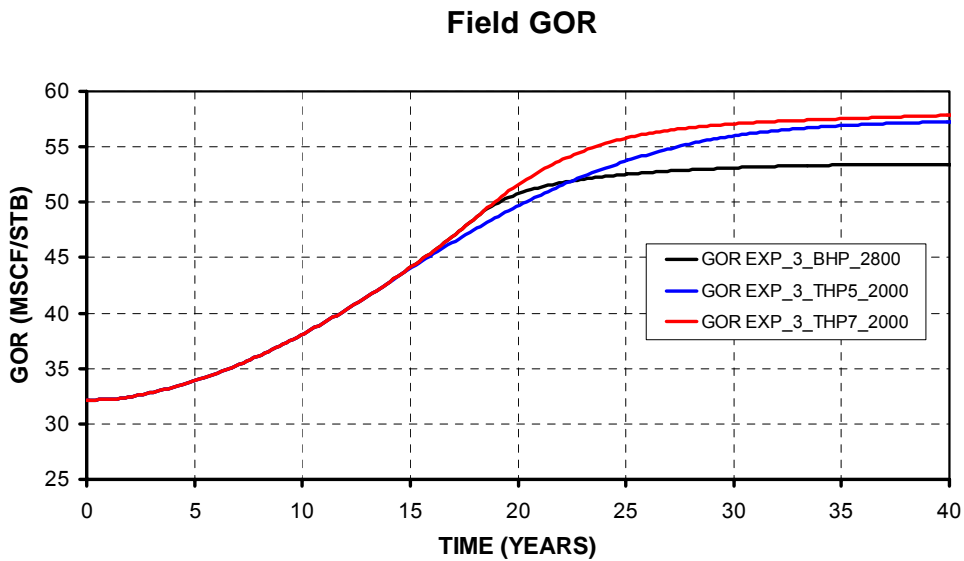


Fig. 77 –Gas Oil Ratio for different pressure constraints

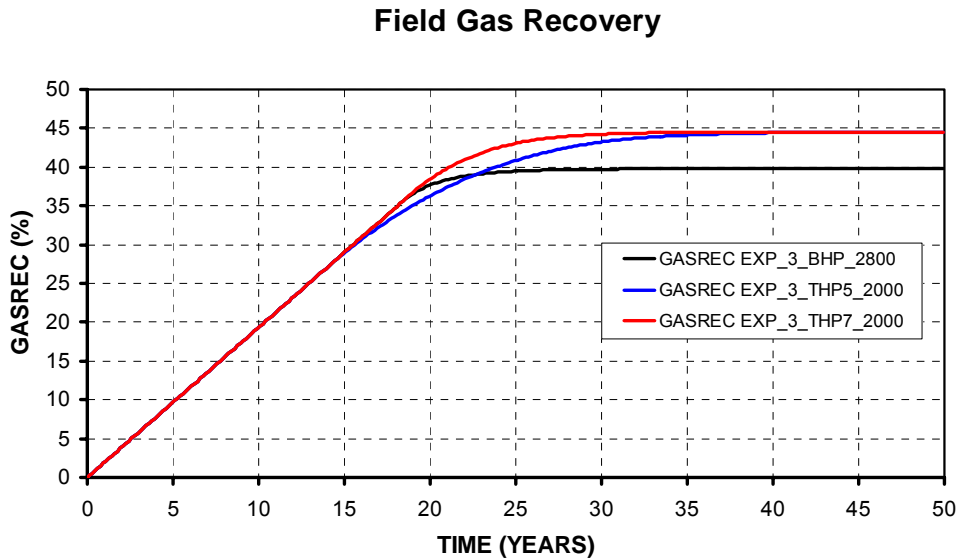


Fig. 78 – Field Gas Recovery for different pressure constraints

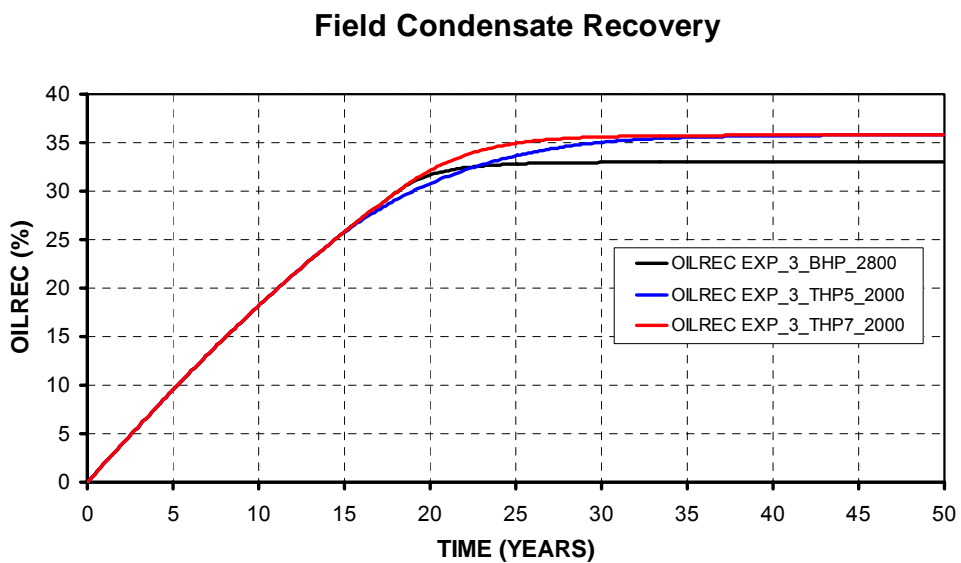


Fig. 79 – Field Condensate Recovery for different pressure constraints

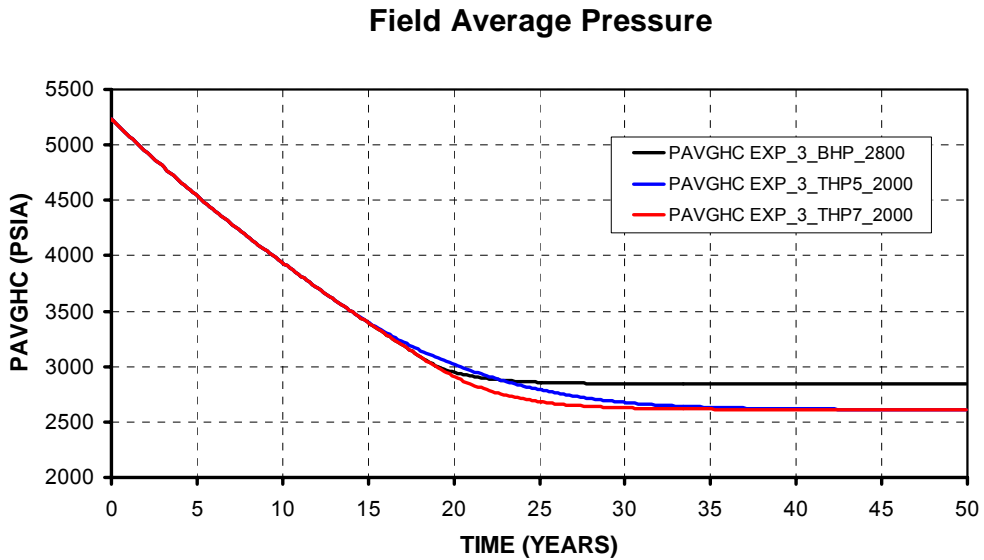


Fig. 80 – Field Average Pressure for different pressure constraints

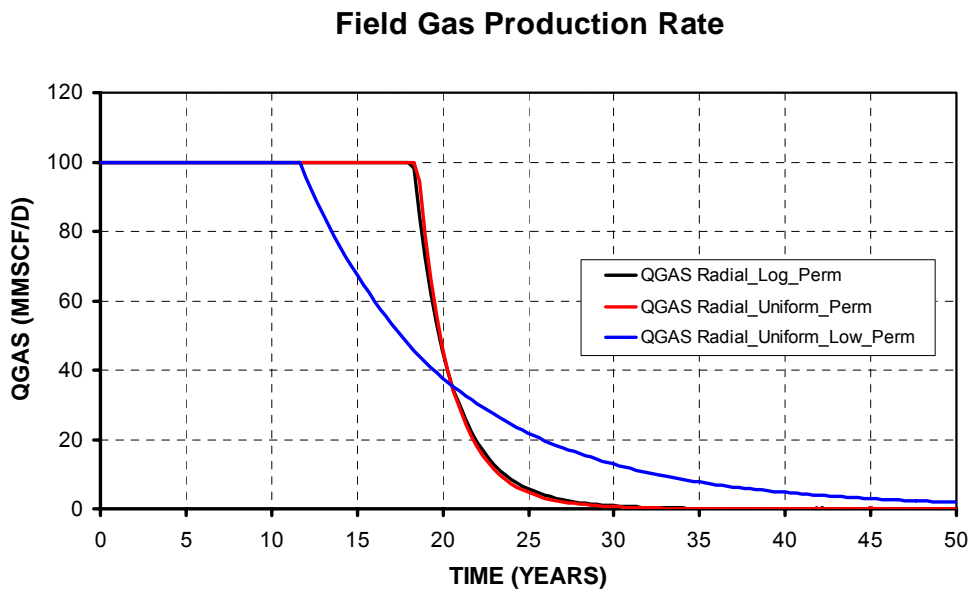


Fig. 81 – Field Gas Production Rate for different permeability distribution

Field Condensate Production Rate

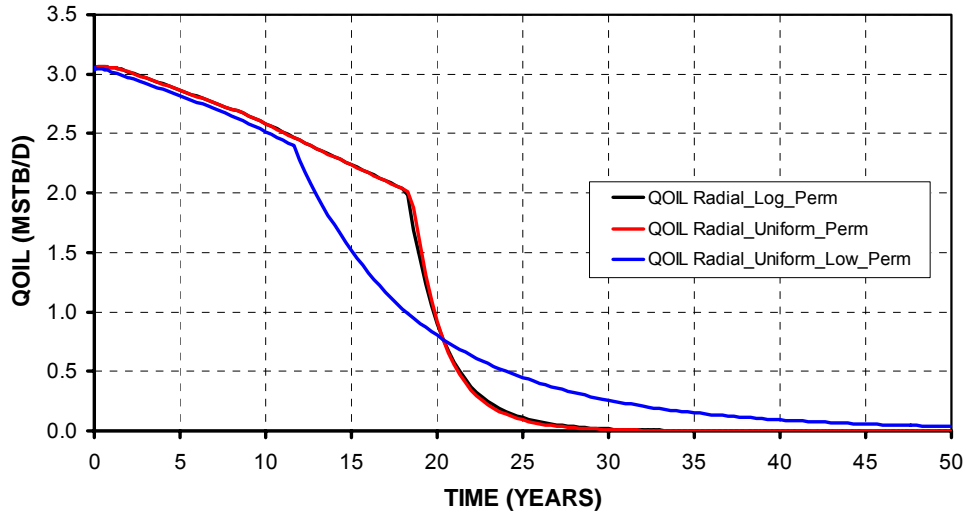


Fig. 82 – Field Condensate Production Rate for different permeability distribution

Field GOR

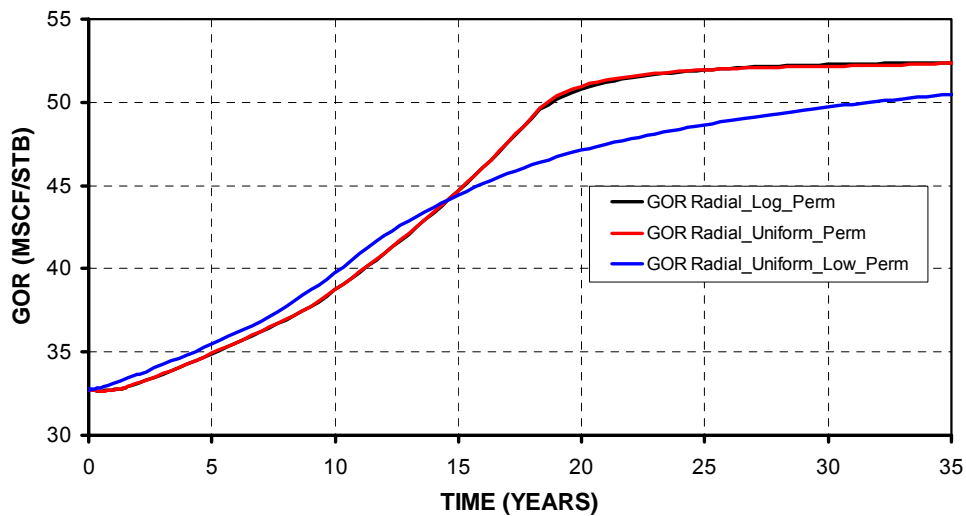


Fig. 83 –Gas Oil Ratio for different permeability distribution

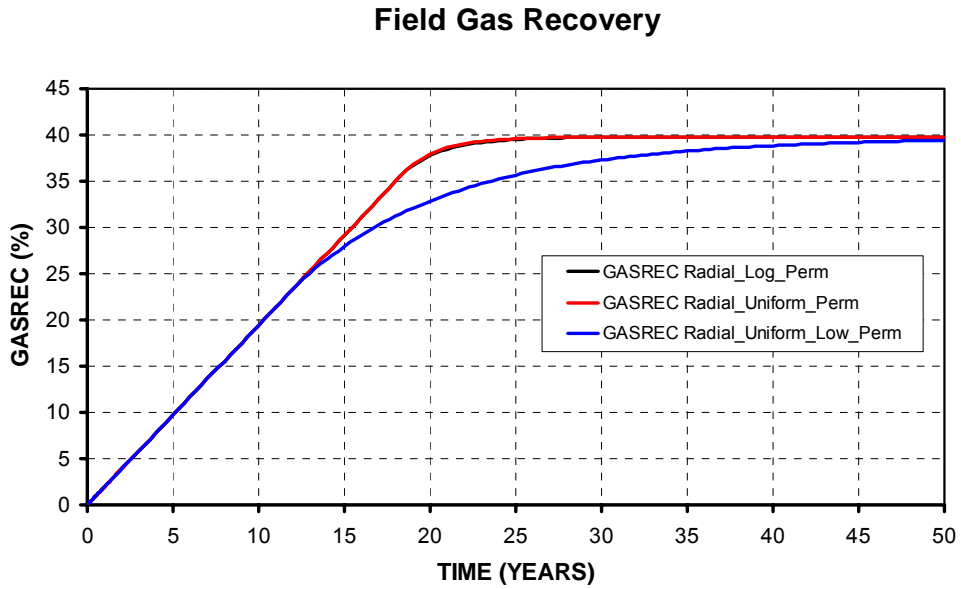


Fig. 84 – Field Gas Recovery for different permeability distribution

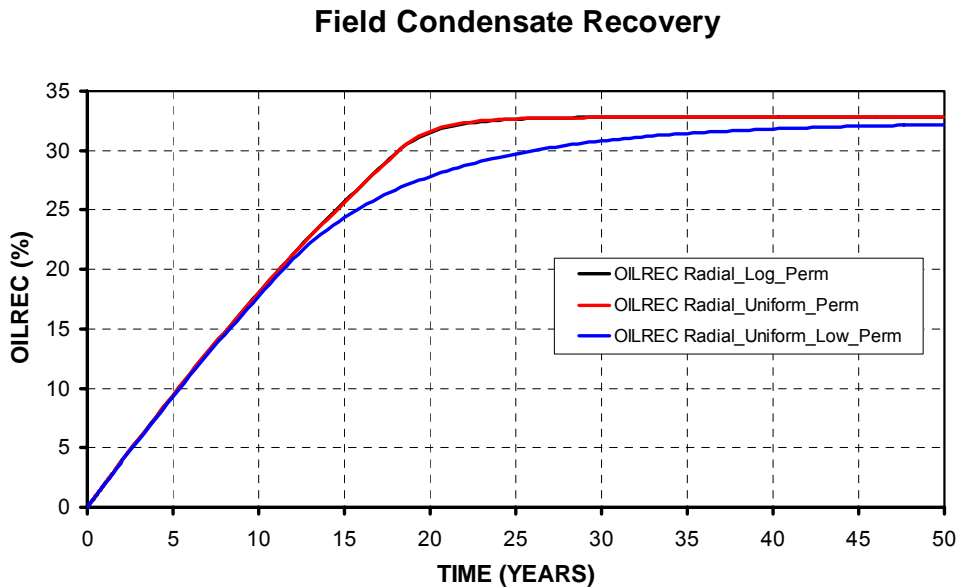


Fig. 85 – Field Condensate Recovery for different permeability distribution

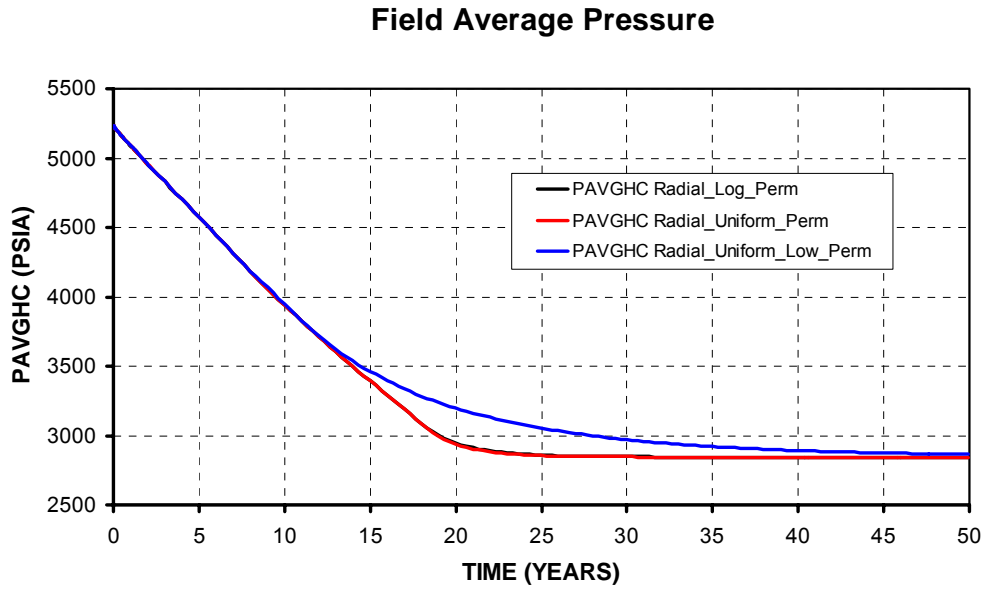


Fig. 86 – Field Average Pressure for different permeability distribution

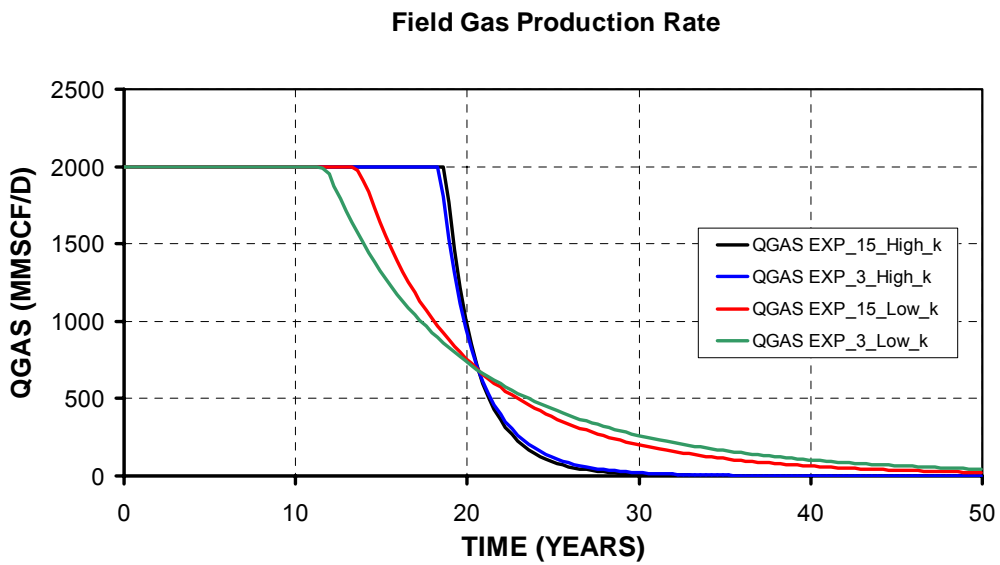


Fig. 87 – Field Gas Production Rate for different permeability distribution and Corey-like exponent

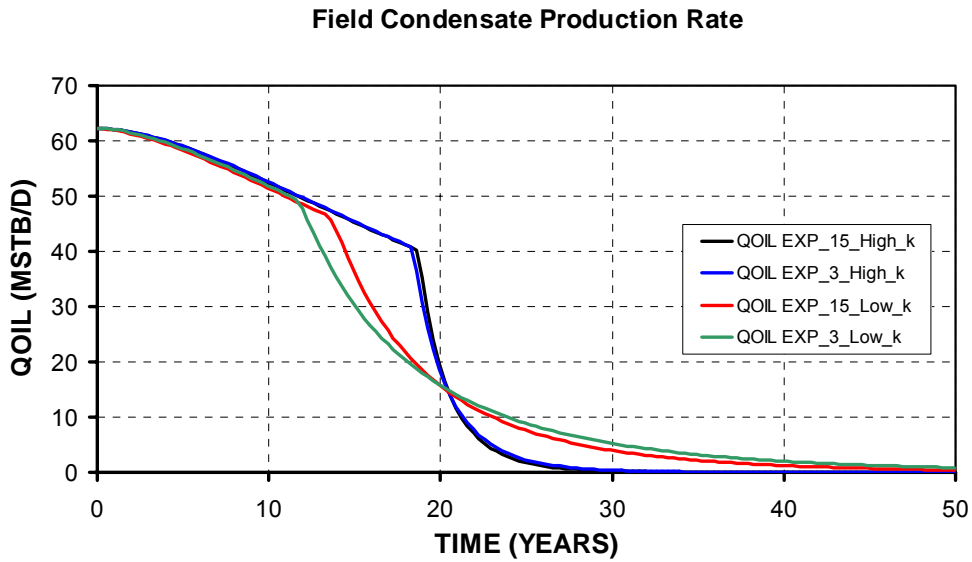


Fig. 88 – Field Condensate Production Rate for different permeability distribution and Corey-like exponent

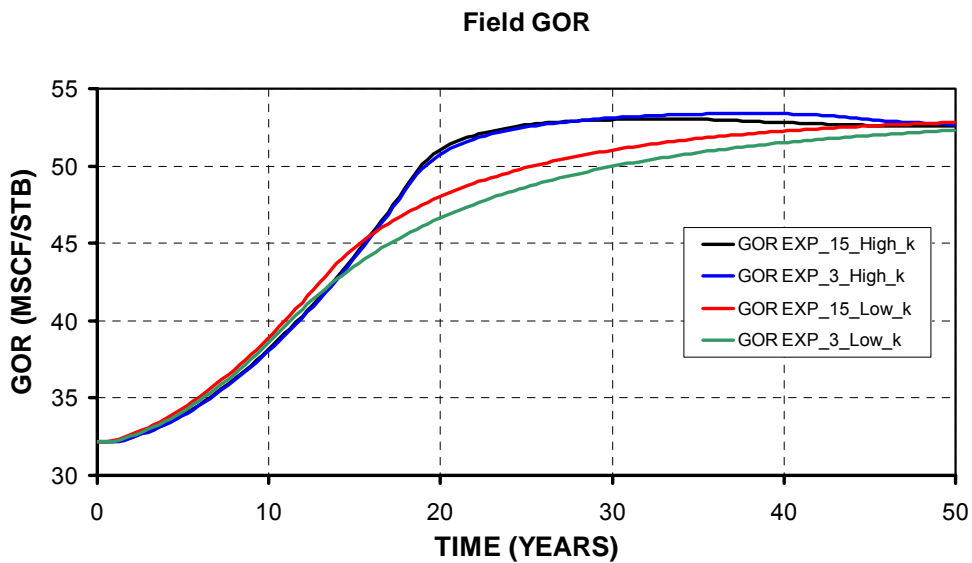


Fig. 89 –Gas Oil Ratio for different permeability distribution and Corey-like exponent

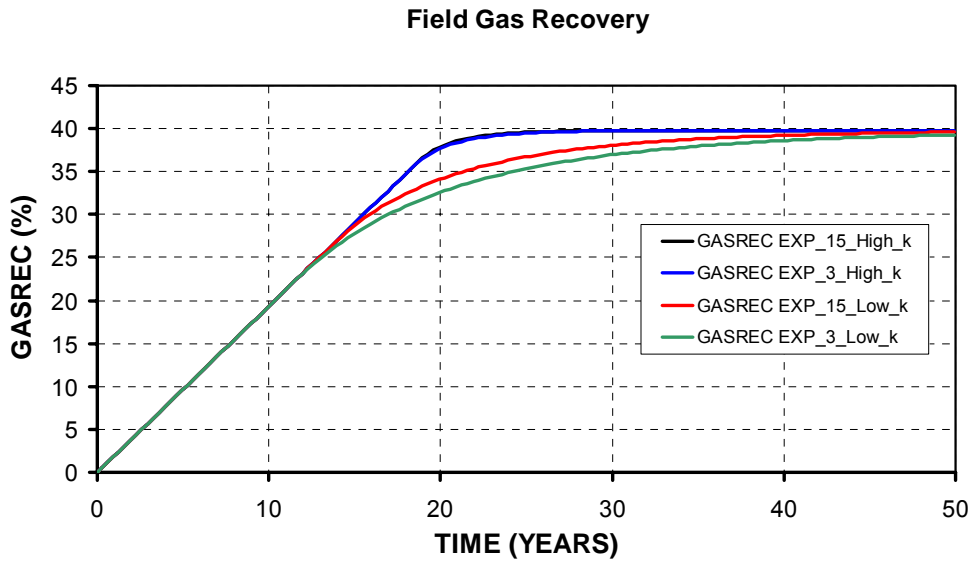


Fig. 90 – Field Gas Recovery for different permeability distribution and Corey-like exponent

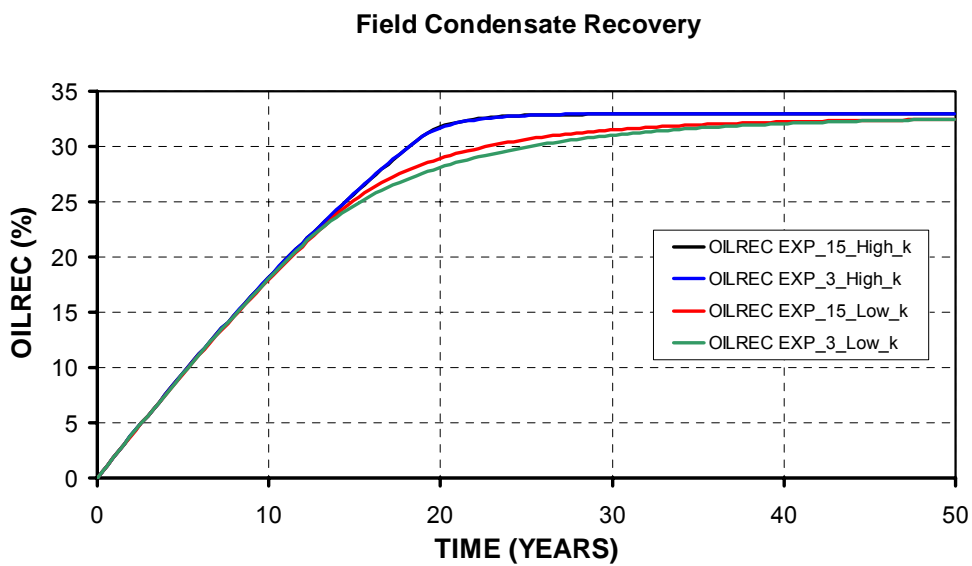


Fig. 91 – Field Condensate Recovery for different permeability distribution and Corey-like exponent

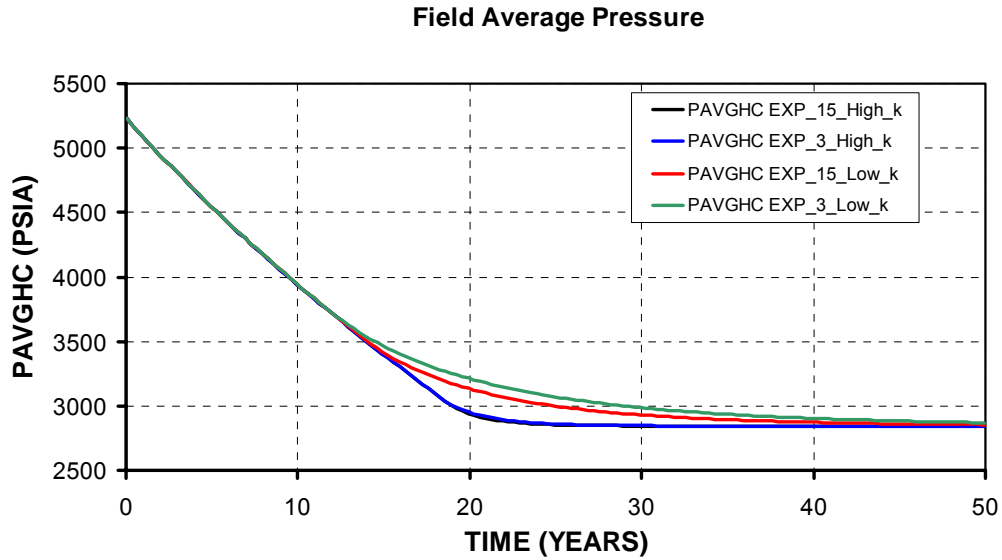


Fig. 92 – Field Average Pressure for different permeability distribution and Corey-like exponent

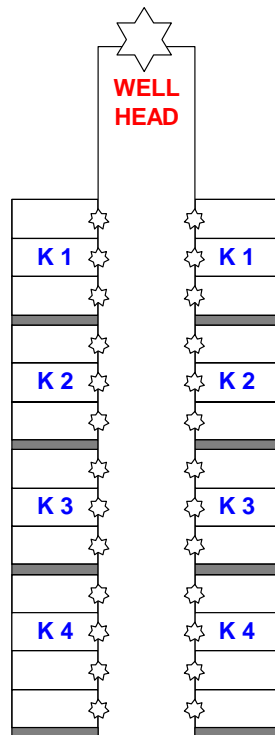


Fig. 93 – Production line structure from well connection level to well level

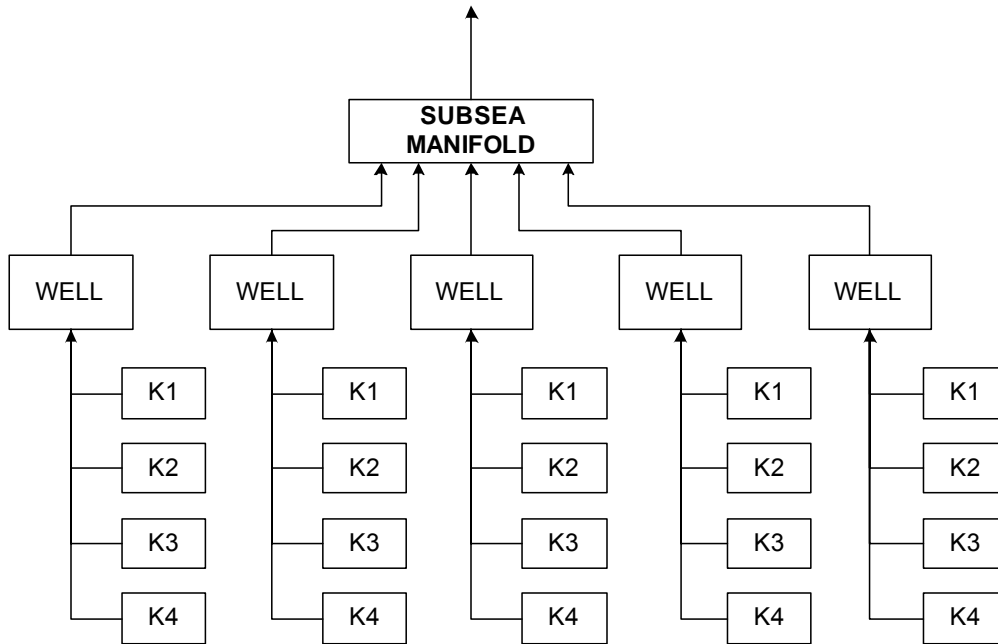


Fig. 94 – Production line structure from well connection level to sub sea manifold level

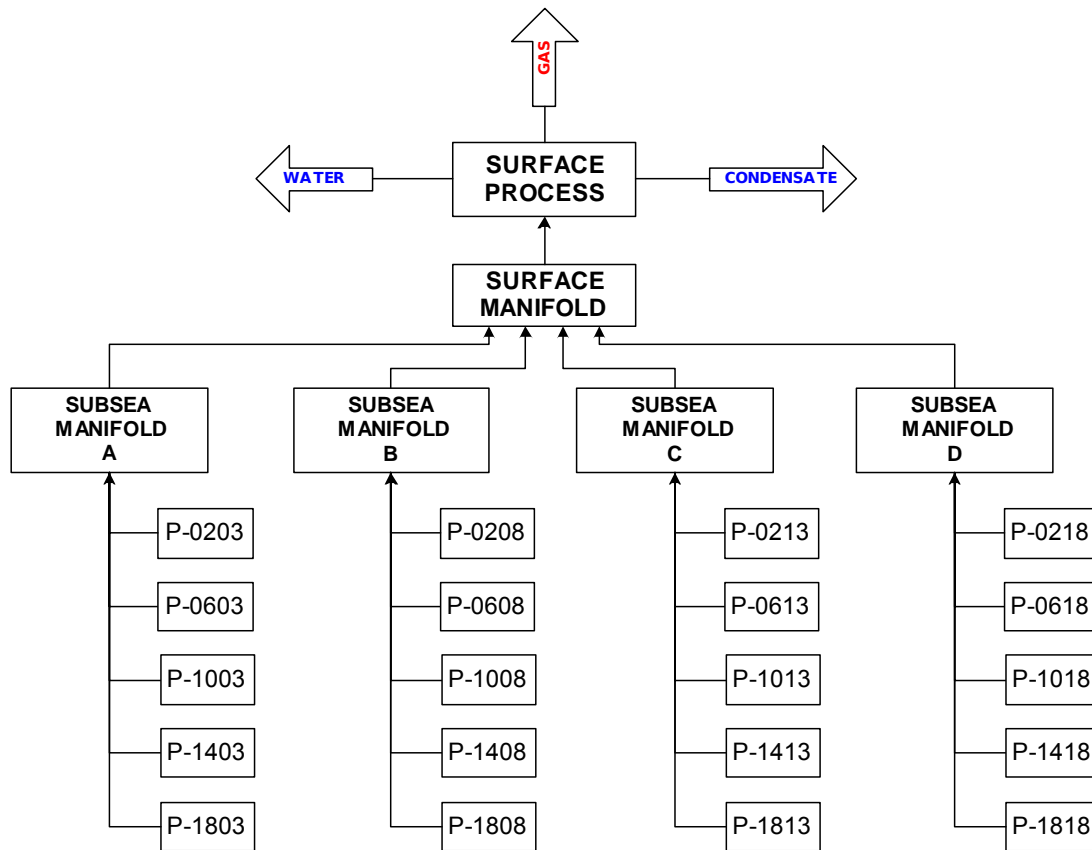


Fig. 95 – Production line structure from well level to surface process level

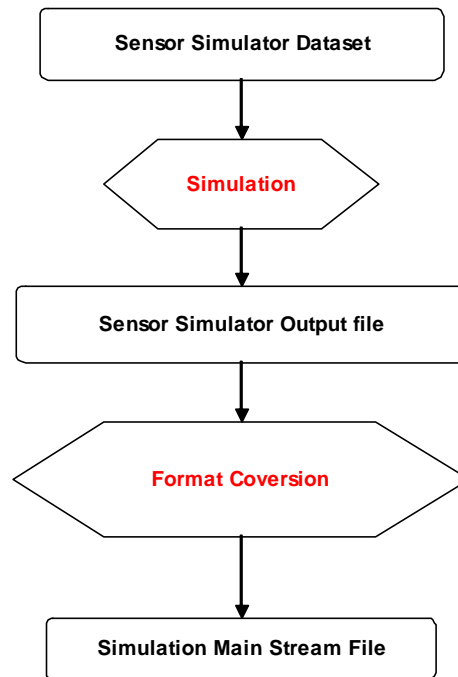


Fig. 96 – The sequence to generate main stream file from Sensor simulator dataset

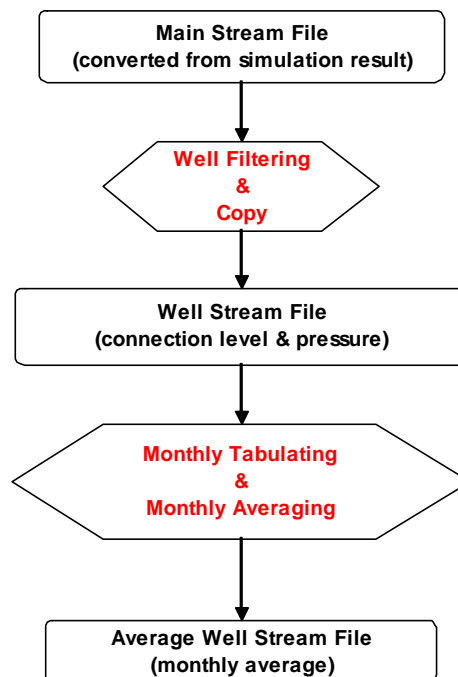


Fig. 97 – The sequence to generate stream files based on individual production well

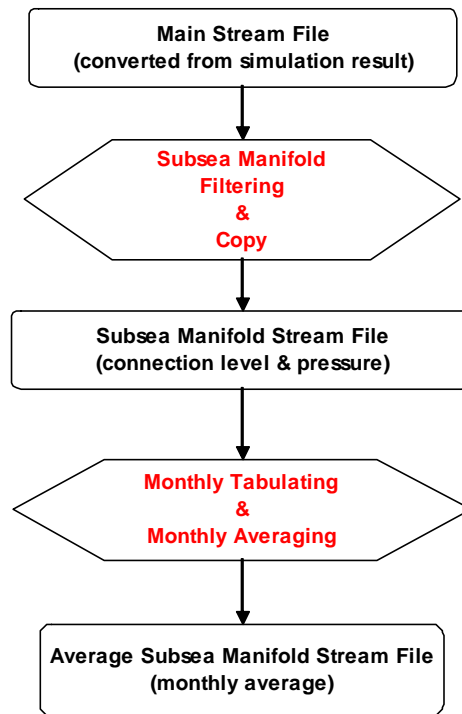


Fig. 98 – The sequence to generate stream files based on subsea manifold

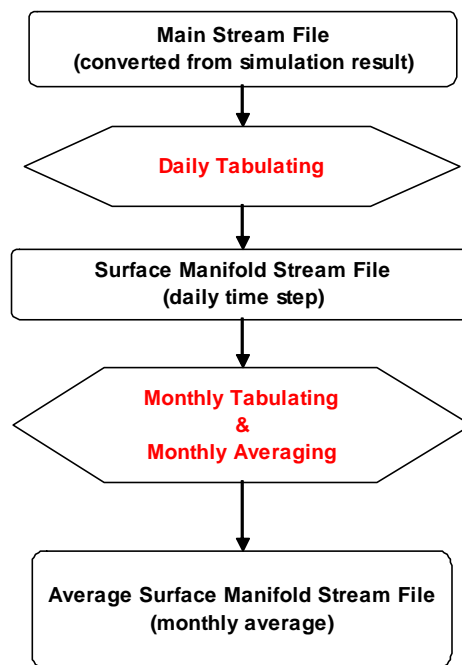


Fig. 99 – The sequence to generate stream files based on surface manifold

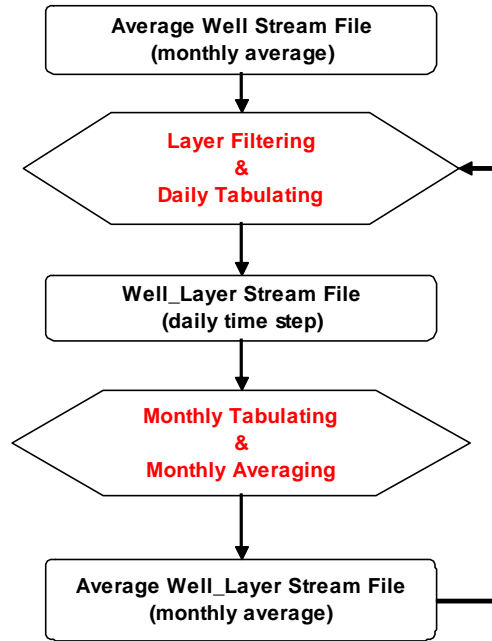


Fig. 100 – The sequence to generate stream files based on geological layer at individual production well

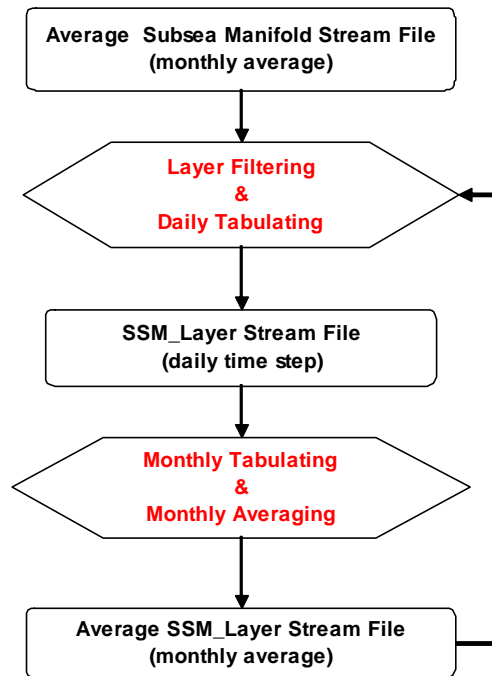


Fig. 101 – The sequence to generate stream files based on geological layer at subsea manifold

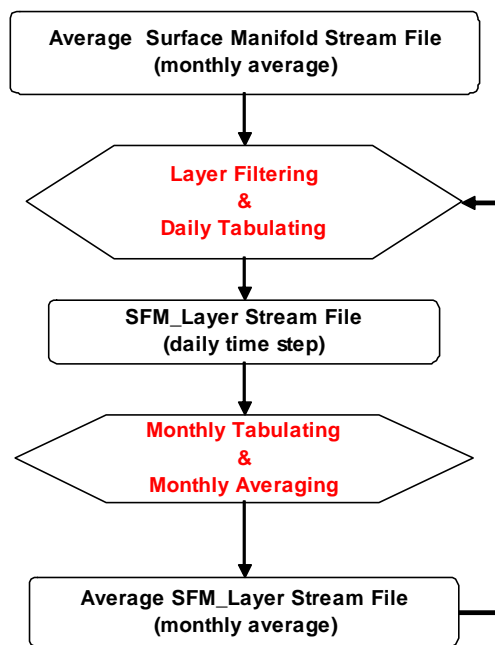


Fig. 102 – The sequence to generate stream files based on geological layer at surface manifold

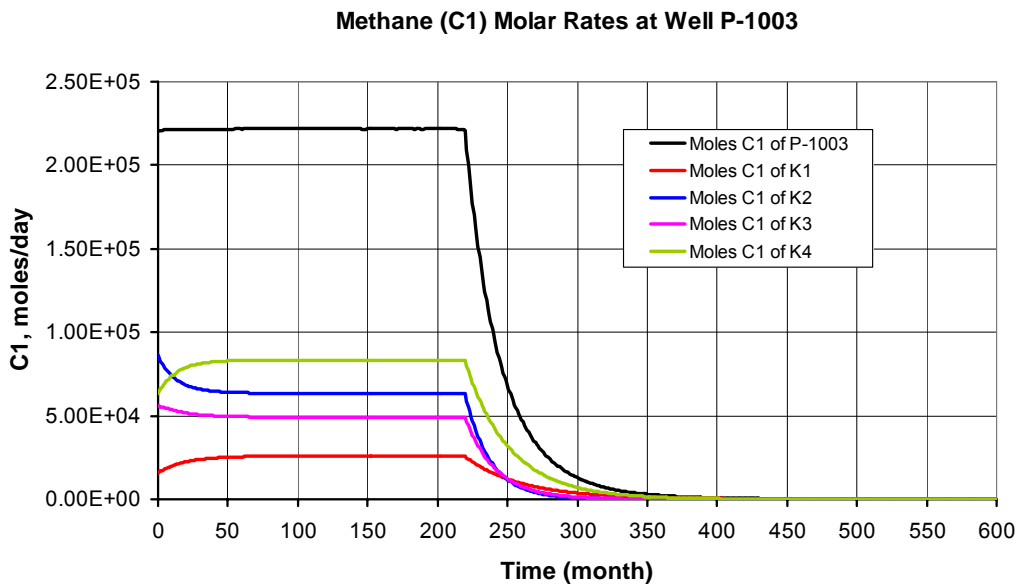


Fig. 103 – Methane molar rate at Well P-1003 and its contribution rate from the geological layers

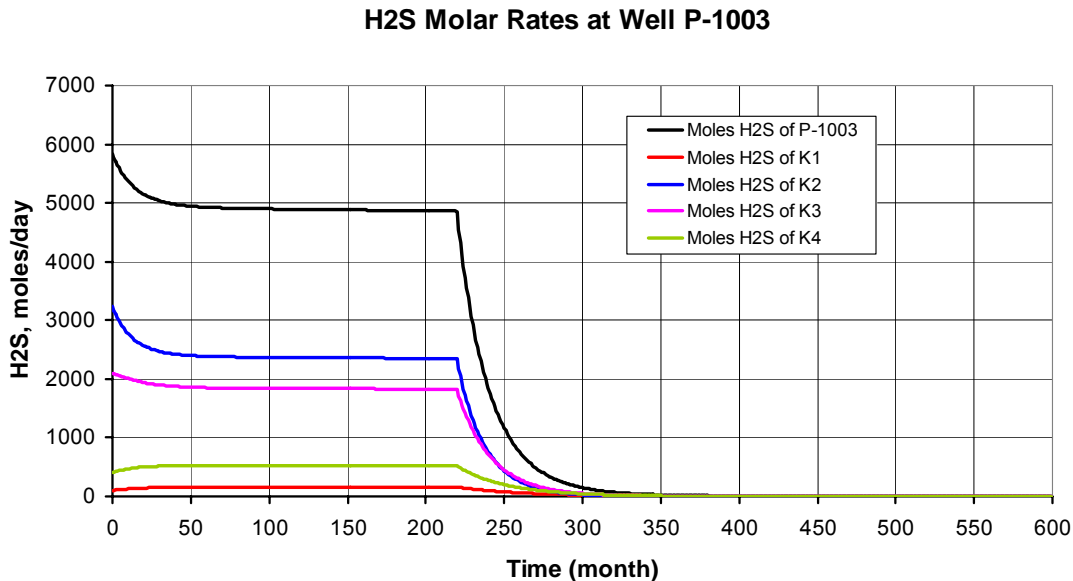


Fig. 104 – H2S molar rate at Well P-1003 and its contribution rate from the geological layers

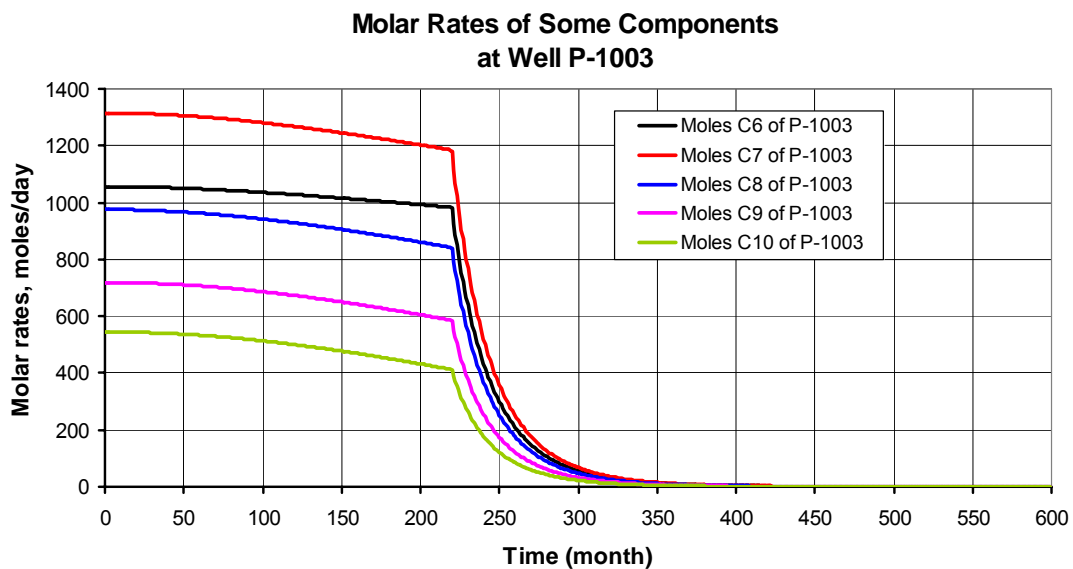


Fig. 105 – Molar rate of some components at Well P-1003

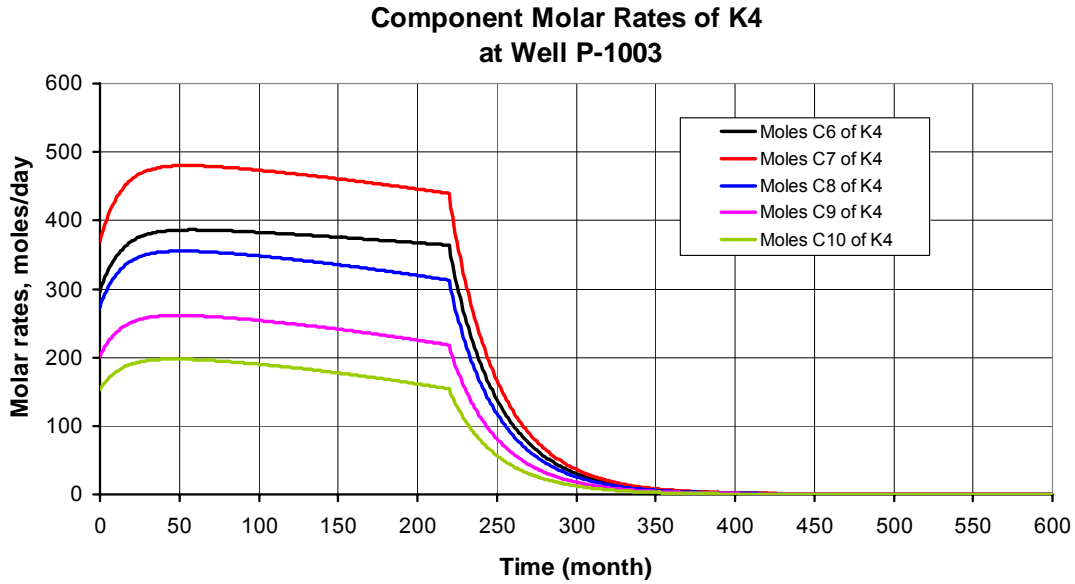


Fig. 106 – Molar rate of some components produced from Layer K4 at Well P-1003

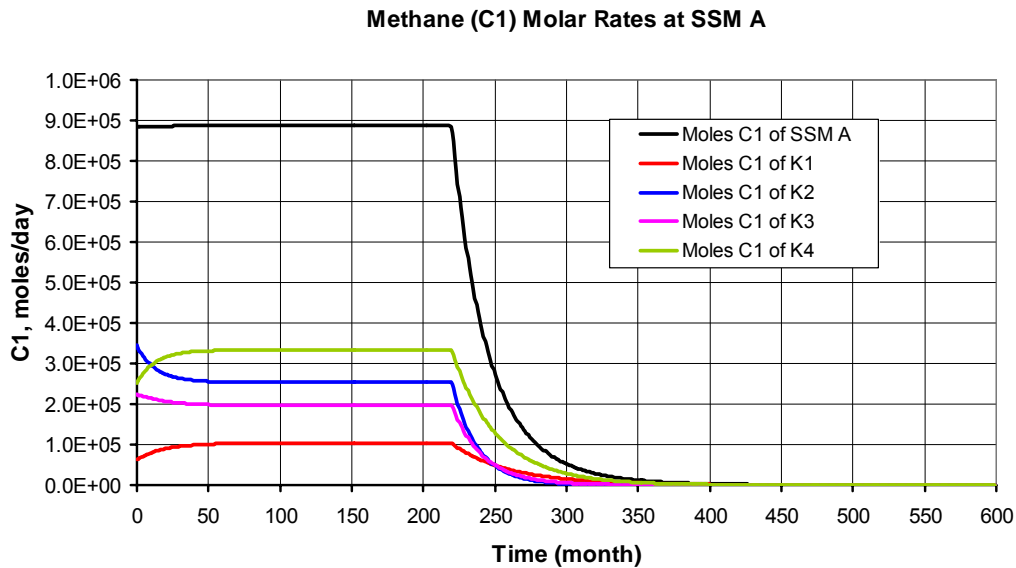


Fig. 107 – Methane molar rate at Subsea Manifold SSM A and its contribution rate from the geological layers

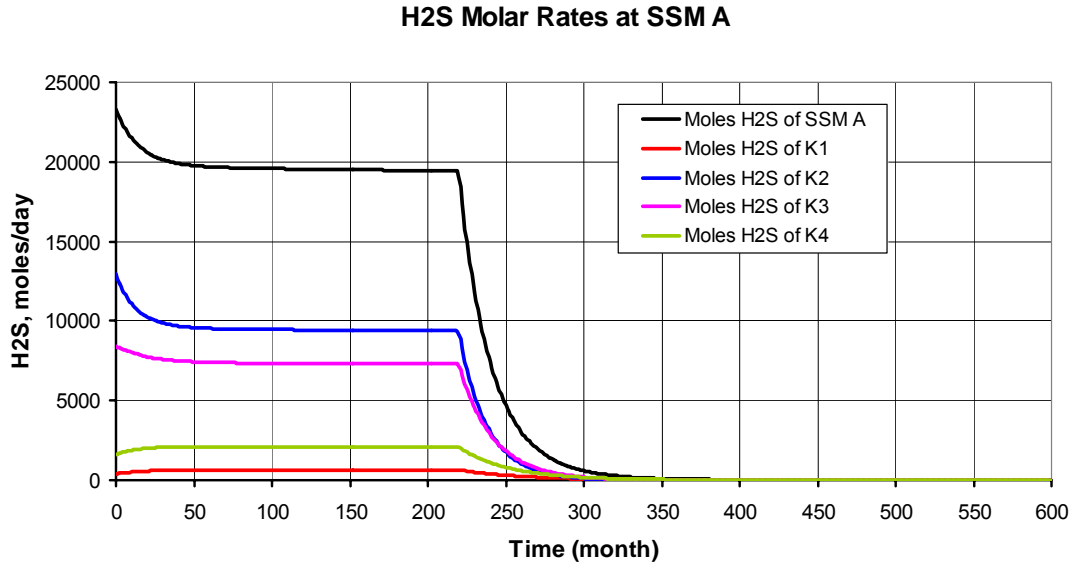


Fig. 108 – H2S molar rate at Subsea Manifold SSM A and its contribution rate from the geological layers

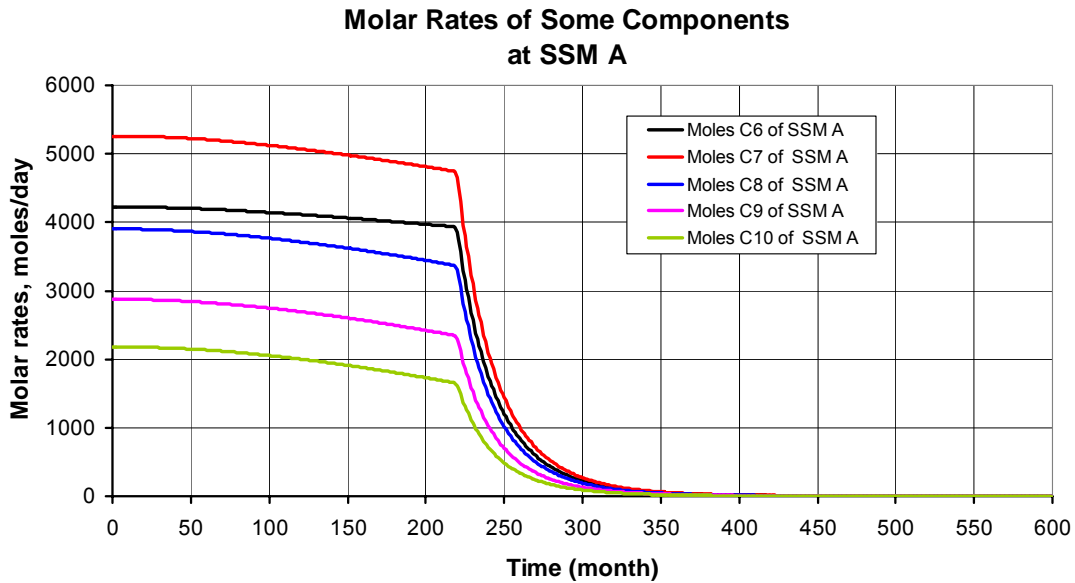


Fig. 109 – Molar rate of some components at Subsea Manifold SSM A

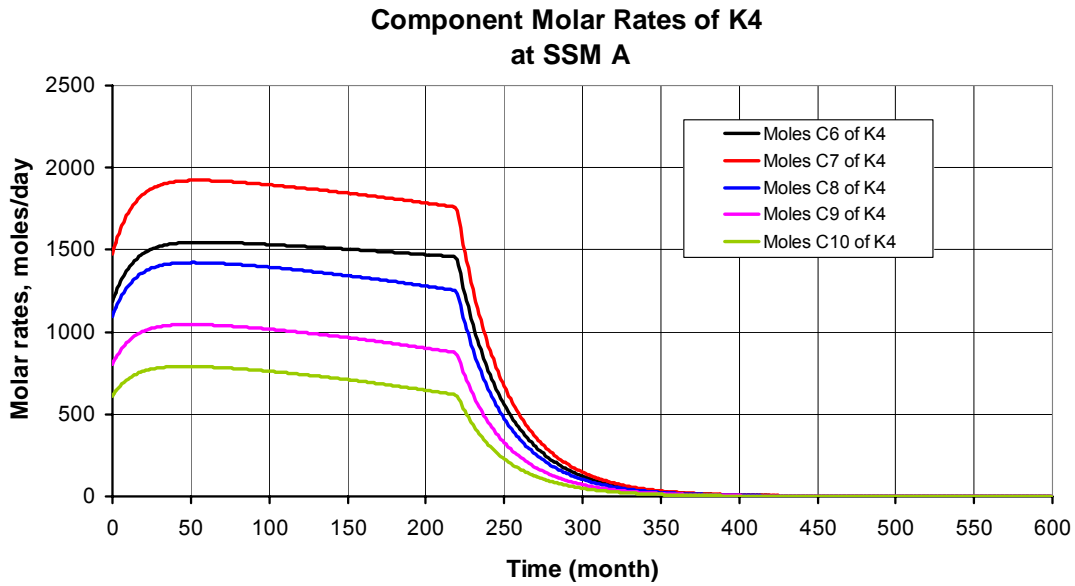


Fig. 110 – Molar rate of some components produced from Layer K4 at Subsea Manifold SSM A

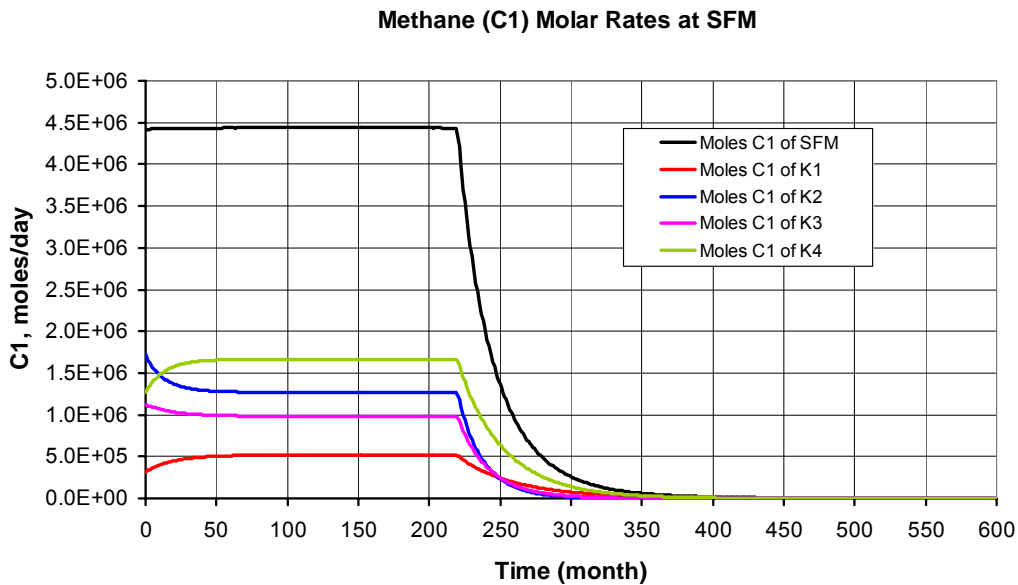


Fig. 111 – Methane molar rate at Surface Manifold SFM and its contribution rate from the geological layers

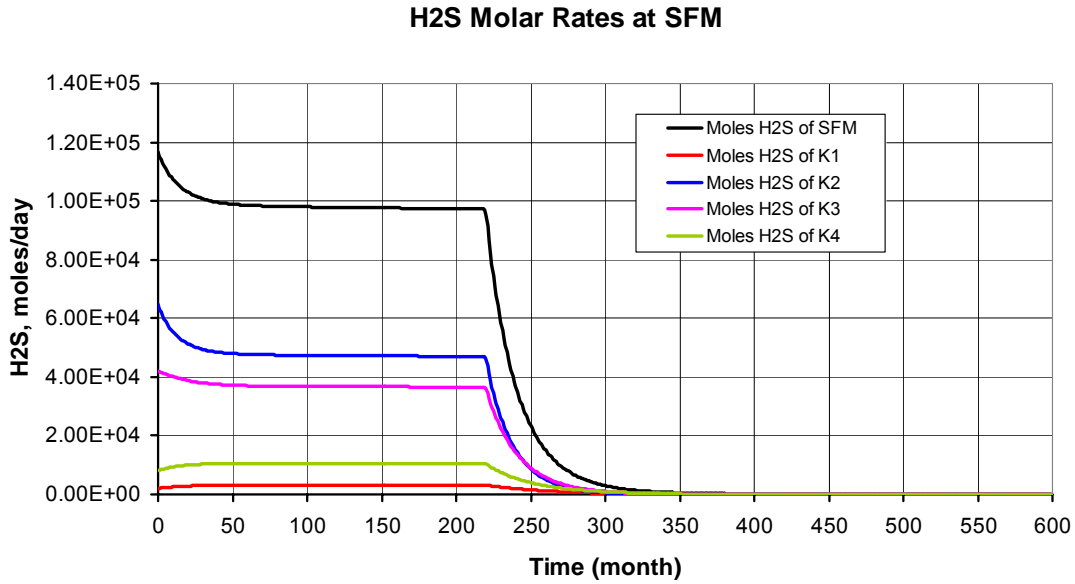


Fig. 112 – H2S molar rate at Surface Manifold SFM and its contribution rate from the geological layers

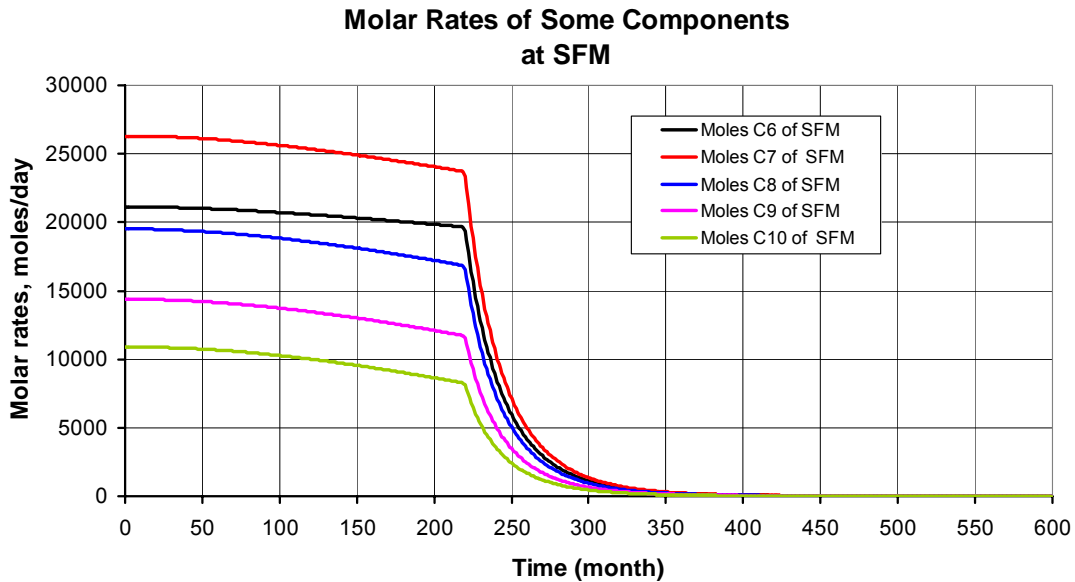


Fig. 113 – Molar rate of some components at Surface Manifold SFM

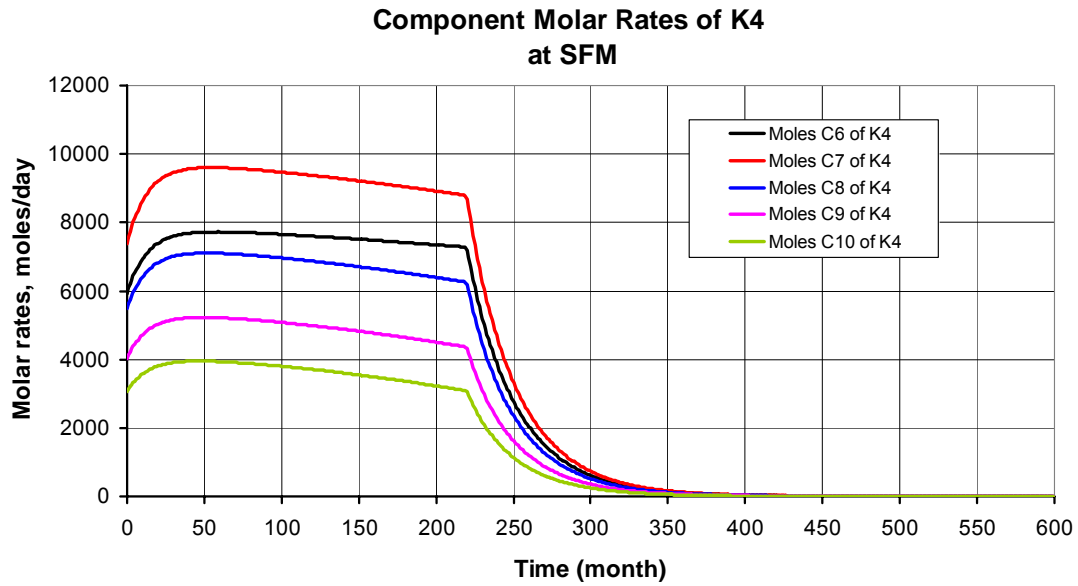


Fig. 114 – Molar rate of some components produced from Layer K4 at Surface Manifold SFM

Appendix A

1. Full Field Reservoir Model Dataset

```

TITLE
  North Field Full Field Cartesian Model
  Covering area of 100 sq.km with 4 major layers K1, K2, K3 and K4
  Gridding System : 20x20x17 = 5200 active blocks with 4 isolation layers
  Compositional Simulation with EOS30+ model
  20 gas production wells
  Swi=0.2 and porosity = 0.15 (K2/K3) and 0.10 (K1/K4)
  20 production wells are open since beginning, 50 years of simulation
  Arif Kuntadi
  30-01-2004
ENDTITLE

RUN
GRID  20    20    17
CPU

MAPSPRINT 1 PV DELX DELY DEPTH POROS KX KY KZ TZ PSAT SG SW P
MAPSFILE 1 SG SO P KRG KRO VISG VISO PSAT POROS

C Grid file
C 20x20x17 Full Field Grid Model
C There are 4 main layers : K1 K2, K3 and K4
C Each layer is separated by isolation layer
C K1 is devided into 3 sublayers
C K2 is devided into 3 sublayers
C K3 is devided into 3 sublayers
C K4 is devided into 4 sublayers
C The main layers are set up as regions

REGION  CON
      0
MOD
C  I1  I2  J1  J2  K1  K2
      1  20  1  20  1   3  = 1
      1  20  1  20  5   7  = 2
      1  20  1  20  9  11  = 3
      1  20  1  20 13  16  = 4
REGNAME
  1 K1-Zone
  2 K2-Zone
  3 K3-Zone
  4 K4-Zone

C Layer K1 and K4 are using the PVTTYPE 1
C Layer K2 and K3 are using the PVTTYPE 1
C All layers are using the same PVTTYPE but different initial gas composition

PVTTYPE CON
      1
C MOD
C  I1  I2  J1  J2  K1  K2
C   1  20  1  20  5   7  = 2
C   1  20  1  20  9  11  = 2

C Area is assumed as 10 km x 10 km
C DX=DY=1640.42 ft, 500 meters in the reservoir zone

C K1 layer has thickness of 204.08 ft
C DZ=68.03 ft for layer 1 - 3 ( Region K1)
C DZ=3.28 ft for layer 4 (isolation layer between K1 and K2)

C K2 layer has thickness of 326.53 ft
C DZ=108.84 ft for layer 5 - 7 ( Region K2)
C DZ=3.28 ft for layer 8 (isolation layer between K2 and K3)

```

```

C K3 layer has thickness of 255.10 ft
C DZ=85.03 ft for layer 9 - 11 ( Region K3)
C DZ=142.86 ft for layer 12 (isolation layer between K3 and K4)

C K4 layer has thickness of 642.86 ft
C DZ=160.71 ft for layer 13 - 16 ( Region K4)
C DZ=142.86 ft for layer 17 (bottom isolation layer)

DELX  CON
      1640.42 ! 500 m

DELY  CON
      1640.42 ! 500 m

THICKNESS ZVAR
3*68.03      ! K1
3.28         ! Isolation layer
3*108.84     ! K2
3.28         ! Isolation layer
3*85.03      ! K3
142.86       ! Isolation layer
4*160.71     ! K4
142.86       ! Isolation layer

C Constant depth to the top surface of the reservoir
DEPTH  CON
      8050 ! ft

C The permeability range of Khuff Formation is 3 - 1800 mD with the average of 30 mD
C K1 and K4 have low permeability, lower than K2 and K3
C K2 and K3 have almost the same permeability
C K1 layer with 3 sublayers, is initially assigned uniform permeability
C K2 layer with 3 sublayers, is initially assigned uniform permeability
C K3 layer with 3 sublayers, is initially assigned uniform permeability
C K4 layer with 4 sublayers, is initially assigned uniform permeability

KX     ZVAR
3*16.7   ! K1
0        ! Isolation layer
3*52.43   ! K2
0        ! Isolation layer
3*46.77   ! K3
0        ! Isolation layer
4*17.7    ! K4
0        ! Isolation layer

C Assuming KY and KZ are equal to KX

KY     EQUALS KX

KZ     EQUALS KX * 0.1

C The porosity is set uniform for K1, K2, K3 and K4

POROS  ZVAR
3*0.10    ! K1
0         ! Isolation layer
3*0.15    ! K2
0         ! Isolation layer
3*0.15    ! K3
0         ! Isolation layer
4*0.10    ! K4
0         ! Isolation layer

C -----

C define Initialization Regions
C IR 1 for K1 and K4 regions
C IR 2 for K2 and K3 regions

```

```

INITREG      CON
  0
MOD
C  I1  I2  J1  J2  K1  K2
  1   20   1   20   1   3   = 1
  1   20   1   20   5   7   = 2
  1   20   1   20   9   11  = 2
  1   20   1   20  13   16  = 1
    
```

C Pref and water and rock properties

C The water has salinity 73 ppm NaCl

```

C      Bwl      cw      denw      visw      cr      Pref
MISC  1.0375  2.635E-6  62.36923  0.65      5E-6      5300
    
```

C EOS30+Model for All Layers

C North Field EOS30+ MODEL

PVTEOS SRK 1

C reservoir temperature, F

220.0

C Fluid characterization, 24-component SRK-EOS

CPT	MW	TC	PC	AC	OMEGA	OMEGB	SHIFT	ZCRIT	PCHOR
N2	28.014	227.160	492.840	0.0370	0.42748	0.0866403	-0.0009	0.29178	59.10
CO2	44.010	547.420	1069.510	0.2250	0.42748	0.0866403	0.21749	0.27433	80.00
H2S	34.082	672.120	1299.970	0.0900	0.42748	0.0866403	0.10153	0.28292	80.10
C1	16.043	343.010	667.030	0.0110	0.42748	0.0866403	-0.00247	0.2862	71.00
C2	30.070	549.580	706.620	0.0990	0.42748	0.0866403	0.05894	0.27924	111.00
C3	44.097	665.690	616.120	0.1520	0.42748	0.0866403	0.09075	0.2763	151.00
i-C4	58.123	734.130	527.940	0.1860	0.42748	0.0866403	0.10952	0.28199	188.80
n-C4	58.123	765.220	550.560	0.2000	0.42748	0.0866403	0.11028	0.27385	191.00
i-C5	72.150	828.700	490.370	0.2290	0.42748	0.0866403	0.09773	0.27231	227.40
n-C5	72.150	845.460	488.780	0.2520	0.42748	0.0866403	0.11947	0.26837	231.00
C6	82.319	924.210	491.320	0.2373	0.42748	0.0866403	0.13411	0.27034	232.57
C7	95.357	988.340	457.180	0.2714	0.42748	0.0866403	0.14292	0.26589	263.86
C8	108.772	1043.920	422.820	0.3094	0.42748	0.0866403	0.15223	0.2614	296.05
C9	121.895	1094.090	389.970	0.3500	0.42748	0.0866403	0.1697	0.25713	327.55
C10	134.784	1138.550	361.660	0.3900	0.42748	0.0866403	0.18619	0.25334	358.48
C11	147.589	1178.850	336.960	0.4295	0.42748	0.0866403	0.20181	0.24986	389.21
C12	160.302	1215.630	315.310	0.4684	0.42748	0.0866403	0.2165	0.2466	419.72
C13	172.914	1249.410	296.270	0.5067	0.42748	0.0866403	0.23022	0.24352	449.99
C14	185.422	1280.570	279.430	0.5444	0.42748	0.0866403	0.24298	0.24056	480.01
C15	197.823	1309.450	264.480	0.5814	0.42748	0.0866403	0.25481	0.2377	509.77
C16	210.113	1336.330	251.140	0.6178	0.42748	0.0866403	0.26573	0.23493	539.27
C17-19	233.389	1383.110	229.290	0.6857	0.42748	0.0866403	0.28431	0.22981	595.13
C20-29	299.514	1493.680	184.610	0.8712	0.42748	0.0866403	0.32394	0.2161	753.83
C30+	477.341	1616.940	167.560	1.0411	0.42748	0.0866403	0.11537	0.20582	1180.62

BIN

```

0      0.12  0.02  0.06  19*0.08
2*0.12 20*0.15
0.07  6*0.06  0.05  13*0.03
19*0  0.06887
19*0
18*0
17*0
16*0
15*0
14*0
13*0
12*0
11*0
10*0
9*0
8*0
7*0
6*0
5*0
4*0
    
```

3*0
2*0
1*0

SEP 1 ! separator conditions are the same as in the PERA-EOS

C	P (psia)	T (F)
	1000	80
	350	70
	14.7	60

C Initialization for a compositional run

C Initialization of K1 and K4 zone

INITIAL 1

DEPTH	! Dew Point Press	Initial gas composition
9600	5134.7	
0.03349140		
0.01755249		
0.00528997		
0.83265138		
0.05157940		
0.01906559		
0.00409428		
0.00699227		
0.00279855		
0.00279921		
0.00390314		
0.00486066		
0.00360525		
0.00265690		
0.00201386		
0.00152830		
0.00116200		
0.00088551		
0.00067654		
0.00051834		
0.00039836		
0.00072976		
0.00062968		
0.00011715		

PINIT 5314.7

ZINIT 9600

C Initialization of K2 and K3 zone

INITIAL 2

DEPTH	! Dew Point Press	Initial gas composition
8500	4944.7	
0.033491		
0.017552		
0.030290		
0.807651		
0.051579		
0.019066		
0.004094		
0.006992		
0.002799		
0.002799		
0.003903		
0.004861		
0.003605		
0.002657		
0.002014		
0.001528		
0.001162		
0.000886		
0.000677		
0.000518		
0.000398		

```

0.000730
0.000630
0.000117

PINIT    5204.7
ZINIT    8500

C Relative Perms
C Two-phase water-oil saturation table
C Swi=0.2
C Water is wetting phase

KRANALYTICAL
.2 .2 .2 .1 ! swc sorw sorg sgc
.5 .33 .9 ! krwro krgro krocw
3 3 3 3 ! nw now ng nog

ENDINIT

PSM

C ----- Recurrent Data -----
C Well data
C There are 20 production wells
C Wells are producing from all layers

WELL
      I      J      K1      K2      SKIN ! header line      calculate well indices internally

P-0203  2      3      1      3      17
        2      3      5      7      13
        2      3      9      11     15
        2      3     13     16     12

P-0208  2      8      1      3      17
        2      8      5      7      13
        2      8      9      11     15
        2      8     13     16     12

P-0213  2     13      1      3      17
        2     13      5      7      13
        2     13      9      11     15
        2     13     13     16     12

P-0218  2     18      1      3      17
        2     18      5      7      13
        2     18      9      11     15
        2     18     13     16     12

P-0603  6      3      1      3      17
        6      3      5      7      13
        6      3      9      11     15
        6      3     13     16     12

P-0608  6      8      1      3      17
        6      8      5      7      13
        6      8      9      11     15
        6      8     13     16     12

P-0613  6     13      1      3      17
        6     13      5      7      13
        6     13      9      11     15
        6     13     13     16     12

P-0618  6     18      1      3      17
        6     18      5      7      13
        6     18      9      11     15
        6     18     13     16     12

P-1003  10     3      1      3      17
        10     3      5      7      13
        10     3      9      11     15

```

	10	3	13	16	12
P-1008	10	8	1	3	17
	10	8	5	7	13
	10	8	9	11	15
	10	8	13	16	12
P-1013	10	13	1	3	17
	10	13	5	7	13
	10	13	9	11	15
	10	13	13	16	12
P-1018	10	18	1	3	17
	10	18	5	7	13
	10	18	9	11	15
	10	18	13	16	12
P-1403	14	3	1	3	17
	14	3	5	7	13
	14	3	9	11	15
	14	3	13	16	12
P-1408	14	8	1	3	17
	14	8	5	7	13
	14	8	9	11	15
	14	8	13	16	12
P-1413	14	13	1	3	17
	14	13	5	7	13
	14	13	9	11	15
	14	13	13	16	12
P-1418	14	18	1	3	17
	14	18	5	7	13
	14	18	9	11	15
	14	18	13	16	12
P-1803	18	3	1	3	17
	18	3	5	7	13
	18	3	9	11	15
	18	3	13	16	12
P-1808	18	8	1	3	17
	18	8	5	7	13
	18	8	9	11	15
	18	8	13	16	12
P-1813	18	13	1	3	17
	18	13	5	7	13
	18	13	9	11	15
	18	13	13	16	12
P-1818	18	18	1	3	17
	18	18	5	7	13
	18	18	9	11	15
	18	18	13	16	12

WELLTYPE

P-0203 - P-1818 MCF ! gas producer, Mscf/D

WELLPLAT ! assign wells to a particular platform

-1 1 ! Assign all gas wells to platform 1
! "-1" means all producers

C Define field production target rate

C The Field Target Rate is 2000 MMSCF/D

PTARG 1 G 2e6 ! Field plateau rate, MCF/D

C Including Tubing Performance Table with 5.5" Production Tubing

```

c include
c thp5_5.inc

BHP
  P-0203 - P-1818  2800  ! Minimum Well Bottom Hole Pressure is set to 2800 psia

C Initially all 20 wells are open for production
C Each well has production rate of 100 MMSCF/D

RATE
  P-0203 - P-1818  100000  ! MCF/D target rate

WELLSUM
  -1  1  ! output summary for all producers

PLATSUM
  -1  0  ! print out platform summary for all timesteps

MAPSFILEFREQ 1

TIME  18250 365

END

```

2. Radial Reservoir Model Dataset

```

TITLE
  North Field Radial Model with single production well
  Covering area of 5 sq.km with 4 major layers K1, K2, K3 and K4
  Gridding System : 25x17x1 = 3525 active blocks with 4 isolation layers
  BO Tables are generated internally with EOS30+ model
  Swi=0.2 and porosity = 15% (K2/K3) and 10% (K1/K4)
  50 years of simulation
  Arif Kuntadi
  23-03-2004
ENDTITLE

RUN
GRID 25 1 145
RUN
CPU
IMPLICIT

MAPSPRINT 1 SG SO P KRG KRO VISG VISO PSAT
MAPSFILE 1 SG SO P KRG KRO VISG VISO PSAT

C Grid file
C 25x17x1 Radial Model
C There are 4 main layers : K1 K2, K3 and K4
C Each layer is separated by isolation layer
C K1 is devided into 20 sublayers
C K2 is devided into 32 sublayers
C K3 is devided into 25 sublayers
C K4 is devided into 64 sublayers
C The main layers are set up as regions

REGION  CON
  0
MOD
C  I1  I2  J1  J2  K1  K2
  1  25  1   1   1   20   = 1
  1  25  1   1  22  53   = 2
  1  25  1   1  55  79   = 3
  1  25  1   1  81 144   = 4
REGNAME
  1  K1-Zone

```

```

2 K2-Zone
3 K3-Zone
4 K4-Zone

C Layer K1 and K4 are using the PVTTYPE 1
C Layer K2 and K3 are using the PVTTYPE 1
C All layers are using the same PVTTYPE but different initial gas composition

PVTTYPE CON
1

C Drainage area was calculated as 1/20 of total area covered in Full Field Model
C Drainage area = 5 km2 (5.38E+07 ft2)
C Drainage radius (re) = 4140 ft

C K1 layer has thickness of 204.08 ft
C DZ=10.20 ft for layer 1 - 20 ( Region K1)
C DZ=3.28 ft for layer 4 (isolation layer between K1 and K2)

C K2 layer has thickness of 326.53 ft
C DZ=10.20 ft for layer 21 - 52 ( Region K2)
C DZ=3.28 ft for layer 8 (isolation layer between K2 and K3)

C K3 layer has thickness of 255.10 ft
C DZ=10.20 ft for layer 53 - 77 ( Region K3)
C DZ=142.86 ft for layer 12 (isolation layer between K3 and K4)

C K4 layer has thickness of 642.86 ft
C DZ=10.04 ft for layer 78 - 141 ( Region K4)
C DZ=142.86 ft for layer 17 (bottom isolation layer)

RADIAL
1 ! grid sizes are generated automatically - equal spacing in log(r)
.583 4140 ! well radius = 7" and outer radius of drainage area (re)
360 ! model full 360 deg round well

THICKNESS ZVAR
20*10.20 ! K1
3.28 ! Isolation layer
32*10.20 ! K2
3.28 ! Isolation layer
25*10.20 ! K3
142.86 ! Isolation layer
64*10.04 ! K4
142.86 ! Isolation layer

C Constant depth to the top surface of the reservoir
DEPTH CON
8050 ! ft

C The permeability range of Khuff Formation is 3 - 1800 mD with the average of 30 mD
C K1 and K4 have low permeability, lower than K2 and K3
C K2 and K3 have almost the same permeability
C K1 layer has 20 sublayers with uniform permeability = 16.7 mD
C K2 layer has 32 sublayers with uniform permeability = 52.43 mD
C K3 layer has 25 sublayers with uniform permeability = 46.77 mD
C K4 layer has 64 sublayers with uniform permeability = 17.7 mD

KX ZVAR
20*16.7 ! K1
0 ! Isolation layer
32*52.43 ! K2
0 ! Isolation layer
25*46.77 ! K3
0 ! Isolation layer
64*17.7 ! K4
0 ! Isolation layer

C Assuming KY and KZ are equal to KX

```

KY EQUALS KX

KZ EQUALS KX * 0.5

C The porosity is set uniform for K1, K2, K3 and K4

POROS ZVAR

```

20*0.10      ! K1
0            ! Isolation layer
32*0.15      ! K2
0            ! Isolation layer
25*0.15      ! K3
0            ! Isolation layer
64*0.10      ! K4
0            ! Isolation layer
    
```

C -----

C define Initialization Regions

C IR 1 for K1 and K4 regions

C IR 2 for K2 and K3 regions

```

      INITREG      CON
      0
MOD
C   I1   I2   J1   J2   K1   K2
    1   25   1    1    1   20   = 1
    1   25   1    1   22   53   = 2
    1   25   1    1   55   79   = 2
    1   25   1    1   81  144   = 1
    
```

C Pref and water and rock properties

C The water has salinity 73 ppm NaCl

```

C      Bwi      cw      denw      visw      cr      Pref
MISC 1.0375  2.635E-6  62.36923  0.65  5E-6  5300
    
```

C EOS30+ are used to generate BO-tables

C Generating BO Tables for Layer K1 and K4

```

C      ipvttype  nsat  ntot
BLACKOIL 1      11   14   EXTEND
PRESSURES
500 1000 1500 1800 2000 2300 2500 3000 3500 4000 4800 5500 6000 6500
    
```

C Equilibrium Gas composition at 4759 psia was taken from SPE 13715

C Initial gas composition was predicted by PhazeComp simulation

```

RESERVOIR FLUID ! Initial reservoir fluid compositions at K4, mole fraction
0.03349140
0.01755249
0.00528997
0.83265138
0.05157940
0.01906559
0.00409428
0.00699227
0.00279855
0.00279921
0.00390314
0.00486066
0.00360525
0.00265690
0.00201386
0.00152830
0.00116200
0.00088551
0.00067654
0.00051834
0.00039836
    
```

0.00072976
 0.00062968
 0.00011715

SEPARATOR ! separator conditions are the same as in the PERA-EOS

C P (psia) T (F)
 1000 80
 350 70
 14.7 60

ENDBLACKOIL

C EOS30+Model for All Layers
 C North Field EOS30+ MODEL

PVTEOS SRK 1

C reservoir temperature, F
 220.0

C Fluid characterization, 24-component SRK-EOS

CPT	MW	TC	PC	AC	OMEGA	OMEGB	SHIFT	ZCRIT	PCHOR
N2	28.014	227.160	492.840	0.0370	0.42748	0.0866403	-0.0009	0.29178	59.10
CO2	44.010	547.420	1069.510	0.2250	0.42748	0.0866403	0.21749	0.27433	80.00
H2S	34.082	672.120	1299.970	0.0900	0.42748	0.0866403	0.10153	0.28292	80.10
C1	16.043	343.010	667.030	0.0110	0.42748	0.0866403	-0.00247	0.2862	71.00
C2	30.070	549.580	706.620	0.0990	0.42748	0.0866403	0.05894	0.27924	111.00
C3	44.097	665.690	616.120	0.1520	0.42748	0.0866403	0.09075	0.2763	151.00
i-C4	58.123	734.130	527.940	0.1860	0.42748	0.0866403	0.10952	0.28199	188.80
n-C4	58.123	765.220	550.560	0.2000	0.42748	0.0866403	0.11028	0.27385	191.00
i-C5	72.150	828.700	490.370	0.2290	0.42748	0.0866403	0.09773	0.27231	227.40
n-C5	72.150	845.460	488.780	0.2520	0.42748	0.0866403	0.11947	0.26837	231.00
C6	82.319	924.210	491.320	0.2373	0.42748	0.0866403	0.13411	0.27034	232.57
C7	95.357	988.340	457.180	0.2714	0.42748	0.0866403	0.14292	0.26589	263.86
C8	108.772	1043.920	422.820	0.3094	0.42748	0.0866403	0.15223	0.2614	296.05
C9	121.895	1094.090	389.970	0.3500	0.42748	0.0866403	0.1697	0.25713	327.55
C10	134.784	1138.550	361.660	0.3900	0.42748	0.0866403	0.18619	0.25334	358.48
C11	147.589	1178.850	336.960	0.4295	0.42748	0.0866403	0.20181	0.24986	389.21
C12	160.302	1215.630	315.310	0.4684	0.42748	0.0866403	0.2165	0.2466	419.72
C13	172.914	1249.410	296.270	0.5067	0.42748	0.0866403	0.23022	0.24352	449.99
C14	185.422	1280.570	279.430	0.5444	0.42748	0.0866403	0.24298	0.24056	480.01
C15	197.823	1309.450	264.480	0.5814	0.42748	0.0866403	0.25481	0.2377	509.77
C16	210.113	1336.330	251.140	0.6178	0.42748	0.0866403	0.26573	0.23493	539.27
C17-19	233.389	1383.110	229.290	0.6857	0.42748	0.0866403	0.28431	0.22981	595.13
C20-29	299.514	1493.680	184.610	0.8712	0.42748	0.0866403	0.32394	0.2161	753.83
C30+	477.341	1616.940	167.560	1.0411	0.42748	0.0866403	0.11537	0.20582	1180.62

BIN

0 0.12 0.02 0.06 19*0.08
 2*0.12 20*0.15
 0.07 6*0.06 0.05 13*0.03
 19*0 0.06887
 19*0
 18*0
 17*0
 16*0
 15*0
 14*0
 13*0
 12*0
 11*0
 10*0
 9*0
 8*0
 7*0
 6*0
 5*0
 4*0
 3*0
 2*0
 1*0

C Generating BO Tables for Layer K2 and K3

```
C      ipvttype  nsat  ntot
BLACKOIL  2      11    14      EXTEND
PRESSURES
500 1000 1500 1800 2000 2300 2500 3000 3500 4000 4400 5500 6000 6500
```

C Initial gas composition was predicted by PhazeComp simulation

```
RESERVOIR FLUID ! Initial reservoir fluid compositions at K2/K3, mole fraction
0.033491
0.017552
0.030290
0.807651
0.051579
0.019066
0.004094
0.006992
0.002799
0.002799
0.003903
0.004861
0.003605
0.002657
0.002014
0.001528
0.001162
0.000886
0.000677
0.000518
0.000398
0.000730
0.000630
0.000117
```

SEPARATOR ! separator conditions are the same as in the PERA-EOS

```
C      P (psia)      T (F)
      1000          80
      350           70
      14.7          60
```

ENDBLACKOIL

C EOS30+Model for All Layers

C North Field EOS30+ MODEL

PVTEOS SRK 2

C reservoir temperature, F

220.0

C Fluid characterization, 24-component SRK-EOS

CPT	MW	TC	PC	AC	OMEGA	OMEGB	SHIFT	ZCRIT	PCHOR
N2	28.014	227.160	492.840	0.0370	0.42748	0.0866403	-0.0009	0.29178	59.10
CO2	44.010	547.420	1069.510	0.2250	0.42748	0.0866403	0.21749	0.27433	80.00
H2S	34.082	672.120	1299.970	0.0900	0.42748	0.0866403	0.10153	0.28292	80.10
C1	16.043	343.010	667.030	0.0110	0.42748	0.0866403	-0.00247	0.2862	71.00
C2	30.070	549.580	706.620	0.0990	0.42748	0.0866403	0.05894	0.27924	111.00
C3	44.097	665.690	616.120	0.1520	0.42748	0.0866403	0.09075	0.2763	151.00
i-C4	58.123	734.130	527.940	0.1860	0.42748	0.0866403	0.10952	0.28199	188.80
n-C4	58.123	765.220	550.560	0.2000	0.42748	0.0866403	0.11028	0.27385	191.00
i-C5	72.150	828.700	490.370	0.2290	0.42748	0.0866403	0.09773	0.27231	227.40
n-C5	72.150	845.460	488.780	0.2520	0.42748	0.0866403	0.11947	0.26837	231.00
C6	82.319	924.210	491.320	0.2373	0.42748	0.0866403	0.13411	0.27034	232.57
C7	95.357	988.340	457.180	0.2714	0.42748	0.0866403	0.14292	0.26589	263.86
C8	108.772	1043.920	422.820	0.3094	0.42748	0.0866403	0.15223	0.2614	296.05
C9	121.895	1094.090	389.970	0.3500	0.42748	0.0866403	0.1697	0.25713	327.55
C10	134.784	1138.550	361.660	0.3900	0.42748	0.0866403	0.18619	0.25334	358.48
C11	147.589	1178.850	336.960	0.4295	0.42748	0.0866403	0.20181	0.24986	389.21
C12	160.302	1215.630	315.310	0.4684	0.42748	0.0866403	0.2165	0.2466	419.72
C13	172.914	1249.410	296.270	0.5067	0.42748	0.0866403	0.23022	0.24352	449.99
C14	185.422	1280.570	279.430	0.5444	0.42748	0.0866403	0.24298	0.24056	480.01
C15	197.823	1309.450	264.480	0.5814	0.42748	0.0866403	0.25481	0.2377	509.77
C16	210.113	1336.330	251.140	0.6178	0.42748	0.0866403	0.26573	0.23493	539.27
C17-19	233.389	1383.110	229.290	0.6857	0.42748	0.0866403	0.28431	0.22981	595.13

C20-29 299.514 1493.680 184.610 0.8712 0.42748 0.0866403 0.32394 0.2161 753.83
 C30+ 477.341 1616.940 167.560 1.0411 0.42748 0.0866403 0.11537 0.20582 1180.62

BIN

0 0.12 0.02 0.06 19*0.08
 2*0.12 20*0.15
 0.07 6*0.06 0.05 13*0.03
 19*0 0.06887
 19*0
 18*0
 17*0
 16*0
 15*0
 14*0
 13*0
 12*0
 11*0
 10*0
 9*0
 8*0
 7*0
 6*0
 5*0
 4*0
 3*0
 2*0
 1*0

C Initialization for a Black-oil run

C Initialization of K1 and K4 zone

INITIAL 1
 DEPTH PSATDP
 9600 5134.7
 PINIT 5314.7
 ZINIT 9600

C Initialization of K2 and K3 zone

INITIAL 2
 DEPTH PSATDP
 8500 4944.7
 PINIT 5204.7
 ZINIT 8500

C Relative Perms

C Two-phase water-oil saturation table

C Swi=0.2

C Water is wetting phase

KRANALYTICAL

.2 .2 .2 .1 ! swc sorw sorg sgc
 .5 .33 .9 ! krwro krgro krocw
 3 3 3 3 ! nw now ng nog

ENDINIT

c PSM

C ----- Recurrent Data -----

C Well data

C There are 20 production wells

C Wells are producing from all layers

WELL

	I	J	K1	K2	! header line	calculate well indices internally
PROD	1	1	1	20		

1	1	22	53
1	1	55	79
1	1	81	144

```
WELLTYPE
  PROD   MCF   !   gas producer, Mscf/D

WELLPLAT ! assign wells to a particular platform
-1      1      ! Assign all gas wells to platform 1
          ! "-1" means all producers

C Define field production target rate
C The Field Target Rate is 100 MMSCF/D

  PTARG  1   G   1e5 ! Field plateau rate, MCF/D

C Including Tubing Performance Table with 7" Production Tubing

C include
C thp7.inc

BHP
  PROD   2800 ! Minimum Well Bottom Hole Pressure is set to 2800 psia

C the production well has production rate of 100 MMSCF/D

RATE
  PROD   1e5      ! MCF/D target rate

WELLSUM
  -1     1      ! output summary for all producers

PLATSUM
  -1     0      ! print out platform summary for all timesteps

MAPSFREQ 1
MAPSFILEFREQ 1
DT .001
TIME 18250 365

END
```

Appendix B

1. Extract of Main stream file which is converted from the simulation result streams.

```

Streamz          1
* =====
* ----- StreamFile generated by Sen2Str -----
* =====

Variable  T1      Time    ; Start time interval
Variable  T2      Time    ; End time interval
Variable  ITIME   Integer ; Time step
Variable  IDAY   Integer ; Day (date)
Variable  IMONTH Integer ; Month (date)
Variable  IYEAR  Integer ; Year (date)
Variable  OTP    Real    ; Ontime for production
Variable  WELL   String  ; Well name
Variable  I_PF   Integer ; I grid cell perforation
Variable  J_PF   Integer ; J grid cell perforation
Variable  K_PF   Integer ; K grid cell perforation
Variable  PVTNUM Integer ; PVT region no.
Variable  IPLAT  Integer ; Platform no.
Variable  PRES   Pressure; Phase pressure
Variable  PFLAG  Integer ; Phase id = 1 for mixture of injection gas and equilibrium gas - Otherwise = 2

Data

Set T1      0 Days
Set T2      2 Days
Set ITIME   1
Set IDAY    0
Set IMONTH  0
Set IYEAR   0

Set WELL    P-0203
Set OTP     1
Set IPLAT   1
Set PVTNUM  1
  I_PF      J_PF      K_PF      PFLAG  PRES (Psia)  Moles N2 (lbmol)  CO2 (lbmol)  H2S (lbmol)  C1 (lbmol)  C2 (lbmol)
  2         3         1         1      5152         204.1            107          32.24        5074        314.3
  2         3         2         1      5159         203.8            106.8        32.19        5067        313.9
  2         3         3         1      5166         203.6            106.7        32.15        5061        313.5
  2         3         5         1      5176         1205            631.3        1089        2.91E+04    1855
  2         3         6         1      5187         1205            631.5        1090        2.91E+04    1856
  2         3         7         1      5199         1206            631.8        1090        2.91E+04    1857
  2         3         9         1      5211         770.7           403.9        697         1.86E+04    1187
  2         3         10        1      5220         771.2           404.2        697.5       1.86E+04    1188
  2         3         11        1      5229         772             404.6        698.2       1.86E+04    1189
  2         3         13        1      5252         630.1           330.2        99.52       1.57E+04    970.4
  2         3         14        1      5269         629.9           330.1        99.49       1.57E+04    970.1
  2         3         15        1      5286         629.8           330.1        99.47       1.57E+04    969.9
  2         3         16        1      5303         629.7           330          99.46       1.57E+04    969.8

Set WELL    P-0208
Set OTP     1
Set IPLAT   1
Set PVTNUM  1
  I_PF      J_PF      K_PF      PFLAG  PRES (Psia)  Moles N2 (lbmol)  CO2 (lbmol)  H2S (lbmol)  C1 (lbmol)  C2 (lbmol)
  2         8         1         1      5152         204.1            107          32.24        5074        314.3
  2         8         2         1      5159         203.8            106.8        32.19        5067        313.9
  2         8         3         1      5166         203.6            106.7        32.15        5061        313.5
  2         8         5         1      5176         1205            631.3        1089        2.91E+04    1855
  2         8         6         1      5187         1205            631.5        1090        2.91E+04    1856
  2         8         7         1      5199         1206            631.8        1090        2.91E+04    1857
  2         8         9         1      5211         770.7           403.9        697         1.86E+04    1187
  2         8         10        1      5220         771.2           404.2        697.5       1.86E+04    1188
  2         8         11        1      5229         772             404.6        698.2       1.86E+04    1189
  2         8         13        1      5252         630.1           330.2        99.52       1.57E+04    970.4
  2         8         14        1      5269         629.9           330.1        99.49       1.57E+04    970.1
  2         8         15        1      5286         629.8           330.1        99.47       1.57E+04    969.9
  2         8         16        1      5303         629.7           330          99.46       1.57E+04    969.8

```

2. Extract of well stream files which is the result of filtering operation of Main stream file.

```

STREAMZ          1
Note             'Converted Streams from Streamz Files:'
Note             'nf'
Note             'C:\Arif\Kuliah\Thesis\Stream\Stz\NF_FFM_COMP_kavg_skin_comb_A.str'
Char             'SRK-SCN-C30+'
Variable         T1          time
Variable         T2          time
Variable         ITIME       integer
Variable         IDAY        integer
Variable         IMONTH      integer
Variable         IYEAR       integer
Variable         OTP         real
Variable         WELL        string
Variable         I_PF        integer
Variable         J_PF        integer
Variable         K_PF        integer
Variable         PVTNUM      integer
Variable         IPLAT       integer
Variable         PRES        pressure
Variable         PFLAG       integer
DATA

Set              T1          0 d
Set              T2          2 d
Set              ITIME       1
Set              IDAY        0
Set              IMONTH      0
Set              IYEAR       0
Set              WELL        'P-1003 '
Set              OTP         1
Set              IPLAT       1
Set              PVTNUM      1

      I_PF      J_PF      K_PF      PFLAG      PRES (psia)  Moles N2  Moles CO2  Moles H2S  Moles C1  Moles C2
      10         3         1         1         5152         204.1     106.9      32.23      5073      314.3
      10         3         2         1         5159         203.8     106.8      32.19      5067      313.9
      10         3         3         1         5166         203.5     106.7      32.15      5060      313.5
      10         3         5         1         5176         1205      631.3      1090      29050     1855
      10         3         6         1         5187         1205      631.6      1090      29060     1856
      10         3         7         1         5199         1206      631.9      1090      29070     1857
      10         3         9         1         5211         770.7     403.9      697       18590     1187
      10         3         10        1         5220         771.3     404.2      697.5     18600     1188
      10         3         11        1         5229         772       404.6      698.2     18620     1189
      10         3         13        1         5252         630       330.2      99.51     15660     970.2
      10         3         14        1         5269         629.8     330.1      99.48     15660     969.9
      10         3         15        1         5286         629.7     330       99.46     15650     969.7
      10         3         16        1         5303         629.6     330       99.45     15650     969.7

Set              T1          2 d
Set              T2          5 d
Set              ITIME       2

      I_PF      J_PF      K_PF      PFLAG      PRES (psia)  Moles N2  Moles CO2  Moles H2S  Moles C1  Moles C2
      10         3         1         1         5148         205.5     107.7      32.45     5108     316.4
      10         3         2         1         5155         205.2     107.5      32.41     5102     316
      10         3         3         1         5162         205       107.4      32.37     5095     315.6
      10         3         5         1         5170         1202      629.9      1087     28980     1851
      10         3         6         1         5182         1202      630.1      1087     28990     1852
      10         3         7         1         5193         1203      630.4      1088     29010     1852
      10         3         9         1         5206         771.5     404.3      697.7     18600     1188
      10         3         10        1         5215         772       404.6      698.2     18620     1189
      10         3         11        1         5224         772.8     405       698.9     18640     1190
      10         3         13        1         5247         630.5     330.4      99.58     15670     971
      10         3         14        1         5264         630.3     330.3      99.55     15670     970.7
      10         3         15        1         5281         630.2     330.3      99.53     15670     970.5
      10         3         16        1         5298         630.1     330.2      99.53     15670     970.4
    
```

3. Extract of average well stream files which is the result of aggregation and averaging operations of well stream file.

```

STREAMZ          1
Note            'Converted Streams from Streamz Files:'
Note            'nf'
Note            'C:\Arif\Kuliah\Thesis\Stream\Temp\temp2.str'
Char            'SRK-SCN-C30+'
Variable        T1            time
Variable        T2            time
Variable        ITIME         integer
Variable        IDAY          integer
Variable        IMONTH        integer
Variable        IYEAR         integer
Variable        OTP           real
Variable        WELL          string
Variable        I_PF          integer
Variable        J_PF          integer
Variable        K_PF          integer
Variable        PVTNUM        integer
Variable        IPLAT         integer
Variable        PRES          pressure
Variable        PFLAG         integer
DATA
    
```

T1 (mo)	T2 (mo)	WELL	Moles N2	Moles CO2	Moles H2S	Moles C1	Moles C2
0	1	'P-1003 '	9060.04	4748.14	5831.2	220839	13952.1
1	2	'P-1003 '	9059.55	4747.99	5763.82	220902	13952.5
2	3	'P-1003 '	9059.17	4748.01	5698.84	220969	13952.6
3	4	'P-1003 '	9059.97	4748.09	5647.15	221033	13954.4
4	5	'P-1003 '	9060.53	4748.1	5599.33	221079	13952.7
5	6	'P-1003 '	9060.02	4748.1	5554.53	221127	13952.5
6	7	'P-1003 '	9060.23	4748.02	5512.89	221157	13951.5
7	8	'P-1003 '	9059.9	4748	5473.99	221203	13952.3
8	9	'P-1003 '	9059.41	4747.92	5437.91	221239	13953.5
9	10	'P-1003 '	9059.53	4748.05	5403.92	221270	13952.6
10	11	'P-1003 '	9059.45	4747.88	5372.36	221299	13951.3
11	12	'P-1003 '	9059.61	4748.02	5348.5	221337	13952.8
12	13	'P-1003 '	9059.5	4748	5314.78	221362	13951.3
13	14	'P-1003 '	9059.6	4748	5288.67	221368	13954
14	15	'P-1003 '	9059.7	4748	5264.13	221397	13952.7
15	16	'P-1003 '	9059.7	4747.9	5241.04	221422	13951.6
16	17	'P-1003 '	9059.79	4747.99	5219.39	221470	13952.2
17	18	'P-1003 '	9059.98	4747.91	5199.46	221476	13952.1
18	19	'P-1003 '	9059.82	4747.72	5181.09	221492	13951.1
19	20	'P-1003 '	9059.98	4747.88	5163.94	221510	13952.1
20	21	'P-1003 '	9060.09	4747.81	5147.81	221511	13950.2
21	22	'P-1003 '	9060.18	4747.8	5132.83	221534	13949
22	23	'P-1003 '	9060.12	4747.8	5119.28	221542	13951.4
23	24	'P-1003 '	9060.34	4747.8	5108.31	221577	13950.9
24	25	'P-1003 '	9060.4	4747.6	5094.51	221585	13951.8
25	26	'P-1003 '	9060.6	4747.6	5083.05	221599	13949.7
26	27	'P-1003 '	9060.7	4747.7	5072.49	221606	13950.1
27	28	'P-1003 '	9060.8	4747.51	5062.6	221615	13950.2
28	29	'P-1003 '	9060.89	4747.69	5053.4	221617	13947.8
29	30	'P-1003 '	9060.9	4747.52	5044.68	221633	13948.8
30	31	'P-1003 '	9060.99	4747.32	5036.58	221644	13947.9

4. Extract of average well layer stream files which is the result of aggregation and averaging operations of well layer stream file.

```

STREAMZ      1
Note        'Converted Streams from Streamz Files:'
Note        'nf'
Note        'C:\Arif\Kuliah\Thesis\Stream\Temp\temp2.str'
Char        'SRK-SCN-C30+'
Variable    T1      time
Variable    T2      time
Variable    ITIME   integer
Variable    IDAY   integer
Variable    IMONTH integer
Variable    IYEAR  integer
Variable    OTP     real
Variable    WELL   string
Variable    I_PF   integer
Variable    J_PF   integer
Variable    K_PF   integer
Variable    PVTNUM integer
Variable    IPLAT  integer
Variable    PRES   pressure
Variable    PFLAG  integer
Variable    Manifold string
Variable    layer  string
DATA
    
```

T1 (mo)	T2 (mo)	WELL	layer	Moles N2	Moles CO2	Moles H2S	Moles C1	Moles C2
0	1	'P-1003 '	'K4'	2539.7	1331.02	401.163	63137.4	3911.3
1	2	'P-1003 '	'K4'	2604.4	1364.91	411.388	64746.3	4011.63
2	3	'P-1003 '	'K4'	2667.85	1398.18	421.421	66326.3	4108.67
3	4	'P-1003 '	'K4'	2717.04	1424.05	429.168	67555.9	4184.81
4	5	'P-1003 '	'K4'	2762.72	1447.91	436.409	68681.1	4254.54
5	6	'P-1003 '	'K4'	2805.04	1470.14	442.991	69740.3	4320.75
6	7	'P-1003 '	'K4'	2844.25	1490.66	449.225	70709.1	4380.81
7	8	'P-1003 '	'K4'	2880.54	1509.69	454.932	71621.5	4436.52
8	9	'P-1003 '	'K4'	2914.33	1527.35	460.371	72462.3	4488.38
9	10	'P-1003 '	'K4'	2945.63	1543.73	465.239	73233.7	4536.39
10	11	'P-1003 '	'K4'	2974.65	1558.94	469.802	73952.5	4580.54
11	12	'P-1003 '	'K4'	2996.54	1570.44	473.196	74505.6	4615.38
12	13	'P-1003 '	'K4'	3027.2	1586.5	478	75260	4661
13	14	'P-1003 '	'K4'	3050.85	1598.97	481.959	75843.9	4699.6
14	15	'P-1003 '	'K4'	3073.15	1610.56	485.497	76393.9	4732.05
15	16	'P-1003 '	'K4'	3093.71	1621.38	488.649	76915	4763.49
16	17	'P-1003 '	'K4'	3113.29	1631.52	491.79	77407.2	4793.96
17	18	'P-1003 '	'K4'	3131.08	1640.9	494.564	77843	4821.64
18	19	'P-1003 '	'K4'	3147.23	1649.24	496.954	78238.9	4845.54
19	20	'P-1003 '	'K4'	3162.26	1657.13	499.309	78614	4869.09
20	21	'P-1003 '	'K4'	3176.23	1664.47	501.665	78952.5	4890.07
21	22	'P-1003 '	'K4'	3188.89	1671.06	503.515	79269.4	4909
22	23	'P-1003 '	'K4'	3200.2	1677.04	505.282	79550.6	4928.47
23	24	'P-1003 '	'K4'	3209.6	1681.88	506.751	79797.1	4941.92
24	25	'P-1003 '	'K4'	3220.9	1687.7	508.5	80080	4960
25	26	'P-1003 '	'K4'	3230.38	1692.59	509.997	80309.5	4972.97
26	27	'P-1003 '	'K4'	3238.73	1697.2	511.273	80515.7	4987.69
27	28	'P-1003 '	'K4'	3246.68	1701.14	512.453	80712.2	4999.53
28	29	'P-1003 '	'K4'	3254.07	1705.07	513.631	80889.7	5009.43
29	30	'P-1003 '	'K4'	3260.88	1708.63	514.716	81066.3	5019.24
30	31	'P-1003 '	'K4'	3267.29	1711.8	515.705	81224.9	5029.05

Appendix C

1. Spreadsheet calculation example for predicting the gas rate with excluding and including the capillary number effect
2. Spreadsheet calculation example for predicting the dry gas rate

Data

Permeability, mD	k	17.7
Outer boundary, ft	re	4140
Well radius, ft	rw	0.583
Reservoir thickness, ft	h	160.71
Skin factor	s	0
Constant for Field Unit	a1	0.00112716
Porosity	phi	0.1
Relative permeability of gas at Sw=Swc, So=Sorg	krgr	0.33
Connate water saturation	Swi	0.2
	C	2.4816
	α	15033

Simulation Result

Layer	Time	GOR	PBH	QG	PAVG	CGR		P*	Remark
	days	scf/stb	psia	mscf/d	psia	stb/mmscf	stb/scf	psia	
K4	1825	44012	2800	17123	3499	22.72	2.272E-05	3426	Region 1 & 2 exist

Gas Rate Comparison between simulation result and manual calculation

PSAT	BO	RS	VISO	rs		BG	VISG	krq/kro	krq_im	kro_im	λg	∫ λg dP
	psia	rb/stb	scf/stb	cp	stb/mmscf	stb/scf	rb/scf					
2800	1.294	502.2	0.823	18.507	1.851E-05	0.001153	0.0193	4.9	0.1	0.0204	4503	459860
2900	1.303	523.1	0.798	19.169	1.917E-05	0.001116	0.0197	5.9	0.103	0.0175	4694	481077
3000	1.313	544.2	0.773	19.839	1.984E-05	0.001082	0.0201	7.3	0.107	0.0146	4928	525221
3100	1.322	565.7	0.75	20.514	2.051E-05	0.001051	0.0205	9.7	0.12	0.0123	5577	590754
3200	1.331	587.5	0.727	21.193	2.119E-05	0.001021	0.0209	14.2	0.133	0.0093	6238	671744
3300	1.341	609.6	0.705	21.871	2.187E-05	0.000994	0.0214	26.1	0.153	0.0059	7196	845103
3400	1.351	632	0.684	22.548	2.255E-05	0.000969	0.0218	130.2	0.205	0.0016	9706	258293
3426											10352	
3426	1.353	637.87	0.679	22.721	2.272E-05	0.000963	0.0219	1000	0.90552	0.0009	42939	3191036
3499	1.360	651.49	0.66	23.21	2.32073E-05	0.000927	0.0221	1000	0.90552	0.0009	44194	

Sum 7.023E+06
 Qg calc. 1.743E+07 SCF/D
 17428 MSCF/D
 Qg error 1.78 %

Gas Rate Calculation considering capillary pressure number effect on relative permeability

PSAT	radius	Vel_Darcy	Vel_pore	Nc	krqM	krq avg	α	FI	krq	kro	λg	∫ λg dP
psia	ft	ft/s	ft/s									
2800	0.58	2.69E-03	3.36E-02	8.99E-05	0.274	0.19	80374	2.00E-01	0.2392	0.0488	10772	1029197
2900	2.07	7.33E-04	9.16E-03	2.69E-05	0.282	0.19	78086	3.73E-01	0.2153	0.0366	9812	912179
3000	7.37	2.00E-04	2.50E-03	8.08E-06	0.290	0.20	75646	5.85E-01	0.1831	0.0249	8432	795068
3100	26.22	5.46E-05	6.82E-04	2.43E-06	0.299	0.21	71720	7.73E-01	0.1607	0.0165	7469	730151
3200	93.23	1.49E-05	1.86E-04	7.28E-07	0.308	0.22	68124	8.91E-01	0.1521	0.0107	7134	735117
3300	331.55	4.08E-06	5.10E-05	2.20E-07	0.318	0.24	63858	9.52E-01	0.1609	0.0062	7569	869384
3400	1179.05	1.12E-06	1.40E-05	6.59E-08	0.327	0.27	56463	9.80E-01	0.2074	0.0016	9819	260353
3426											10398	
3426											42939	3191036
3499											44194	

Sum 8.522E+06
 Qg calc. 2.115E+07 SCF/D
 21149 MSCF/D

Data

Permeability, mD	k	17.7
Outer boundary, ft	re	4140
Well radius, ft	rw	0.583
Reservoir thickness, ft	h	160.71
Skin factor	s	0
Constant for Field Unit	a1	0.00112716
Porosity	phi	0.1
Relative permeability of gas at Sw=Swc, So=Sorg	krgr	0.33
Connate water saturation	Swi	0.2
	C	2.4816

Simulation Result

Layer	Time	GOR	PBH	QG	PAVG	CGR		P*	Remark
	days	scf/stb	psia	mscf/d	psia	stb/mmcf	stb/scf	psia	
K4	1825	44012	2800	17123	3499	22.72	2.272E-05	3426	Region 1 & 2 exist

Dry Gas Rate Calculation

PSAT	BO	RS	VISO	rs		BG	VISG	krq	λg	krq ∫ λg dP
psia	rb/stb	scf/stb	cp	stb/mmcf	stb/scf	rb/scf	cp			
2800	1.294	502.2	0.823	18.507	1.851E-05	0.001153	0.0193	0.90552	44938	4093997
2900	1.303	523.1	0.798	19.169	1.917E-05	0.001116	0.0197	0.90552	45485	4141213
3000	1.313	544.2	0.773	19.839	1.984E-05	0.001082	0.0201	0.90552	45981	4183241
3100	1.322	565.7	0.75	20.514	2.051E-05	0.001051	0.0205	0.90552	46413	4223172
3200	1.331	587.5	0.727	21.193	2.119E-05	0.001021	0.0209	0.90552	46863	4250231
3300	1.341	609.6	0.705	21.871	2.187E-05	0.000994	0.0214	0.90552	47011	4271796
3400	1.351	632	0.684	22.548	2.255E-05	0.000969	0.0218	0.90552	47339	1105027
3426									47424	
3426	1.353	637.87	0.679	22.721	2.272E-05	0.000963	0.0219	0.90552	47419	3190989
3499	1.360	651.49	0.66	23.21	2.32073E-05	0.000927	0.0221	0.90552	48805	

Sum 2.946E+07
 Qg calc. 7.311E+07 SCF/D
 73107 MSCF/D